



LUND UNIVERSITY

Crosstalk in Wideband Wireline Systems -- Curse and Blessing

Huang, Yezi

2015

Document Version:

Publisher's PDF, also known as Version of record

[Link to publication](#)

Citation for published version (APA):

Huang, Y. (2015). *Crosstalk in Wideband Wireline Systems -- Curse and Blessing*. [Licentiate Thesis, Faculty of Engineering, LTH]. Lund University.

Total number of authors:

1

General rights

Unless other specific re-use rights are stated the following general rights apply:

Copyright and moral rights for the publications made accessible in the public portal are retained by the authors and/or other copyright owners and it is a condition of accessing publications that users recognise and abide by the legal requirements associated with these rights.

- Users may download and print one copy of any publication from the public portal for the purpose of private study or research.
- You may not further distribute the material or use it for any profit-making activity or commercial gain
- You may freely distribute the URL identifying the publication in the public portal

Read more about Creative commons licenses: <https://creativecommons.org/licenses/>

Take down policy

If you believe that this document breaches copyright please contact us providing details, and we will remove access to the work immediately and investigate your claim.

LUND UNIVERSITY

PO Box 117
221 00 Lund
+46 46-222 00 00

Crosstalk in Wideband Wireline Systems — Curse and Blessing

Yezi Huang



LUND UNIVERSITY

Licentiate Thesis
Lund, October 2015

Yezi Huang
Department of Electrical and Information Technology
Lund University
Box 118, SE-221 00 LUND
SWEDEN

This thesis is set in Computer Modern 10pt
with the L^AT_EX Documentation System

Series of licentiate and doctoral theses
No. 78
ISSN 1654-790x
ISBN 978-91-7623-536-2 (print)
ISBN 978-91-7623-537-9 (pdf)

© Yezi Huang 2015
Printed in Sweden by *Tryckeriet i E-huset*, Lund.
October 2015.

*To my parents
Hao and Manbing*

ℰ

to Ruoyang

Abstract

The fourth generation broadband (4G BB) concept aims for ubiquitous and high-speed data communication over the existing twisted copper pairs between the last distribution point and the customer premise equipment. Although it saves deployment cost for the last-mile communication, using the existing copper infrastructure makes the system vulnerable to crosstalk due to electromagnetic coupling from the neighboring pairs.

Crosstalk is frequency-dependent and its interfering effects vary with implementation scenarios. When exploring higher frequencies and more functionality for the copper-based infrastructure, new practical problems emerge which opens up a space of unknowns to be investigated. This thesis deals with crosstalk, its effects, its mitigation, and approaches to exploit it in emerging systems and applications. Dividing the frequency range into three bands and taking into account the respective architecture's characteristics, precoding schemes are proposed that properly process the crosstalk to improve end-users' quality of experience.

Chapters I–III of this thesis cope with sudden termination changes that significantly degrade the delivered throughput to active users when using a frequency range from 30 MHz to 180 MHz. A general model that interprets the changed coupling environment is presented and analyzed. Efficient precoder updating procedures are proposed for both linear and non-linear precoding systems which minimize the disturbed period to active end-users.

Chapter IV designs modified linear precoders for rate-boosting by utilizing strong crosstalk between 150 MHz and 300 MHz. Taking advantage of a common network topology in a novel way, the proposed precoding schemes can add a decent amount of extra data-rate to target end-user(s) on top of the normal precoding schemes.

Finally, Chapters V–VII revisit the frequencies below 30 MHz and investigate the potential of using the existing copper-based infrastructure as the analog fronthaul for small-cell densification of the mobile networks. An LTE-over-copper system is sketched and analyzed invoking 3GPP requirements. A

time-domain precoding scheme is proposed that performs channel estimation using carried LTE signals and yields an effective channel that is crosstalk-free and has identical direct paths.

Preface

This licentiate thesis is comprised of two parts. The first part gives an overview of the research field in which I have been working during my Ph.D. studies and a brief summary of my contribution to it. The second part is composed of the following submitted journal paper, patent application, and conference contributions:

- I. Yezi Huang, Thomas Magesacher, Eduardo Medeiros, Chenguang Lu, Per-Erik Eriksson, and Per Ödling, “Mitigating Disorderly Leaving Events in G.fast,” in *Proc. 2015 IEEE International Conference on Communications (ICC)*, London, U.K., June 2015.
- II. Yezi Huang, Thomas Magesacher, Eduardo Medeiros, Chenguang Lu, and Per-Erik Eriksson, “Mitigation Scheme for Disorderly Leaving Event in G.fast,” *Patent application*, September 2014.
- III. Yezi Huang, Thomas Magesacher, Chenguang Lu, and Per Ödling, “Fast Mitigation of Sudden Termination Changes in Wideband Wireline Systems,” submitted to *IEEE Transactions on Communications*.
- IV. Yezi Huang, Thomas Magesacher, Eduardo Medeiros, Chenguang Lu, Per-Erik Eriksson, and Per Ödling, “Rate-Boosting Using Strong Crosstalk in Next Generation Wireline Systems,” in *Proc. 2015 IEEE Global Communications Conference (GLOBECOM)*, San Diego, USA, December 2015.
- V. Yezi Huang, Eduardo Medeiros, Stefan Höst, Thomas Magesacher, Per-Erik Eriksson, Chenguang Lu, Per Ödling, and Per Ola Börjesson, “Enabling DSL and Radio on the Same Copper Pair,” in *Proc. 2015 IEEE International Conference on Communications (ICC)*, London, U.K., June 2015.

-
- VI. Yezi Huang, Eduardo Medeiros, Nilma Fonseca, Stefan Höst, Thomas Magesacher, Per-Erik Eriksson, Chenguang Lu, Per Ödling, and Per Ola Börjesson, “LTE over Copper – Potential and Limitations,” in *Proc. IEEE 26th Annual International Symposium on Personal, Indoor and Mobile Radio Communications (PIMRC)*, Hong Kong, China, September 2015.

 - VII. Yezi Huang, Eduardo Medeiros, Thomas Magesacher, Stefan Höst, Chenguang Lu, Per-Erik Eriksson, Per Ödling, and Per Ola Börjesson, “Time-Domain Precoding for LTE-over-Copper Systems,” submitted to *2016 IEEE International Conference on Communications (ICC)*, Kuala Lumpur, Malaysia.

Acknowledgements

“I am a Ph.D. student from Lund University stationed at Ericsson Research in Kista”—this is the most used introduction to my position. Thanks to this unique combination, I am exposed to the most relevant problems and have learnt loads from my academic and industrial colleagues. The outcome of this Licentiate thesis is the instantiation of the collective wisdom and assistance that I am very grateful for.

My deep gratitude goes first to my supervisor Thomas Magesacher who is knowledgeable, precise, encouraging and patient. Doing my master thesis with Thomas enlightened me on the way of conducting research, and later guided me to this Ph.D. position. Those countless and inspiring discussions ever since add considerably to my signal processing experience and lead to many meaningful results.

I am indebted to my co-supervisor Per Ödling who helps me tremendously in my scientific and personal development. He always provides important insights into research topics and the better ways to present ideas. Thanks to the brilliant “business lunch project” that links me to many competent people from all kinds of backgrounds.

I always appreciate my co-supervisor Per Ola Börjesson for generously sharing his technical expertise. His consistent enthusiasm and contributions to research continuously motivate the whole group.

My appreciation also extends to Eduardo Medeiros for the day-by-day discussions and for being such a good friend. Many thanks to my dear colleagues and friends Pernilla Schuber, Stefan Höst, Kaan Bür, Jens A Andersson in the broadband communication group of the department of Electrical and Information Technology for providing advice and support in many aspects of my work and life. As I started entirely as a rookie both in the DSL world and in the research group, their continuous help is invaluable.

As for Ericsson Research, I am particularly grateful to Henrik Almeida and his team in Small Cell Transport. Thanks for providing me with this precious working environment inside the group and being able to work closely with the

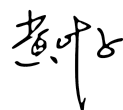
top-notch researchers and projects. Special thanks to Chenguang Lu and Per-Erik Eriksson for the insightful discussions and fruitful co-authorship. Thanks to Boris Dortschy and Miguel Berg for their time and patient instructions in the lab. And thanks to Jaume Rius i Riu, Antoni Fertner, Neiva Lindqvist, Keke Zu for sharing all kinds of knowledge and information with genuine kindness.

Thanks to Per and Per Ola's strong connections with industry, I obtain precious opportunities to meet and discuss with the insiders from BT, Orange, Deutsche Telekom, Alcatel-Lucent, ADTRAN, Telnet, Skipio, TNO and FTW. Thanks for sharing your expertise and experience. I acknowledge the support from Celtic-Plus and VINNOVA—the Swedish Governmental Agency for Innovation Systems for the HFCC/G.fast and GOLD projects, the European Horizon 2020 project Xhaul and the EXAM project of EIT Digital.

I am also grateful to Bogdan Timus, Sara Landström, Patryk Urban, Ning He, Fredrik Lindqvist, and Jiajia Chen for those inspiring lunch talks.

Many thanks to Fredrik Rusek, Victor Ufnarovski, Hui Li for giving inspiring Ph.D. lectures. Since I am mostly working from Stockholm, those course trips to Lund and special working needs would not have been possible without the administrative assistance from Pia Bruhn, Anne Andersson and Buon Kiong Lau. Thank you all for always being helpful.

I owe immeasurable gratitude to my parents, who are always caring and supportive. Thanks for letting me pursue my career in Sweden even if they preferred to have me stay close by. And finally, I acknowledge my husband Ruoyang for his love, understanding and support.



Yezi Huang
October 23, 2015

List of Acronyms and Abbreviations

eos	embedded operations channel
los	loss of signal
ACLR	adjacent channel leakage power ratio
ACS	adjacent channel selectivity
ASIC	application-specific integrated circuitry
BBU	baseband unit
CIR	channel impulse response
CO	central office
CP	customer premise
CPE	customer premise equipment
CRS	cell-specific reference signal
CWDD	column-wise diagonal dominant
DFT	discrete Fourier transform
DLE	disorderly leaving event
DMT	discrete multi-tone modulation
DP	distribution point
DPC	dirty paper coding

DSL	digital subscriber line
DSLAM	digital subscriber line access multiplexer
EVM	error vector magnitude
FDD	frequency-division duplexing
FEXT	far-end crosstalk
FIR	finite impulse response
FRN	FEXT-reflected-NEXT
FTTH	fiber-to-the-home
IF	intermediate frequency
IFFT	inverse fast Fourier transform
IIR	infinite impulse response
IRS	impulse response shortening
IRS	impulse response shortening filter
ISI	inter-symbol interference
LoC	LTE-over-copper
LP	linear precoder
MRC	maximum ratio combining
NEXT	near-end crosstalk
OLE	orderly leaving event
PLD	programmable logic device
PSD	power spectrum density
PSTN	public switched telephone network
RB	Resource Block
RE	Resource Element
RF	radio frequency

RMC	robust management channel
RN	reflected-NEXT
ROC	robust embedded operations channel
RRH	remote radio head
RRU	remote radio unit
SEM	spectrum emission mask
SNR	signal-to-noise ratio
SoC	system on chip
SSNR	shortening signal-to-noise ratio
STC	sudden termination change
TDD	time-domain duplex
THP	Tomlinson-Harashima precoder
UE	user equipment
VCE	vectoring control entity
VDSL2	very-high-bit-rate digital subscriber line

Contents

Abstract	v
Preface	vii
Acknowledgements	ix
List of Acronyms and Abbreviations	xi
Contents	xv
Introduction	1
I. Mitigating Disorderly Leaving Events in G.fast	9
1 Introduction	11
2 FEXT-Reflected-NEXT (FRN) Model for DLE	12
3 Residual Crosstalk Analysis	15
4 Proposed Residual-Crosstalk-Free Channel Estimation . . .	17
5 Simulation Results	20
6 Conclusion	24
II. Patent Application: Mitigation Scheme for Disorderly Leaving Event in G.fast	29
1 Technical Field	31
2 Background	31
3 Summary	32
4 Brief Description of the Drawings	33
5 Detailed Description	33
6 Claims	48

III. Fast Mitigation of Sudden Termination Changes in Wide-band Wireline Systems	57
1 Introduction	59
2 Wireline System Model	61
3 Residual Crosstalk Analysis	65
4 Precoder Update When Deactivating the Disruptive Line .	70
5 Precoder Update When (Re)Activating an Additional Line	78
6 Conclusion	84
IV. Rate-Boosting Using Strong Crosstalk in Next Generation Wireline Systems	89
1 Introduction	91
2 Channel Characteristics at High Frequencies	92
3 Maximum Ratio Combining (MRC) Precoding Scheme for Rate-Boosting	94
4 Optimized Precoding Scheme for Rate-Boosting	98
5 Conclusion	104
V. Enabling DSL and Radio on the Same Copper Pair	109
1 Introduction	111
2 Why and Where	112
3 Coexistence and Capacity	114
4 Band Placement with Fixed Filter Structure	118
5 Conclusion	121
VI. LTE over Copper – Potential and Limitations	127
1 Introduction	129
2 System Architecture	129
3 Uplink Path	131
4 Downlink Path	136
5 Design Implications	139
6 Conclusion	140
VII. Time-Domain Precoding for LTE-over-Copper Systems	145
1 Introduction	147
2 Precoding Architecture	148

3	Time-Domain Channel Estimation	150
4	Time-Domain Precoding	154
5	Conclusion	160

Introduction

1 Background

After almost 140 years of their debut, copper telephone wires are still playing an essential role in communication. Far beyond delivering analog vocal signals, as they were originally designed for, the copper wires have been exploited to provide various forms of service ranging from traditional computer network connections to data-rate-intensive applications such as cloud-based storage, HD video communication and next generation IPTV. The enabling technologies behind this evolution are generally referred to as digital subscriber line (DSL).

One major impairment of DSL systems comes from the crosstalk due to electromagnetic couplings between twisted wire pairs. According to different transeiving routes, the crosstalk is classified into near-end crosstalk (NEXT) and far-end crosstalk (FEXT). In DSL systems, NEXT can be effectively mitigated by duplexing schemes such as frequency-division duplexing (FDD) or time-division duplex (TDD), whereas FEXT is suppressed by vectoring [1, 2], as indicated in VDSL2 [3] and G.fast [4] standards.

As illustrated in Fig.1, both direct and FEXT couplings are highly frequency-dependent. While direct couplings are generally decreasing with increasing frequencies, FEXT shows different trends within different frequency ranges, which are categorized into three parts in this thesis.

For the frequencies below 30 MHz, FEXT increases with frequency. Within this range, the magnitude of FEXT is much smaller than signals received via direct paths, and it is where the prevailing xDSL systems operate.

When frequency extends up to 106 MHz, FEXT reaches its highest levels while the direct couplings keep on decreasing. As a result, the magnitudes of the two kinds of couplings become closer, but still keep a considerable gap in between. This frequency range corresponds to the band used by emerging wideband communication systems over short multi-pair copper cables such as the first version of G.fast.

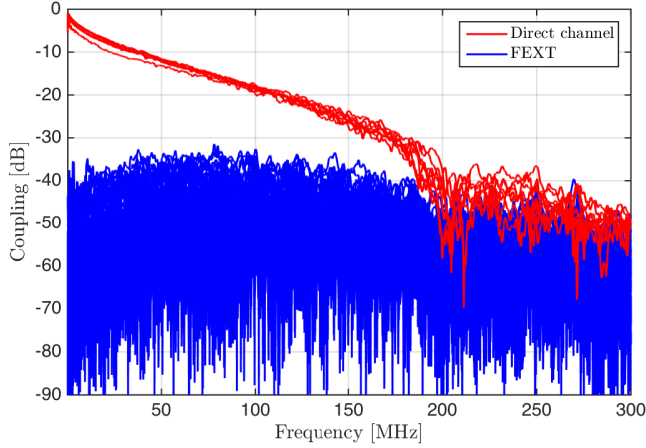


Fig. 1: Channel measurements for a 30-pair, 100-meter, 0.5 mm cable. $K = 8$ pairs are randomly picked from the same binder.

Considering a wideband discrete multi-tone modulation (DMT) system with a group of K twisted-pairs, the channel condition on each sub-carrier can be represented by a $K \times K$ matrix. The first two frequency categories below 106 MHz share the property that the channel matrix on each sub-carrier is diagonally dominant. Accordingly, a simple and effective linear diagonalizing precoder [5] can be used in the downstream direction to cancel out FEXT.

As the frequency goes beyond 106 MHz (up to 300 MHz in this thesis), the coupling magnitude of FEXT paths becomes comparable to that of the direct paths, which makes the diagonal dominance of channel matrices invalid. The performance of the traditional linear precoder degrades significantly due to a high normalization penalty. Non-linear precoder applying Tomlinson-Harashima precoding [6] is then conceived as an alternative.

2 Contributions of this Thesis

Based on the frequency range division illustrated above, the following content of this thesis is subdivided into three parts.

The first part studies a new practical issue observed above 30 MHz, which are the frequencies used in next generation wideband wireline systems, *e.g.*, G.fast. This issue is termed sudden termination change (STC), which leads to a disrupted vectoring operation and accompanying service interruption to

active end-users. Its influence within a vectored group is captured by a model, which further induces the proposed updating schemes at the distribution point (DP)-side.

- Chapters I and II deal with a typical STC case, namely disorderly leaving event (DLE) for the frequency range from 30 MHz to 106 MHz. A FEXT-reflected-NEXT (FRN) model is described for DLE with an ideal initial status, where all terminations at the customer premise equipment (CPE)-side are perfectly matched. Based on this model, a parameterized channel estimation is proposed for linear precoding systems, which reduces the estimation effort from $\mathcal{O}(K^2)$ to $\mathcal{O}(K)$. Compared to the state-of-the-art method, the period during which active users are disturbed is significantly reduced to just the time it takes to detect the DLE.
- Chapter III extends the model to cover a general STC scenario, and propose solutions for both deactivating and (re)activating STC events. Since the studied frequencies are also extended up to 180 MHz, the impact of an STC on both linear and non-linear precoding systems are analyzed. Low complexity precoder updating procedures are presented, which avoid full matrix inversion for the linear precoder and full matrix QR-decomposition for the non-linear precoder. The advantage of a minimized disturbed period for active users is also maintained for the extended scenarios.

The second part focuses on an even higher frequency range, from 150 MHz to 300 MHz. Since in this scenario FEXT couplings become comparable to the direct coupling, the FEXT paths can be exploited to support data transmission instead of being responsible for destructive crosstalk.

- Chapter IV exploits the strong crosstalk in a constructive manner on unused lines or in unused spectrum on neighboring lines to boost data-rate for active users. At the same time, the destructive crosstalk is effectively mitigated while the regulated spectral power limit per line is still fulfilled. Two linear precoding schemes, based on maximum ratio combining (MRC) and convex optimization respectively, are proposed which can deliver decent amount of additional data-rate to each active user compared to the normal linear precoding scheme.

The third part looks back to the frequencies used by currently operative DSL systems. The coexistence of LTE and DSL signals is investigated within this range to explore the potential of having the existing copper-based infrastructure serve as the analog fronthaul for rolling out small cells. The target is to deliver a relatively small amount but dedicated LTE data-rate to indoor mobile users over twisted copper pairs, which have already connected to a multitude of small cell deploying sites.

- Chapters V and VI discuss the bandplan for running LTE and DSL signals on the same copper pair, and the possible deploying distance from street cabinets to customer premises when invoking 3GPP requirements. The main target is to make the system architecture between remote radio unit (RRU) and remote radio heads (RRHs) transparent to mobile end-users. A “black-box” study on the overall in-band amplification and out-of-band suppression of the RRH is conducted for uplink and downlink respectively.
- Chapter VII deals with crosstalk cancellation for LTE signals in the downstream direction when transmitting over copper pairs. Since the LTE signal generated by the RRU is typically in time-domain, a time-domain precoding application is proposed, which cancels crosstalk and creates effective direct paths that are identical for all involved pairs.

References

- [1] ITU, “Self-FEXT cancellation (vectoring) for use with VDSL2 transceivers,” Recommendation ITU-T G.993.5, April 2010. [Online]. Available: <https://www.itu.int/rec/T-REC-G.993.5/en>
- [2] G. Ginis and J. Cioffi, “Vectored Transmission for Digital Subscriber Line Systems,” *IEEE Journal on Selected Areas in Communications*, vol. 20, no. 5, pp. 1085-1104, June 2002.
- [3] ITU, “Very high speed digital subscriber line transceivers 2 (VDSL2),” Recommendation ITU-T G.993.2, December 2011. [Online]. Available: <https://www.itu.int/rec/T-REC-G.993.2-201112-I/en>
- [4] ITU, “Fast Access to Subscriber Terminals - Physical Layer Specification,” Recommendation Draft ITU-T G.9701, 2014. [Online]. Available: <https://www.itu.int/rec/T-REC-G.9701/en>
- [5] R. Cendrillon, G. Ginis, E. Van den Bogaert, and M. Moonen, “A Near-Optimal Linear Crosstalk Precoder for Downstream VDSL,” *IEEE Transactions on Communications*, vol. 55, no. 5, pp. 860-863, May 2007.
- [6] G. Ginis and J. Cioffi, “A Multi-User Precoding Scheme Achieving Crosstalk Cancellation with Application to DSL Systems”, in *Proc. Conference Record of the Thirty-Fourth Asilomar Conference on Signals, Systems and Computers*, vol.2, pp. 1627-1631, October 2000.

Paper I

Mitigating Disorderly Leaving Events in G.fast

Abstract

Vectoring is a vital component of wideband wireline communication systems. A disorderly leaving event (DLE) disturbs the vectoring operation since the precoder, which was designed for the channel before the change, is no longer up to date. Measurements indicate that the impact of a DLE can be serious for frequencies beyond 30 MHz, which corresponds to the band used by emerging wideband communication systems over short multi-pair copper cables such as G.fast. As an alternative to the state-of-the-art update procedure, this paper presents an approach to mitigating the DLE problem. By interpreting DLE with the FEXT-reflected-NEXT (FRN) model, we propose a scheme that enables the showtime lines to return to disturbance-free transmission once the loss of signal on a certain line is detected while updating the precoder as a background process. Furthermore, the estimation complexity for a K -user vectoring group is reduced from $\mathcal{O}(K^2)$ to $\mathcal{O}(K)$.

Based on: Y. Huang, T. Magesacher, E. Medeiros, C. Lu, P.-E. Eriksson, and P. Ödling, "Mitigating Disorderly Leaving Events in G.fast," in *Proc. 2015 IEEE International Conference on Communications (ICC)*, London, U.K., pp. 939–944, June 2015. © 2015 IEEE. Reprinted with permission.

1 Introduction

The widespread deployment of cloud-based services and video-on-demand offerings continues to drive data rate and quality of service requirements for last-mile connections. In response to this trend, the wireline access industry advances towards a fiber to the last distribution point paradigm [1]. In this scenario, the recently consented G.fast standard [2] exploits shorter copper pairs and high bandwidth to provide up to around 1 Gbits/s aggregate net data rate.

Modern wideband wireline communication systems (such as G.fast) employ techniques referred to as vectoring [3] in order to cooperatively mitigate crosstalk. As vectoring relies on accurate channel information, changes of the terminating impedance in the multi-port wireline channel may cause severe performance degradation in terms of signal-to-noise ratio (SNR) as exemplified in Fig. 1. A change of impedance alters the perceived channel coupling conditions, and leads to residual crosstalk caused by an outdated precoder (or equalizer).

A particular event resulting in sudden termination change occurs when a modem *within* an active vectored group is turned off abruptly or is disconnected due to line disruption. This occurrence is called a disorderly leaving event (DLE), and was first reported during the development of vectored VDSL2 [3]. A fast channel tracking method was proposed in [4] to deal with DLEs in VDSL2. Unfortunately, it cannot be applied to G.fast since it is based on the assumption that only one column of the channel matrix changes.

In [5], a procedure is described that allows G.fast transceivers to leave a vectored group without negatively impacting the performance of other lines in the same bundle. The main idea is to allow coordination between transceivers at both ends, and acquire information necessary to update the precoder/equalizer before the line leaves and its termination impedance changes. While solving the problem of orderly leaving events, [5] does not address situations where there is no previous intent announced by the leaving transceiver(s).

This paper has two main contributions: First, we extend the model presented in [6, 7] to address DLEs, and identify the source of DLE disturbance that we can control. Second, we develop a novel precoder update procedure that does not disturb other lines while performing channel estimation as a background process.

The paper is organized as follows. In Section 2 a system model is presented to explain DLE. Taking advantage of this model, we formulate the DLE disturbance in Section 3 and propose in Section 4 a parameter-based channel estimation procedure that minimizes the impact of DLEs for the remaining active users. Section 5 demonstrates the effectiveness of the proposed method with channel measurements and simulations. Section 6 concludes the work.

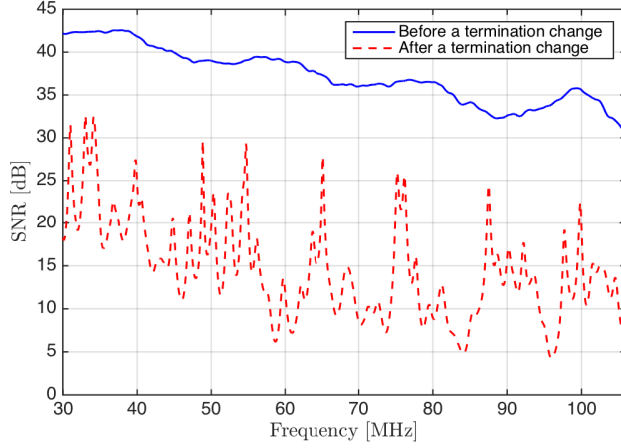


Fig. 1: SNR on one victim line before and after a termination change. The SNR drop represents the impact of a disrupted vectoring.

Notation: Bold capital letters (*e.g.*, \mathbf{A}) and bold lower-case letters (*e.g.*, \mathbf{a}) denote matrices and column vectors, respectively. $a_{i,j}$ is an element on the i -th row and j -th column of \mathbf{A} and a_i is the i -th element of \mathbf{a} . $\mathbf{I}_{n \setminus i}$ is an n -dimensional identity matrix excluding the i -th row. $\mathcal{M}_i\{\mathbf{A}\}$ denotes an operator deleting both the i -th row and column from \mathbf{A} . Operator “ \setminus ” excludes certain element(s) on the right-hand side from the set on the left-hand side.

2 FEXT-Reflected-NEXT (FRN) Model for DLE

Consider a wideband discrete multi-tone modulation (DMT) system with a group of K twisted pairs (or equivalently, users). The twisted pairs connect the transceivers at the distribution point (DP) with the customer premise equipment (CPE).

In [6, 7], a FEXT-reflected-NEXT (FRN) model is proposed to characterize the changed coupling condition due to an alien-line impedance mismatch at the CPE. A DLE is similar—except now the impedance change happens within the vectored group as illustrated in Fig. 2. Without loss of generality, we illustrate the DLE coupling model in downstream on a certain sub-carrier. Since G.fast employs time-division duplex (TDD), the model for downstream applies, *mutatis mutandis*, to upstream.

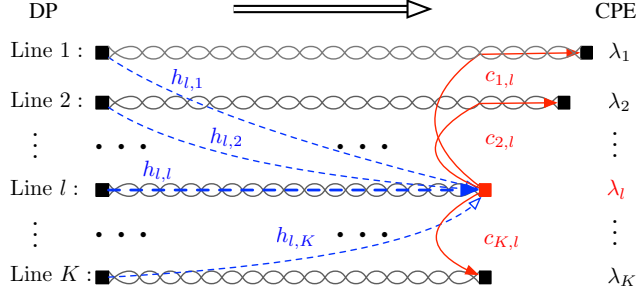


Fig. 2: Downstream FRN model. *Dash lines:* Channel paths from DP to the mismatched termination l . *Solid lines:* near-end coupling paths from the mismatched termination l to the remaining CPEs.

Let $\mathbf{H} \in \mathbb{C}^{K \times K}$ denote the frequency-domain channel matrix on a certain sub-carrier for the perfectly-terminated case, where diagonal and off-diagonal elements are direct-channel coefficients and far-end crosstalk (FEXT) coefficients, respectively. For the sake of simple notation, but without loss of generality, the sub-carrier index is omitted. Let $\mathbf{\Lambda} = \text{diag}([\lambda_1, \lambda_2, \dots, \lambda_K]) \in \mathbb{C}^{K \times K}$ denote a diagonal matrix with termination reflection coefficients and let $\mathbf{C} \in \mathbb{C}^{K \times K}$ denote the near-end crosstalk (NEXT) coupling matrix at the CPE-side. For scenarios with unequal pair-lengths, \mathbf{C} denotes attenuated NEXT (as illustrated in Fig. 2 for the l -th column of \mathbf{C}). The diagonal entries of \mathbf{C} , corresponding to the CPE-side echo coefficients, are assumed to be 0. The channel matrix \mathbf{H}' for the general case is

$$\mathbf{H}' = \mathbf{H} + \mathbf{\Delta},$$

where $\mathbf{\Delta} = \mathbf{C}\mathbf{\Lambda}\mathbf{H}$ quantifies the deviation from the all-terminated case according to the FRN model. When the terminations at the CPE are perfectly matched (*i.e.*, $\lambda_i = 0$ for $i = 1, \dots, K$), then $\mathbf{\Delta} = \mathbf{0}$ and thus $\mathbf{H}' = \mathbf{H}$.

Vectoring enables cooperative signal processing within the group. A properly designed precoder in downstream and equalizer in upstream at the DP significantly reduces FEXT. In this work, we focus on linear precoding and thus on the frequency range up to 106 MHz (cf. [2]). Specifically in downstream, let $\mathbf{G} = \text{diag}([g_1, g_2, \dots, g_K]) \in \mathbb{R}^{K \times K}$ denote a diagonal matrix with the gain adjusters for each line on the main diagonal. Assume that the cyclic prefix of DMT is not shorter than the impulse responses of the coupling paths. Furthermore, assume that the inverse fast Fourier transform (IFFT) for the group users is well synchronized. After including linear precoder \mathbf{P}_o , transmitting $\mathbf{x} \in \mathbb{C}^{K \times 1}$ at the DP-side yields the receive signal $\mathbf{y} \in \mathbb{C}^{K \times 1}$ given

by

$$\mathbf{y} = \mathbf{H}'\mathbf{P}_o\mathbf{G}\mathbf{x} + \mathbf{n},$$

where $\mathbf{n} \in \mathbb{C}^{K \times 1}$ denotes the background noise. An ideal precoder designed for \mathbf{H} at DP neutralizes the crosstalk effectively such that for the input symbols \mathbf{x}

$$\mathbf{H}\mathbf{P}_o\mathbf{G}\mathbf{x} = \mathbf{\Sigma}\mathbf{x}, \quad (1)$$

where $\mathbf{\Sigma} \in \mathbb{C}^{K \times K}$ is diagonal.

In practice, most often only one diagonal element of $\mathbf{\Lambda}$ will deviate significantly from 0 as a result of a DLE (*i.e.*, mismatch of a single line only). Assume line l exhibits a DLE, which is quantified by a reflection coefficient $|\lambda_l| \gg 0$. Consequently, $\mathbf{\Delta} \neq \mathbf{0}$ and all FEXT coupling coefficients change. The new FEXT arriving at termination k , ($k \neq l$) is determined by

$$(\mathbf{h}'_k)^T = \mathbf{h}_k^T + c_{k,l}\lambda_l\mathbf{h}_l^T,$$

where \mathbf{h}_l^T indicates the l -th row of \mathbf{H} , and $(\mathbf{h}'_k)^T$ is the k -th row of \mathbf{H}' . The outdated precoding with \mathbf{P}_o fulfilling Eq. (1) yields the disturbed receive signal

$$\mathbf{y}' = \underbrace{\mathbf{H}\mathbf{P}_o\mathbf{G}\mathbf{x} + \mathbf{n}}_{\mathbf{y}_d} + \underbrace{\mathbf{C}\mathbf{\Lambda}\mathbf{H}\mathbf{P}_o\mathbf{G}\mathbf{x}}_{\mathbf{\xi}}, \quad (2)$$

where \mathbf{y}_d is the desired receive signal obtained in the perfectly-terminated case and $\mathbf{\xi}$ is the residual crosstalk due to the DLE. Equivalently, the effective channel changes from \mathbf{H} to $\mathbf{H}' = \mathbf{H} + \mathbf{\Delta}$.

The FRN model described in [6, 7] suggests that FEXT arrives at and is reflected by the alien mismatched termination only. Compared to the alien-line case, in a DLE the leaving line is always active. As the direct path $h_{l,l}$ has a lower channel attenuation than the FEXT paths $h_{l,k}$, $k \in \{1, \dots, K\} \setminus l$, the residual-crosstalk issue in a DLE could be even worse.

We demonstrate the impact of a DLE on the channel coupling conditions by means of crosstalk-paths and direct-path measurements from a 30-pair, 100 m, 0.5 mm cable [8]. 10 pairs from a single binder were chosen at random. The measurement points follow a 51.75 kHz sub-carrier spacing, and we consider 2048 sub-carriers in total corresponding to the frequency range up to 106 MHz. The all-terminated case and a DLE-case where line $l = 10$ is left unterminated yield two 10×10 matrices \mathbf{H} and \mathbf{H}' respectively. The 10-th row of \mathbf{H}' is left the same as that of \mathbf{H} . The corresponding channel-matrix deviation is thus given by $\mathbf{\Delta} = \mathbf{H}' - \mathbf{H}$. We quantify the impact of this DLE on vectoring in terms of the worst residual crosstalk $\mathcal{P}_k^{\text{rx}}$ over all lines

$$\mathcal{P}_k^{\text{rx}} = \mathcal{P}^{\text{tx}} + 20 \log_{10}(\max_i |\delta_{i,k}|), \quad (3)$$

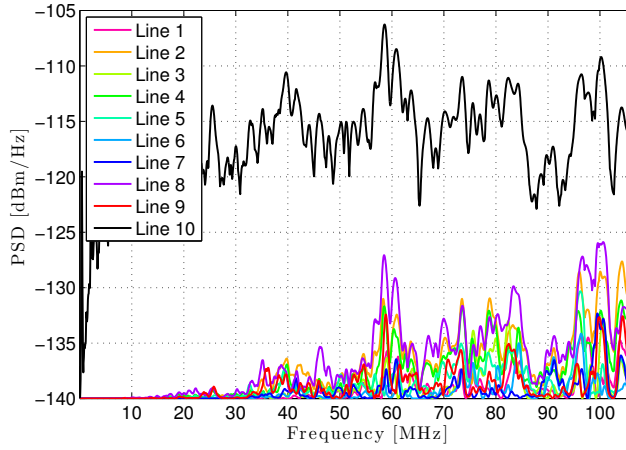


Fig. 3: Comparison of the strongest crosstalk caused by each column of Δ , when having a vectored group size of $K = 10$ and line $l = 10$ is leaving.

when line k is excited by a signal with transmit power spectrum density (PSD) \mathcal{P}^{tx} . In essence, Eq. (3) evaluates the maximum power of the k -th column of Δ .

Fig. 3 shows the crosstalk power for $\mathcal{P}^{\text{tx}} = -76$ dBm/Hz with respect to the background noise of -140 dBm/Hz. Clearly, the channel changes in the column $l = 10$ (black curve) are dominant, which is consistent with the assumption in [4]. However, channel changes in the other columns become disturbing for frequencies beyond 30 MHz. Except for the l -th row, every other entry of Δ contributes to the new channel \mathbf{H}' . Equivalently, almost every element of \mathbf{H} changes due to a DLE.

3 Residual Crosstalk Analysis

In downstream direction, changed channel coupling conditions result in an outdated precoder. Specifically, the linear precoder as in [9] defines

$$\mathbf{P}_o = \mathbf{H}^{-1} \mathbf{H}_\Sigma, \quad (4)$$

where the diagonal matrix \mathbf{H}_Σ contains direct channel coefficients of the all-terminated channel \mathbf{H} .

Consider the DLE case where line l leaves while all other lines are perfectly terminated. Thus, $\mathbf{\Lambda} = \text{diag}([0, \dots, 0, \lambda_l, 0, \dots, 0])$ and the resulting reflection-

followed-by-NEXT paths $\mathbf{C}\mathbf{\Lambda}$ are given by

$$\mathbf{C}\mathbf{\Lambda} = [\mathbf{0} \quad \dots \quad \mathbf{0} \quad \mathbf{v}_l \quad \mathbf{0} \quad \dots \quad \mathbf{0}], \quad (5)$$

where the reflecting crosstalk coefficients are defined in a vector as

$$\mathbf{v}_l = \lambda_l [c_{1,l}, \dots, c_{i,l}, \dots, c_{K,l}]^T. \quad (6)$$

According to Eq. (2), the residual crosstalk when using the outdated precoder \mathbf{P}_o is given by

$$\begin{aligned} \boldsymbol{\xi} &= \mathbf{C}\mathbf{\Lambda}\mathbf{H}\mathbf{P}_o\mathbf{G}\mathbf{x} \\ &= \mathbf{C}\mathbf{\Lambda}\mathbf{H}_\Sigma\mathbf{G}\mathbf{x}. \end{aligned} \quad (7)$$

Using Eq. (5), the expression (7) for the residual crosstalk simplifies to

$$\begin{aligned} \boldsymbol{\xi} &= \mathbf{v}_l h_{l,l} g_l x_l \\ &= \mathbf{v}_l \sigma_l x_l, \end{aligned} \quad (8)$$

where x_l is the l -th element of \mathbf{x} , and $\sigma_l = h_{l,l} g_l$ is the effective gain for path l .

Eq. (8) reveals that retaining the outdated precoder \mathbf{P}_o can eliminate the possible FEXT-reflected-NEXT components since the precoder keeps doing its job of mitigating/eliminating FEXT arriving at the reflective surface of termination l . The only source of the residual crosstalk $\boldsymbol{\xi}$ is the transmitted signal x_l on the leaving line via the l -th direct channel $h_{l,l}$ (see the bold dash line in Fig. 2), which is then reflected and couples to other CPEs via \mathbf{v}_l .

A traditional reaction to DLE, however, is to stop transmission on the leaving line as soon as possible, and quickly update the linear precoder at the DP to $\bar{\mathbf{P}}$ fulfilling

$$\mathcal{M}_l\{\mathbf{H}\} \bar{\mathbf{P}} \mathcal{M}_l\{\mathbf{G}\} = \mathcal{M}_l\{\boldsymbol{\Sigma}\}, \quad (9)$$

to diagonalize the dimension-reduced original channel $\mathcal{M}_l\{\mathbf{H}\}$. The FRN model implies that stopping transmission on the leaving line only avoids FEXT from line l (*i.e.*, the l -th column of \mathbf{H}), but does not avoid FEXT to line l (*i.e.*, the l -th row of \mathbf{H}). Instant update of the precoder to $\bar{\mathbf{P}}$ does not cancel FEXT through paths $h_{l,k}$ for $k \in \{1, \dots, K\} \setminus l$, which are then reflected at mismatched port and couple as NEXT to the victim lines resulting in residual crosstalk. Moreover, immediate line shutoff is sensitive to DLE false alarm or detection failure [4], which leads to unnecessary retraining of the transceivers.

In the upstream direction, the FRN model suggests that the leaving line l “emits” an unwanted upstream signal as a result of “incoming” NEXT being reflected by the mismatched port at the CPE side. The resulting upstream

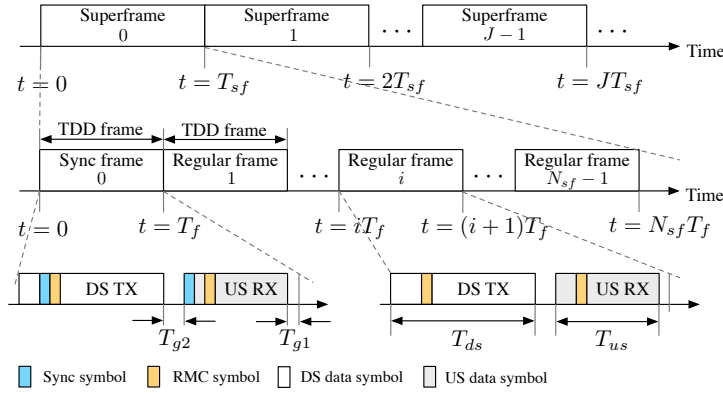


Fig. 4: G.fast TDD structure at the DP-side. Time gaps are reserved between paired down- and up-stream as T_{g2} and between upstream and next downstream as T_{g1} . The sum of the T_{g1} and T_{g2} equals to one DMT symbol duration.

FEXT through coupling into $k \in \{1, \dots, K\} \setminus l$ is taken care of by the interference canceler, whose coefficients are still correct for coupling paths from line l at the CPE to lines $k \in \{1, \dots, K\} \setminus l$ at the DP. The resulting upstream FEXT coefficients from lines $k \in \{1, \dots, K\} \setminus l$ into line l change and cause residual FEXT at the interference canceler output on line l , which is no problem since transmission on line l is interrupted anyway.

4 Proposed Residual-Crosstalk-Free Channel Estimation

A reference time-line for G.fast TDD frames is shown in Fig. 4. A typical TDD frame is $T_f = 750 \mu s$ long and consists of $N_f = 36$ DMT symbols. A superframe for this setting consists of $N_{sf} = 8$ TDD frames. The first frame of each superframe is a sync-frame, which contains one synchronization symbol located at a predefined symbol position in both directions. The sync-frame is then followed by 7 regular frames without synchronization symbols.

Assume that a DLE happens at time instant t_l at the CPE. In case t_l falls into a downstream transmission interval of the i -th TDD frame ($t_l \in [(i-1)T_f, (i-1)T_f + T_{ds}]$), the DP will detect this event during the next upstream transmission period ($t \in [(i-1)T_f + T_{ds} + T_{g2}, iT_f - T_{g1}]$). The DP initiates upstream channel tracking and in the next downstream transmission period and onwards ($t \geq iT_f$), it transmits *idle symbols* [2] at non-synchronization

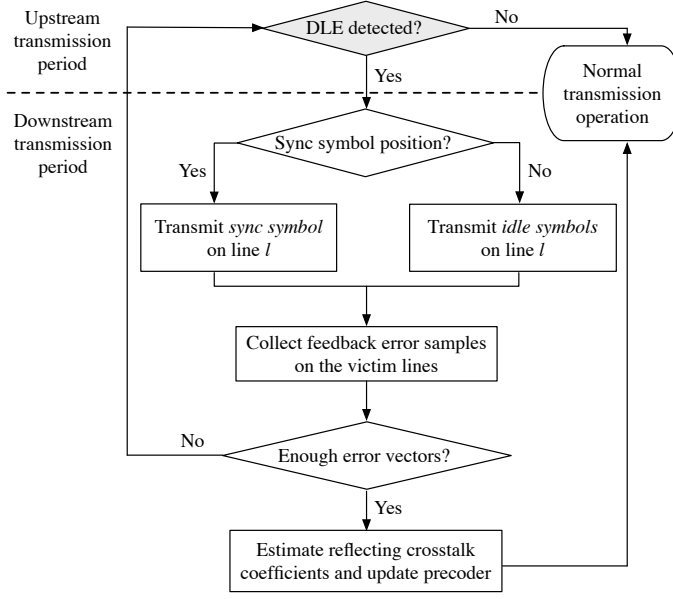


Fig. 5: Flowchart of proposed operation at the DP-side

symbol positions on the leaving line l . The main idea is to mute the data symbols on line l but keep transmitting the anti-crosstalk signals to cancel out FEXT arriving at the mismatched termination of line l at the CPE. According to the FRN model (cf. Fig. 2), there is thus no energy to cause reflections and subsequent NEXT into the other lines. A more detailed illustration for this special operation will be given below. If the DLE occurs during an upstream transmission interval, the channel tracking for upstream and “muting line l ” for downstream launch directly.

Generally, instead of turning off the leaving line immediately after detecting a loss of signal (*los*), channel estimation and precoder update in downstream direction is accomplished by alternating two kinds of special symbols: idle symbols and synchronization symbols (as illustrated in Fig. 5).

Silent mode By modifying the l -th gain adjuster to be $g_l = 0$ at non-synchronization symbol positions, idle symbols are transmitted on the leaving line. The residual crosstalk ξ in Eq. (8) on the victim lines becomes $\xi = \mathbf{v}_l h_{l,l} x_l \cdot 0 = 0$. It enables “silent” estimation and updating in the sense that active users remain undisturbed. Thus, we call this kind of transmission

mode *silent mode*. The DLE noisy period is at most $T_{ds} + T_{g2}$ before *los* on line l is detected.

Synchronization mode Synchronization symbols are transmitted every 6 ms (*i.e.*, one superframe duration) on each line in G.fast. Assume J superframes are required before the estimation is completed. Let t_j be the time instant to transmit the j -th downstream synchronization symbol. In this specific time slot, the l -th gain adjuster is set back to g_l , which is used for transmission before DLE. According to Eq. (1), Eq. (2) and Eq. (8), transmitting synchronization symbol $\mathbf{s}(t_j) = [s_1(t_j), \dots, s_l(t_j), \dots, s_K(t_j)]^T$ yields

$$\begin{aligned}\mathbf{q}(t_j) &= \mathbf{\Sigma}\mathbf{s}(t_j) + \mathbf{v}_l\sigma_l s_l(t_j) + \mathbf{n} \\ &= \mathbf{\Sigma}(\mathbf{s}(t_j) + \mathbf{e}(t_j)),\end{aligned}$$

where $\mathbf{e}(t_j) = \mathbf{\Sigma}^{-1}(\mathbf{v}_l\sigma_l s_l(t_j) + \mathbf{n})$. The synchronization error samples $\mathbf{I}_{K \setminus l}\mathbf{e}(t_j)$ on the victim lines are then fed back to the DP [2].

After sending the synchronization symbol at the scheduled time instant, the transmission on line l goes back to idle symbols for all non-synchronization symbol positions. Keep on alternatively sending idle symbols and synchronization symbols on the leaving line until DP collects J error symbols on the victim lines as

$$\begin{aligned}\mathbf{E} &= \mathbf{I}_{K \setminus l}[\mathbf{e}(t_1), \mathbf{e}(t_2), \dots, \mathbf{e}(t_J)] \\ &= \mathbf{I}_{K \setminus l}\mathbf{\Sigma}^{-1}\mathbf{v}_l\sigma_l\mathbf{s}_l^T + \mathbf{N},\end{aligned}$$

where $\mathbf{s}_l = [s_l(t_1), \dots, s_l(t_J)]^T$ is the synchronization sequence transmitted on the leaving line l at t_j ($j = 1, \dots, J$), and $\mathbf{N} \in \mathbb{C}^{(K-1) \times J}$ is the equalized additive noise on victim lines for J synchronization time instants. The contributing reflecting crosstalk coefficients in Eq. (6) can be estimated by

$$\hat{\mathbf{v}}_l = \frac{\mathcal{M}_l\{\mathbf{\Sigma}\}\mathbf{E}\mathbf{s}_l^* (\mathbf{s}_l^T \mathbf{s}_l^*)^{-1}}{\sigma_l}, \quad \hat{\mathbf{v}}_l \in \mathbb{C}^{(K-1) \times 1}, \quad (10)$$

where \mathbf{s}_l^* is the conjugate of \mathbf{s}_l . Although the full channel matrix of $\mathcal{M}_l\{\mathbf{H}\}$ is changed due to a single DLE, the estimation effort of the proposed method reduces from $(K-1)^2$ parameters to $K-1$ by modelling the changed coupling condition with reflecting crosstalk coefficients in \mathbf{v}_l .

During the whole process, the DP-side is still able to track the received signal power on line l . In case of, for example, a false alarm of DLE, no channel retraining is required and it is fast to get back to the normal transmission by a simple setting on g_l .

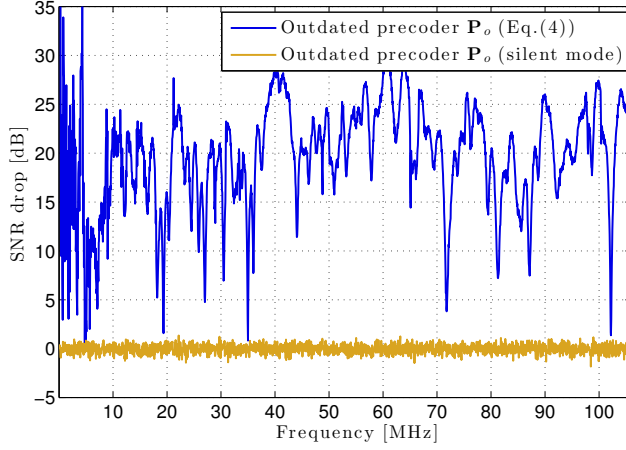


Fig. 6: SNR drop on victim line 1 after DLE, given full line transmission with the outdated precoder \mathbf{P}_o .

With \mathbf{v}_l estimated, the precoder can be updated for the new channel matrix $\mathcal{M}_l\{\mathbf{H}'\}$ according to the FRN model, *i.e.*,

$$\hat{\mathbf{P}} = \left(\mathcal{M}_l\{\mathbf{H}\} + \hat{\mathbf{v}}_l \mathbf{E}_l^T \mathbf{H} \mathbf{I}_{K \setminus l}^T \right)^{-1} \mathcal{M}_l\{\mathbf{H}'_\Sigma\}, \quad (11)$$

where \mathbf{E}_l is an elementary column vector with only 1 on the l -th position and 0s elsewhere.

5 Simulation Results

In order to evaluate the proposed scheme, we consider a vectoring system with $K = 3$ users operating on the 100 m-cable [8] introduced in Section 2. A DLE occurs on line $l = 3$. We use G.fast system parameters [2] and focus on the frequency-range up to 106 MHz. The special silent mode we propose in Section 4 is appraised in terms of SNR drop, introduced in Fig.1. We also compare our operation with the traditional method both in frequency and in time based on the PSD of the resulting residual crosstalk.

Fig.6 shows that the SNR drop caused by a DLE on the victim lines can be mitigated by setting the gain scaling factor of line l to zero, which would essentially solve the DLE problem. However, keeping the analog front-end running to send pure anti-crosstalk signals consumes power. If the line has

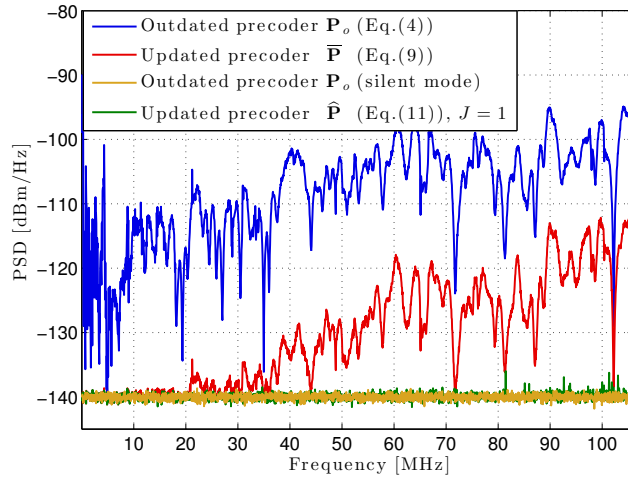


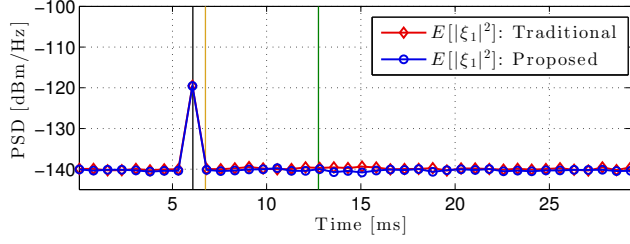
Fig. 7: Residual crosstalk in frequency after DLE on victim line 1.

already left, it is thus desirable to invoke the second mode in order to update the precoder for the new dimension-reduced channel $\mathcal{M}_l\{\mathbf{H}'\}$.

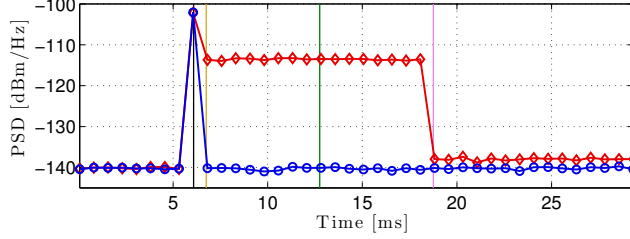
Fig. 7 presents the residual crosstalk PSD on one of the victim lines in the vectored group. By stopping transmission on the leaving line and updating the precoder to $\bar{\mathbf{P}}$ based on the dimension-reduced original channel $\mathcal{M}_l\{\mathbf{H}\}$ (*i.e.*, the traditional operation as defined by Eq. (9)), there is an improvement in SNR (comparing the second curve to the top one). However, the residual crosstalk power level is still far above the background noise level, especially for high frequencies where the crosstalk channel has a power level closer to that of the direct channel. Thus, further channel tracking is needed.

In contrast, both modes in our proposed operation suppress the residual crosstalk down to the background noise level throughout the studied frequency range. The victim lines are able to retrieve the residual-crosstalk-free transmission via the silent mode (yellow curve). With $J = 1$ synchronization symbol, the estimated precoder $\hat{\mathbf{P}}$ can effectively take care of the new channel matrix $\mathcal{M}_l\{\mathbf{H}'\}$ (green curve).

Assume no persistent detection of *los* requirement as in [3] is considered for now, and no signal processing time is counted in. Fig. 8 and Fig. 9 compare the residual crosstalk on a certain sub-carrier when the DLE happens at two extreme time slots (time instants indicated by the black line): Fig. 8 shows the longest time distance to the next synchronization symbol, and Fig. 9 presents the shortest time distance. The average residual crosstalk power on victim line



(a) Average residual crosstalk on a sub-carrier at 20 MHz



(b) Average residual crosstalk on a sub-carrier at 100 MHz

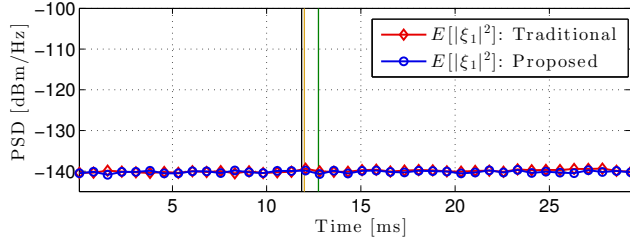
Fig. 8: Average residual crosstalk $E[|\xi_1|^2]$ in time on victim line 1 in downstream at the worst situation: DLE happens one symbol after the synchronization symbol during downstream transmission interval.

k is calculated over one frame on one sub-carrier as

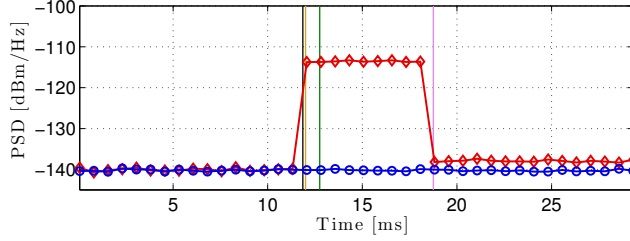
$$E[|\xi_k|^2] = \frac{1}{N_{ds}} \sum_{j=1}^{N_{ds}} |\xi_k(j)|^2,$$

where N_{ds} is the number of DMT symbols assigned to downstream transmission in one frame.

As indicated with different vertical time lines in Fig. 8 and Fig. 9, both the traditional and our proposed method deal with the DLE disturbance in two steps. Once los is detected, the first step is taken in the next frame (time instant marked by the yellow line). For the traditional method, the channel dimension is reduced and the precoder is updated to $\bar{\mathbf{P}}$. For our proposed method, the silent mode is activated by transmitting idle symbols on the leaving line. Both methods work well on low-frequency sub-carriers (*e.g.*, 20 MHz in Fig. 8a and Fig. 9a). However, on higher-frequency sub-carriers (*e.g.*, 100 MHz), $\bar{\mathbf{P}}$ is not adequate for crosstalk cancellation, as shown by the error plateau in Fig. 8b and Fig. 9b. Residual crosstalk severely disturbs the active users before enough



(a) Average residual crosstalk on a sub-carrier at 20 MHz



(b) Average residual crosstalk on a sub-carrier at 100 MHz

Fig. 9: Average residual crosstalk $E[|\xi_1|^2]$ in time on victim line 1 in downstream at the best situation: DLE happens one frame before the synchronization frame during upstream transmission interval.

error samples can be collected (time instant marked by the pink line) to proceed with a second step, aiming at a precoder update based on the acquired estimates. A traditional way is to perform an elementwise estimation of the dimension-reduced new channel $\mathcal{M}_l \{\mathbf{H}'\}$ using synchronization symbols and pilot sequences. When Hadamard sequences are applied, $2^{\lceil \log_2(K-1) \rceil}$ synchronization symbols are required to estimate $(K-1)^2$ channel matrix elements. For example, a single DLE in a vectored group of $K = 100$ would keep on disturbing the active users for at least $128 \times 6 = 768$ ms, and require an estimation of $99^2 = 9801$ entries for each sub-carrier.

The proposed operation, instead, keeps residual crosstalk close to the background noise level during and after the process of estimation and update (time instant marked by the green line), and makes the dimension-reducing operation unnoticeable. Once the DP is aware of the *los*, there is no more crosstalk disturbing the victim lines. Given persistently detected *los* on line l and accomplished estimation of the new channel matrix, it is safe then to completely remove line l from the vectored group.

It is worth noting that keeping the precoder the same as before the DLE

during channel estimation has three advantages. First, other active users in showtime are not disturbed, thanks to the silent mode. Second, it enables FRN-based modelling, which significantly reduces the estimation effort. A traditional method requires orthogonal synchronization sequences to estimate $(K - 1)^2$ channel coefficients, while our parameter-based method can exploit the synchronization symbols on line l as a unique reference for estimating the $K - 1$ reflecting coefficients only. Third, our estimation does not rely on the orthogonality property. The traditional method shows a slightly higher residual crosstalk-PSD level on severely impacted sub-carriers (cf. Fig. 8b and Fig. 9b), since the required orthogonality is degraded by background noise.

6 Conclusion

A sudden termination change due to a DLE alters the original channel matrix of a vectored group, which can have serious consequences for the vectoring operation. Based on the FRN model, we identify the sources and paths for residual crosstalk after the DLE and introduce a model that is parameterized by reflecting crosstalk coefficients. A procedure for channel estimation and precoder update in the downstream direction is proposed. Temporarily retaining the outdated precoder after a DLE narrows potential residual crosstalk paths down to only the direct channel of the leaving line. Compared to the state-of-the-art method, the period during which active users are disturbed can be significantly shortened to the time it takes to detect the loss of signal and the estimation complexity for a K -user system is reduced from $\mathcal{O}(K^2)$ to $\mathcal{O}(K)$.

References

- [1] P. Ödling, T. Magesacher, S. Höst, P. O. Börjesson, M. Berg, and E. Areizaga, "The Fourth Generation Broadband Concept," *IEEE Communications Magazine*, vol. 47, no. 1, pp. 62-69, January 2009.
- [2] ITU, "Fast Access to Subscriber Terminals - Physical Layer Specification," Recommendation Draft ITU-T G.9701, 2014. [Online]. Available: <https://www.itu.int/rec/T-REC-G.9701/en>
- [3] ITU, "Self-FEXT cancellation (vectoring) for use with VDSL2 transceivers," Recommendation ITU-T G.993.5, April 2010. [Online]. Available: <https://www.itu.int/rec/T-REC-G.993.5/en>

- [4] C. Lu and P.-E. Eriksson, "A Fast Channel Estimation Method for Disorderly Leaving Events in Vectored DSL Systems, in *Proc. 2011 IEEE International Conference on Communications (ICC)*, pp. 1-6, June 2011.
- [5] Alcatel-Lucent, "Influence of an Impedance Change on a Leaving Line onto the Direct and Crosstalk Channels of the Active Lines," ITU-T SG15 Contribution 2013-10-Q4-058, October 2013.
- [6] Futurewei Technologies, "G.fast: SNR Drop and FEXT Channel Variations due to Change of Alien Termination," ITU-T SG15 contribution 2013-10-q4-046, March 2013.
- [7] E. Medeiros, T. Magesacher, P. Ödler, D. Wei, X. Wang, Q. Li, P.-E. Eriksson, C. Lu, J. Boschma, and B. van den Heuvel, "Modeling Alien-Line Impedance Mismatch in Wideband Vectored Wireline Systems," *IEEE Communications Letters*, vol. 18, no. 9, pp. 1527-1530, September 2014.
- [8] Ericsson AB, *Access Network Pair cable, TEL 312*, 2010. [Online]. Available: <http://goo.gl/4RdCXc>
- [9] R. Cendrillon, G. Ginis, E. Van den Bogaert, and M. Moonen, "A Near-Optimal Linear Crosstalk Precoder for Downstream VDSL," *IEEE Transactions on Communications*, vol. 55, no. 5, pp. 860-863, May 2007.

Paper II

Patent Application: Mitigation Scheme for Disorderly Leaving Event in G.fast

Abstract

Vector Control Entity and method therein for Disorderly Leaving Events, DLEs, causing Sudden Termination Change in a DSL system. The method comprises, when a DLE occurs on a line l in a vectored group of DSL lines, and the transmission on line l is, at least partly, continued: obtaining at least one error sample from CPEs connected to other lines in the vectored group of DSL lines, and calculating an estimate of the channel coefficients, \mathbf{H}' , changed due to the DLE. The estimate is calculated based on the at least one error sample, and thus a channel estimate is provided. The method further comprises modifying a downstream precoder, based on the channel estimate, such that retraining of the other lines in the vectored group due to the DLE is avoided. The estimate of the channel coefficients is calculated based on the model $\mathbf{H}' = \mathbf{H} + \mathbf{CAH}$.

Based on: Yezi Huang, Thomas Magesacher, Eduardo Medeiros, Chenguang Lu, and Per-Erik Eriksson, "Mitigation Scheme for Disorderly Leaving Event in G.fast," *Patent application*, September 2014.

1 Technical Field

The invention relates to a method and an arrangement in a Digital Subscriber Line, DSL, system, in particular to the handling of Disorderly Leaving Events, DLE, in a DSL vectoring system.

2 Background

Vectoring technology cancels the FEXT (far-end crosstalk) between DSL lines, and therefore maximizes DSL system performance. Vectoring technology enables offering 100 Mbps per user with DSL lines *e.g.*, between the end of a fiber network and the Customer Premises Equipment, CPE.

The Telecommunication Standardization Sector of the International Telecommunication Union, ITU-T, has been standardizing a vectoring standard G.993.5 [1], and the first recommendation of G.993.5 was approved on April 22nd, 2010. The cancellation of the FEXT is done at the DSLAM (Digital Subscriber Line Access Multiplexer) side. The downstream FEXT is pre-cancelled by a precoder in the DSLAM, while the upstream FEXT is cancelled by an upstream crosstalk canceller in the DSLAM. The recommendation provides a way to estimate the FEXT channel in both downstream and upstream and utilize the estimated channel to cancel the crosstalk.

A Disorderly Leaving Event, DLE, which may alternatively be denoted *e.g.* Disorderly Shutdown Event, DSE, on a DSL line occurs *e.g.*, when a user unplugs the telephone cable or turns off the CPE abruptly. The disorderly shutdown of a DSL line may change the crosstalk channel characteristics, *i.e.* the crosstalk coupling to other lines, due to the impedance change at the CPE end which is disorderly shut down.

However, when using vectoring, the precoder in the DSLAM remains unchanged after a DLE and continues to be optimized for the original channel characteristics, *i.e.*, the channel characteristics before the DLE. This could result in a significant SNR (Signal to Noise Ratio) drop for other lines, since the precoder is outdated and thus cannot completely cancel the crosstalk from the line which is disorderly shut down. A DLE on one line can make other lines retrain. In VDSL2, retraining a line may take 30 seconds, which is a considerable interruption, *e.g.*, in IP-TV services. Even though the retrain time is significantly shorter in G.fast, it is still several seconds, which would still cause undesirable service interruption.

A method for handling DLEs is presented in [2], which is the work of two of the inventors of the present disclosure, and which is incorporated herein

by reference. According to this method, a partial channel estimate is derived after the DLE, and is combined with a channel estimate derived before the DLE. That is, a part of the original channel estimate, in form of a channel coefficient matrix, is replaced with a new estimate, *e.g.*, a column of the channel coefficient matrix. This method works very well for frequencies where the crosstalk between lines is within certain limits. However, when using higher frequencies for communication, such as in G.fast [3], the crosstalk between lines is larger, and thus all parts of the channel coefficient matrix are affected to a larger extent, even though the change in some parts may still be dominant. Measurements indicate that the impact of DLE is serious for frequencies around 30 MHz and beyond, which is of interest for G.fast.

Thus, there is a need for a fast method for estimating a channel, a channel tracking method, which works well also for higher frequencies.

3 Summary

An object of the invention is to provide a fast channel tracking mechanism for handling Disorderly Leaving Events, DLEs in DSL systems.

According to a first aspect, a method is provided for handling DLEs causing Sudden Termination Change, STC, in a DSL system. The method comprises, when a DLE occurs on a line l in a vectored group of DSL lines, and the transmission on line l is, at least partly, continued: obtaining at least one error sample from CPEs connected to other lines in the vectored group of DSL lines, and calculating an estimate of the channel coefficients, \mathbf{H}' , changed due to the DLE. The estimate is calculated based on the at least one error sample, and thus a channel estimate is provided. The method further comprises modifying a downstream precoder, based on the channel estimate, such that retraining of the other lines in the vectored group due to the DLE is avoided, and errors are also minimized. The estimate of the channel coefficients is calculated based on the model $\mathbf{H}' = \mathbf{H} + \mathbf{CAH}$.

According to a second aspect, a Vectoring Control Entity, VCE, is provided for handling DLEs causing Sudden Termination Change, STC, in a DSL system. The VCE is configured to: when a DLE occurs on a line l in a vectored group of DSL lines, and the transmission on line l is, at least partly, continued: obtain at least one error sample from CPEs connected to other lines in the vectored group of DSL lines, and further to calculate an estimate of the channel coefficients, \mathbf{H}' , changed due to the DLE, based on the at least one error sample, thus providing a channel estimate. The VCE is further configured to modify a downstream precoder, based on the channel estimate, such that retraining of the other lines in the vectored group due to the DLE is avoided and errors are

also minimized. The VCE is further configured to calculate the estimate of the channel coefficients based on the model $\mathbf{H}' = \mathbf{H} + \mathbf{CAH}$.

4 Brief Description of the Drawings

The foregoing and other objects, features, and advantages of the technology disclosed herein will be apparent from the following more particular description of embodiments as illustrated in the accompanying drawings. The drawings are not necessarily to scale, emphasis instead being placed upon illustrating the principles of the technology disclosed herein.

Fig. 1 shows a DS FEXT-reflected-NEXT model for OLE/DLE, where $\mathbf{H}(i, j)$ denotes the entry on the i -th row and j -th column of \mathbf{H} . Same notation is used for \mathbf{C} .

Fig. 2 illustrates G.fast TDD structure at VCE/DP/CO.

Fig. 3–4 illustrate procedures performed by a VCE/DP/CO, according to exemplifying embodiments.

Fig. 5–6 show a VCE/DP/CO according to exemplifying embodiments.

5 Detailed Description

Briefly described, a solution is provided for enabling a fast update of the precoder for after a sudden impedance change on a line termination. A fast channel estimation method is provided to fast track the channel change and quickly update the precoder accordingly. The fast channel estimation, or tracking, method utilizes a new model for estimating the channel, and is applicable for all frequencies used for DSL communication, also for higher frequencies around 30 MHz and beyond.

The solution described herein relates in particular to emerging wideband communication systems over multi-pair copper cables, such as the recently drafted standard ITU-T G.fast [3]. In general, it is distinguished between sudden impedance changes, caused by lines inside a vectoring group, hereinafter referred to as disorderly leaving lines, and outside a vectoring group, hereinafter referred to as alien-line termination changes. This invention focuses on the former, i.e. disorderly leaving lines, especially when occurring on the CPE side.

Tracking the channel according to the standardized state-of-the-art way, *i.e.*, relying solely on sync symbols and updating the entire channel matrix using the mechanisms described in the standard, causes far-end crosstalk (FEXT) for other users for a considerable amount of time, until the update is completed.

Modems that are suddenly, *i.e.*, without prior warning or preemptive actions, turned off, change their operating mode, or are disconnected due to line disruption, cause sudden changes of the termination impedance, which they present to a multi-port wireline channel. In the prior art, such events are often referred to as Disorderly Leaving Events, DLEs or Disorderly Shutdown Event, DSE, as stated previously. These terms will also be used herein for denoting such events. Another term which may be used herein to denote such events is Sudden Termination Changes, STCs. Any change in the termination impedance on one or more of the channels line(s) manifests itself as a change of a channel coefficient matrix. In general, a DLE alters all the coefficients of a channel matrix, and the changes increase with increasing frequencies. As previously mentioned, measurements indicate that the impact of DLE is serious for frequencies around 30 MHz and beyond.

Advanced wideband wireline communication systems employ signal coordination in order to mitigate crosstalk among lines. Corresponding techniques, referred to as vectoring, rely on accurate channel information. Sudden channel changes disturb the vectoring operation since a precoder, which was designed for the channel before the change, is no longer up to date. The mismatch may result in residual crosstalk causing a signal-to-noise ratio, SNR, drop that is beyond a reserved SNR margin and makes active end users suffer from packet errors and losses.

An exemplifying procedure according to an embodiment of the herein disclosed solution will be described below as comprising three parts, where at least b) is optionally performed in order to reduce interference to other lines in a vectored group.

- a) A DLE at the CPE side is detected by a power detector. Particularly if a CPE is unplugged in a DLE, the received power in upstream will go down to zero. In this case, a loss of signal will be detected. In a TDD system like G.fast, if a DLE happens at the CPE side during an upstream, US, slot, it may be detected in the same slot and counter measures (described in b) below) can be taken in the following downstream, DS, slot. If an STC happens during a DS slot, it may be detected in the next US slot and counter measures can be taken in the following DS slot. In a FDD system like VDSL2, the detection process starts as it happens.
- b) As soon as a DLE has been detected, the DS data signal intended to the disorderly leaving line i may be replaced by zeroes. That is, during data symbol slots, zeroes are transmitted. The precoder then generates a low-power “anti-crosstalk” signal that cancels the FEXT at the CPE port. In this case, on the disorderly leaving line, the direct signal intended to its own CPE is gone. On each victim line, the precompensated signal

associated with the direct signal of the disorderly leaving line is also gone, while the precompensated signals associated with the direct signal of all other victim lines are kept unchanged. Based on the FRN-model, which will be described below, there is no signal entering the port, thus there is no signal to be reflected and subsequently coupled via NEXT to the other ports—the other lines remain undisturbed during DS transmission. An alternative to sending zeroes is sending the DS data signal intended to the disorderly leaving line in a sufficiently low power.

- c) During synch-symbol slots, regular synch symbols, and not zeroes as in the data symbol slots, are transmitted, and a specific channel estimation scheme is employed. The scheme, which will be described below is based on the FRN model and reduces the complexity from estimating $(K - 1) \times K$ channel coefficients, *i.e.*, all changed coefficients, needed by the state-of-the-art approach to only $K - 1$ reflection coupling coefficients, in order to track all changed coefficients.

In step b), it has been realized by the inventors that it is advantageous to set the gain scaling factor of the leaving line to zero during the data symbols and other non-sync symbols after the detection of a DLE, or loss of signal on the line, while keeping the precoder coefficients unchanged, especially the coefficients on the columns associated with the victim lines. On the disorderly leaving line, only the direct signal intended to its own CPE is muted, while the precompensated signal from other lines to the disorderly leaving line is kept. On other lines, we keep transmitting both direct signals and the precompensated signals among these victim lines. Therefore, this operation does not stop the transmission on the leaving line completely. If the line is completely stopped, no signal would be present on the leaving line and the precompensated signal component from other lines to the leaving line would also disappear. Basically, the signals associated with the data symbols intended to the leaving line CPE are disappeared on all lines. It should be noted that data symbols here may include all non-sync symbols, if other symbols are also needed to be protected. In this document, we show mathematically and also experimentally via simulations that when using the suggested solution, there will be no residual crosstalk due to the mismatch of the outdated precoder and the changed channel. Note that in this step, the precoder is kept unchanged. At a DLE, the crosstalk channel changes are due to the reflected signals from the disconnected port of the leaving line to other lines. By keeping the original precoder, at least of the coefficients associated with the victim lines, no crosstalk signals from the victim lines will arrive at the disconnected port and thereby no crosstalk will be reflected. And the signal of the disorderly leaving line is also muted. No crosstalk is caused by the leaving line either. Therefore, no residual crosstalk

will be present in the system.

Although the method of muting the direct signal of the leaving line described above takes away the residual crosstalk at the CPE end, it may cause unnecessary erasures, *i.e.*, errors, on the leaving line in the case of a false detection of a DLE. If step b) above is not performed, and regular transmission is continued and step c) is performed directly, the fast tracking algorithm is very robust with false detections. However, step b) is easy to implement and also relax the time requirement for the fast tracking implementation. With step b), step c) can gain more time for the algorithm execution while not causing errors and therefore reduce the hardware complexity for fast tracking. As previously stated, the muting method is advantageous but optional. An alternative to the muting method/step b) is to continue the transmission on the leaving line as before the DLE. As explained above, the solution described herein would still be applicable. Note that during the transmission of sync symbols, the gain scaling factor of the leaving line is not set to zero. So, when applying an exemplifying embodiment comprising the muting method, the gain scaling factor may alternate between zero, or close to zero, and the original value during data symbols and sync symbols, respectively. In other words, during transmission of sync symbols, the gain scaling factor is equal to, or at least in parity with, the gain scaling factor used for transmission before the DLE; and during transmission in data symbol positions after the DLE, the gain scaling factor is set to zero, or at least close to zero. In principle, during sync symbols, gain scaling can be set to any non-zero number. When the non-zero number is known by the VCE/CO, the channel estimation can be resolved. However, using original value is of interest of practical implementation.

In order to update the precoder to match the channel after the DLE, it is necessary to track the channel change. The precoding coefficients of the other lines, *i.e.*, lines other than the leaving line, should be updated such that residual crosstalk is cancelled by the (updated) precoder when the transmission on the leaving line has been completely stopped. In this invention, the crosstalk channel change is modelled as the reflected crosstalk from the leaving line. Based on this model, a fast channel estimation method is proposed to estimate only the modelled reflected crosstalk coefficients, which are modelled as a vector with the elements of the number of other lines. The estimated elements of the vector are much fewer than that of a matrix. Thus, the channel change can be estimated with only one error sample report corresponding to one sync symbol, which is much faster than for a prior art conventional channel estimation scheme. For example, for 10 lines, a normal conventional channel estimation scheme needs the error samples of 16 sync symbols. Thus, the invented method is potentially much faster.

Method in a Vectoring Control Entity, VCE.

Below, examples of embodiments of a method performed by a VCE will be described with reference to Fig. 3–4. The method is suitable for handling DLE causing STC in a DSL system. The VCE is a function block which is operable to provide vectoring for a group of lines in a DSL system. Physically, the VCE may be; be comprised in Central Office, CO, or Distribution Point, DP. The VCE may be comprised in a DSLAM, connectable to wirelines in the DSL system. Usually, for a small system with a small number of lines, VCE is integrated in to a DSLAM. Alternatively, the VCE may be comprised in a node outside a DSLAM, which is often the case when the system is large and the VCE needs to coordinate multiple DSLAMs.

A method performed by a VCE is illustrated in Fig. 3. The network node determines 301 whether a DLE has occurred on a line in a vectored group of DSL lines. When a DLE occurs on a line l , at least one error sample is obtained 303 from Customer Premises Equipments, CPEs, connected to other lines in the vectored group of DSL lines. The transmission on line l , which may also be denoted *e.g.*, the leaving line, is at least partly continued after the DLE, which will be further described below. Further, an estimate is calculated 304, of the channel coefficients, \mathbf{H}' , changed due to the DLE. The estimate is calculated based on the obtained at least one error sample, thus providing a channel estimate. The method further comprises modifying 305 a downstream precoder, based on the channel estimate. The estimate of the channel coefficients is calculated based on the model $\mathbf{H}' = \mathbf{H} + \mathbf{C}\mathbf{A}\mathbf{H}$, where \mathbf{C} is a near-end crosstalk coupling matrix for the CPE end of the vectored group; \mathbf{A} is a diagonal matrix with the reflection coefficients, after the DLE, of the CPE-end of the cables associated with the vectored group; \mathbf{H} is a matrix with the channel coefficients before the DLE; and \mathbf{H}' is a matrix with the estimated channel coefficients after the DLE.

By performing the actions described above, retraining of the other lines in the vectored group due to the DLE on line l may be avoided, and errors are also minimized, which is very advantageous.

The error samples may be obtained by transmitting an error feedback request to the CPEs connected to the other lines in the vectored group. By “other lines” is here meant “other than line l ”. That is, the error samples may be received from the CPEs in response to such error feedback requests. Such requests may be transmitted to the CPEs over a robust management channel. In VDSL2, it is called robust embedded operations channel, ROC. In G.fast, it is called the Robust Management Channel (RMC). Such requests can also be transmitted to the CPEs over the embedded operations channel (eoc) without robustness enhancement.

Regarding the continued transmission on line l after the DLE, there are a few alternatives, of which two different are illustrated in Fig. 3. In one embodiment, the transmission is continued 302:1 on line l after the DLE just as it was before the DLE. That is, the transmission on line l is not changed in response to the detection of a DLE on line l . In another embodiment, the transmission on line l may be changed 302:2 in response to the DLE, in order to mitigate the interference subjected to the other lines during the channel tracking procedure. For example, in an embodiment comprising the alternative 302:2, the transmission of sync signals in sync symbol positions could be continued but the transmission of the direct signal in line l in data symbol positions on line l could be muted, *e.g.*, by setting a gain value to zero, which will be further described below. Other alternatives for the continued transmission are also possible, and considered to be encompassed by the present disclosure.

It should be noted that at a Disorderly Leaving Event, DLE, which is the case that is discussed herein (as opposed to orderly leaving event, OLE), there are two problems that arises related to the channel matrix. First, the channel matrix is fully changed, at least in certain frequency ranges, as a consequence of the DLE; and second, the channel matrix dimension is reduced, since a line is leaving. It should further be noted that it is fully possible that more than one line is subjected to a DLE. In the examples herein, in order to facilitate understanding, it is, however, assumed that only one line at a time exhibits an STC of a DLE.

As stated above, according to the invention, the change in the channel matrix is modelled as $\Delta = \mathbf{CAH}$. If assuming three lines, the channel matrix will be of the dimension 3×3 , and could be denoted \mathbf{H}_3 . The channel, or channel matrix, could then be described, after DLE, as $\mathbf{H}_{3,\text{DLE}} = \mathbf{H}_3 + \Delta_3$, where Δ_3 is the change

$$\Delta_3 = \mathbf{CAH}_3 + \begin{bmatrix} 0 & c_{12} & c_{13} \\ c_{21} & 0 & c_{23} \\ c_{31} & c_{32} & 0 \end{bmatrix} \begin{bmatrix} 0 & 0 & 0 \\ 0 & 0 & 0 \\ 0 & 0 & \lambda_3 \end{bmatrix} \mathbf{H}_3.$$

\mathbf{C} being a near-end crosstalk coupling matrix for the CPE end of the vectored group, as previously mentioned. The coefficients in this matrix are changed after the DLE, and are thus unknown when initiating the fast channel tracking described herein. $\mathbf{\Lambda}$ is a diagonal matrix with the reflection coefficients, after the STC, of the CPE-end of the cables associated with the vectored group, as previously mentioned. It is assumed here that all CPEs, except for the one subjected to a DLE, are perfectly matched to the lines. In this example with three lines, let line 3 be the leaving line. This means that there will be no reflection for lines 1 and 2, since the CPE impedance, alt. termination, is perfectly matched. Thus the reflection coefficients, on the diagonal of $\mathbf{\Lambda}$, are

zero for lines 1 and 2. However, for line 3, the DLE entails that the termination is no longer matched, and thus the reflection coefficient will not be zero, *i.e.*, $\lambda_3 \neq 0$. For example, if $\lambda_3 = 1$, the signal arrived at the disconnected port will be fully reflected back. Performing the matrix multiplication will give:

$$\begin{aligned} \Delta_3 = \mathbf{C}\Lambda\mathbf{H}_3 &= \begin{bmatrix} 0 & 0 & c_{13}\lambda_3 \\ 0 & 0 & c_{23}\lambda_3 \\ 0 & 0 & 0 \end{bmatrix} \mathbf{H}_3 = \begin{bmatrix} c_{13}\lambda_3 h_{31} & c_{13}\lambda_3 h_{32} & c_{13}\lambda_3 h_{33} \\ c_{23}\lambda_3 h_{31} & c_{23}\lambda_3 h_{32} & c_{23}\lambda_3 h_{33} \\ 0 & 0 & 0 \end{bmatrix} \\ &= \begin{bmatrix} c_{13} \\ c_{23} \\ 0 \end{bmatrix} \begin{bmatrix} h_{31} & h_{32} & h_{33} \end{bmatrix}. \end{aligned}$$

Above, it is seen that 6 channel coefficients have been changed in the channel matrix. In a normal tracking method, all these 6 coefficients need to be estimated. In our fast tracking method, a combined reflection coupling coefficient from port j to port i is defined $c_{ij}\lambda_j$, following the model above, to estimate the channel change Δ_3 . Thus, in this example, only two reflection coupling coefficients need to be estimated, *i.e.*, $c_{13}\lambda_3$ and $c_{23}\lambda_3$, since the original channel vector $[h_{31}, h_{32}, h_{33}]$ can be known, either stored in the memory or derived from the original precoder. These two reflection coupling coefficients can be derived from error samples obtained on lines 1 and 2 after the STC. Could alternatively be expressed as after the DLE. Since there are only two unknowns to solve in the equation system above, only one error sample from line 1 and line 2, respectively, will be needed to solve the equations. Then, the precoder can be updated accordingly to adapt to the channel change. Thus, the herein described fast tracking method is potentially much faster than a normal tracking scheme.

When the fast channel tracking is performed, the transmission on line 3 will eventually be stopped. The channel matrix will then have a reduced dimension, *i.e.*, 2×2 in this example. Denoting the 2×2 channel matrix after DLE $\mathbf{H}_{2,\text{DLE}}$:

$$\begin{aligned} \mathbf{H}_{2,\text{DLE}} &= \mathbf{H}_2 + \Delta_2 = \mathbf{H}_2 + \begin{bmatrix} c_{13}\lambda_3 h_{31} & c_{13}\lambda_3 h_{32} \\ c_{23}\lambda_3 h_{31} & c_{23}\lambda_3 h_{32} \end{bmatrix} \\ &= \mathbf{H}_2 + \begin{bmatrix} c_{13}\lambda_3 \\ c_{23}\lambda_3 \end{bmatrix} \begin{bmatrix} h_{31} & h_{32} \end{bmatrix}, \end{aligned}$$

where \mathbf{H}_2 is part of the original matrix \mathbf{H}_3 , *i.e.*, the channel matrix for the three lines before the DLE. Here, there are two cases depending on if step b) is implemented or not.

If step b) is not implemented, the precoder may first be updated by fast tracking to adapt to the change while the leaving line, *i.e.*, line 3, keeps transmitting until it is believed left already. During this time, the fast tracking

algorithm may be applied to estimate the channel and calculate the precoder accordingly for the reduced 2-lines system, *i.e.*, only line 1 and line 2. Then the leaving line stops its transmission totally while the precoder is updated with the calculated precoder coefficients simultaneously.

The transmission in data symbol positions on other lines than line l , before the DLE, comprises far-end crosstalk precompensation signals, including the precompensated signal from line l , and a direct signal of its own. After the DLE, the far-end crosstalk precompensation signal from line l may be stopped on the other lines, while the other signals are continued after the DLE, such that the reflection of cross-talk from the precompensated signal from line l on other lines become zero. In other words, the respective signals which precompensate cross-talk from line l on the other lines before the DLE, may be stopped after the DLE, when there is no cross-talk from line l if the direct signal of line l is stopped when step b is performed. As an alternative to stopping the respective precompensated signal from line l on the other lines, this signal could be reduced in power after the DLE, as compared to the power of the signal before the DLE. Herein, a “precompensated signal from line l ” is a signal which precompensates for crosstalk from line l . This signal may be generated by the precoder based on the direct signal on line l .

Below, an exemplifying procedure according to an embodiment of the herein disclosed solution will be described in more detail.

Consider a vectoring system with K lines, or users. For simplicity, analysis is performed on a certain sub-carrier and at a certain time instant. Signal transceiving in frequency-domain in downstream, DS, direction can be described independently as $\mathbf{y} = \mathbf{H}\mathbf{x} + \mathbf{n}$, where the transmit and receive signals are $\mathbf{x} \in \mathbb{C}^{K \times 1}$ and $\mathbf{y} \in \mathbb{C}^{K \times 1}$ respectively; the channel matrix seen by the vectored group is $\mathbf{H} \in \mathbb{C}^{K \times K}$, and additive background noise on the copper pairs is $\mathbf{n} \in \mathbb{C}^{K \times 1}$. The direct channel of each line locates on the diagonal of \mathbf{H} , whereas the FEXT composes its off-diagonal entries.

Vectoring enables the cooperative signal processing within the vectored group by configuring an appropriate precoder for the downstream and a crosstalk canceller, in upstream at the DP/CO to cancel FEXT. Specifically in DS, let $\mathbf{G} \in \mathbb{R}^{K \times K}$ denote a diagonal matrix with the gain adjuster, *i.e.*, gain scaling factor as stated before, for each line on the main diagonal, namely $\mathbf{G} = \text{diag}([g_1, g_2, \dots, g_K])$. After including precoding, \mathbf{P}_o , the transmitting of \mathbf{x} at DP/CO yields $\mathbf{y} = \mathbf{H}\mathbf{P}_o\mathbf{G}\mathbf{x} + \mathbf{n}$. An ideal precoder neutralizes crosstalk effectively such that for the input symbol \mathbf{x}

$$\mathbf{\Sigma}\mathbf{x} = \mathbf{H}\mathbf{P}_o\mathbf{G}\mathbf{x} \quad (1)$$

where $\mathbf{\Sigma}$ is a $K \times K$ diagonal matrix.

A DLE at the CPE side exhibits STC and changes the whole channel coupling environment. Equivalently, every entry of the matrix \mathbf{H} changes. Before further processed, the outdated precoder \mathbf{P}_o fails at anti-crosstalk and makes all receiving ends suffer from residual crosstalk.

By modelling the changed coupling condition with near-ends coupling coefficients, the estimation effort reduces from $(K-1)xK$ parameters to $K-1$. Fast estimation and adaption may further be supported by controlling the transmitted signal on the leaving line.

Specifically, let $\mathbf{\Lambda} \in \mathbb{C}^{K \times K}$ denote a diagonal matrix with the reflection coefficients of the CPEs, or rather of the CPE end of the cables in the vectored group, on the main diagonal, *i.e.*, $\mathbf{\Lambda} = \text{diag}([\lambda_1, \lambda_2, \dots, \lambda_K])$. The near-end coupling matrix $\mathbf{C} \in \mathbb{C}^{K \times K}$ describes the NEXT or attenuated NEXT at the CPE end, depending on the relative cable length, which is also illustrated in Fig. 1 for the l -th column of \mathbf{C} . When the terminations at the CPEs are perfectly matched, there will be no reflection, which gives the reflection coefficients $\lambda_i = 0$ for $i = 1, \dots, K$ ideally. Then, the CPE-near-end coupling matrix \mathbf{C} has no contribution on the whole coupling environment.

After a DLE, when the termination of one line in a vectored group has changed and is mismatched, one diagonal element of $\mathbf{\Lambda}$ will deviate significantly from 0. Assume line no. l exhibits an STC, which is quantified by that the reflection coefficient $\lambda_l \neq 0$. In this case, $\boldsymbol{\xi} = \mathbf{\Lambda}\mathbf{y} = \mathbf{\Lambda}\mathbf{H}\mathbf{P}_o\mathbf{G}\mathbf{x}$ is reflected by mismatched CPE termination. The reflected signal $\boldsymbol{\xi}$ couples back to the CPEs via \mathbf{C} , and adds

$$\boldsymbol{\delta} = \mathbf{C}\mathbf{\Lambda}\mathbf{H}\mathbf{P}_o\mathbf{G}\mathbf{x} \quad (2)$$

to the expected receive signal \mathbf{y} . So the received signal after DLE becomes

$$\begin{aligned} \mathbf{y}' &= \mathbf{y} + \boldsymbol{\delta} \\ &= \mathbf{H}\mathbf{P}_o\mathbf{G}\mathbf{x} + \mathbf{C}\mathbf{\Lambda}\mathbf{H}\mathbf{P}_o\mathbf{G}\mathbf{x} + \mathbf{n} \\ &= (\mathbf{I} + \mathbf{C}\mathbf{\Lambda})\mathbf{H}\mathbf{P}_o\mathbf{G}\mathbf{x} + \mathbf{n} \\ &= (\mathbf{H} + \mathbf{\Delta})\mathbf{P}_o\mathbf{G}\mathbf{x} + \mathbf{n}. \end{aligned} \quad (3)$$

Equivalently, the channel changes from \mathbf{H} to $\mathbf{H}' = \mathbf{H} + \mathbf{\Delta}$, where $\mathbf{\Delta} = \mathbf{C}\mathbf{\Lambda}\mathbf{H}$.

A near-optimal linear precoder has been proposed in the prior art as $\mathbf{P}_o = \mu\mathbf{H}^{-1}\mathbf{H}_\Sigma$, where $\mathbf{H}_\Sigma = \text{diag}(\text{diag}(\mathbf{H}))$ is the diagonal matrix of \mathbf{H} and the scaling factor $\mu = \max_i \|\mathbf{H}^{-1}\mathbf{H}_\Sigma\|_{\text{row } i}$. For example, assume $K = 3$ and

$l = 2$. The mismatched error in Eq. (2) is actually

$$\begin{aligned}
\boldsymbol{\delta} &= \mu \mathbf{C} \boldsymbol{\Lambda} \mathbf{H} \mathbf{H}^{-1} \mathbf{H}_{\Sigma} \mathbf{G} \mathbf{x} \\
&= \mu \begin{bmatrix} 0 & c_{12} & c_{13} \\ c_{21} & 0 & c_{23} \\ c_{31} & c_{32} & 0 \end{bmatrix} \begin{bmatrix} 0 & 0 & 0 \\ 0 & \lambda_2 & 0 \\ 0 & 0 & 0 \end{bmatrix} \mathbf{H}_{\Sigma} \mathbf{G} \mathbf{x} \\
&= \mu \begin{bmatrix} 0 & \lambda_2 c_{12} & 0 \\ 0 & 0 & 0 \\ 0 & \lambda_2 c_{32} & 0 \end{bmatrix} \begin{bmatrix} h_{11}g_1 & 0 & 0 \\ 0 & h_{22}g_2 & 0 \\ 0 & 0 & h_{33}g_3 \end{bmatrix} \begin{bmatrix} x_1 \\ x_2 \\ x_3 \end{bmatrix} \\
&= \mu \begin{bmatrix} 0 & \lambda_2 c_{12} & 0 \\ 0 & 0 & 0 \\ 0 & \lambda_2 c_{32} & 0 \end{bmatrix} \begin{bmatrix} h_{11}g_1x_1 \\ h_{22}g_2x_2 \\ h_{33}g_3x_3 \end{bmatrix} \\
&= \mu \lambda_2 \begin{bmatrix} c_{12} \\ 0 \\ c_{32} \end{bmatrix} h_{22}g_2x_2.
\end{aligned}$$

The above implies that, in the general case, the mismatched error can be written as:

$$\boldsymbol{\delta} = \mathbf{v}_l \mu h_{ll} g_l x_l, \quad (4)$$

where $\mathbf{v}_l = \lambda_l [c_{1l}, \dots, c_{Kl}]$.

The equation above reveals, and the inventors have realized, that the activating source of mismatched error $\boldsymbol{\delta}$ only comes from the transmit signal x_l on the leaving line via the l -th direct channel h_{ll} (see solid line in line l in Fig. 1), which is then reflected and couples to CPE receivers via \mathbf{v}_l , the reflection coupling vector of line l .

With the mismatched errors' source and paths targeted, we propose an operation as follows to accomplish changed channel estimation and precoder update while minimizing the disturbance to active end users.

A reference time-line for G.fast TDD frames is shown in Fig. 2. A typical TDD frame duration is $T_f = 750 \mu\text{s}$, corresponding to $N_f = 36$ symbol periods (T_s). Time gaps are reserved between paired DS and US as T_{g2} , and between US and next DS as T_{g1} . The number of TDD frames in one superframe, binding to $N_f = 36$, is $N_{sf} = 8$. The first frame of each superframe is specified as sync frame, which contains one sync symbol locating on predefined symbol position in both directions. The sync frame is then followed by 7 regular frames.

Consider a DLE at time instant t_l at a CPE connected to line l during the first superframe in Fig. 2, *i.e.*, $t_l \in [0, T_{sf}]$. If the DLE occurs during a DS transmission interval of the i -th TDD frame ($t_l \in [(i-1)T_f, (i-1)T_f + T_{ds}]$), the VCE/DP/CO will be notified about the event during next US transmission period ($t \in [(i-1)T_f + T_{ds} + T_{g2}, iT_f - T_{g1}]$). In the next DS transmission

period and onwards ($t > iT_f$), the VCE/DP/CO may transmit the *muted signal* on data symbol positions by controlling the gain adjuster g_l on the leaving line. The detailed illustration for this special operation will be given below. If a DLE occurs during an US transmission interval, the “muting” for DS may launch directly, if step b) is implemented.

According to current standard, the transmission on the leaving line is turned off immediately when a DLE is detected. However, according to the solution disclosed herein, the precoder is kept “outdated” as \mathbf{P}_o until estimation is completed if step b) is implemented. That is, the precoder, which is optimized for the channel as it was before the DLE, is kept also after the DLE, even though it then is outdated. The DS operation for new channel estimation, or “fast tracking”, may be accomplished by sending two kinds of special symbols: muted symbol and sync symbol. An exemplifying embodiment is illustrated in Fig. 4.

Specifically, by modifying the l -th gain adjuster to be $\hat{g}_l = \epsilon$ ($\epsilon \rightarrow 0$) at the data symbol positions, symbols are transmitted in what herein is denoted *muting mode*, *i.e.*, muted symbols are transmitted at non-sync symbol positions on the leaving line. The mismatched error δ in Eq. (4) adding on the victim lines becomes negligible as $\delta = \mathbf{v}_l \mu h_{ll} \epsilon x_l \rightarrow 0$ for $\epsilon \rightarrow 0$. This enables the whole process to be “silent” to active end users. Muted symbols can also be obtained by change the symbol constellation points to zeros or close to zeros in the QAM symbol encoder/mapper.

NOTE: in the G.fast standard, idle symbols are defined as:

10.2.1.7 Idle symbol encoding

For all sub-carriers of an idle symbol the symbol encoder shall generate a constellation point $X_i = 0, Y_i = 0$.

If precoding is enabled, transmission of an idle symbol may result in non-zero power at the U interface due to adding of FEXT pre-compensation signals from (k,n) reference point (see Figure 10-1).

If precoding is disabled, transmission of idle symbol results in zero power at the U interface. Therefore, in upstream direction transmission of idle symbol results in a quiet symbol period.

The idle symbols are equivalent to the muted symbols here if set the gain scaling factor to zero or set the symbol constellation points to zero. Here, the expression muted symbols is considered to also cover the alternative option of continuing to transmit the symbols, but at a very low power.

Sync symbols are transmitted every 6 ms, *i.e.*, one superframe duration, on each line in G.fast (c.f. Fig. 2). Assume that J superframes are required before the update is completed. Let t_j^{sc} be the time instant to transmit the

j -th DS sync symbol. On this specific time slot, the l -th gain adjuster is set back to g_l , which may be stored *e.g.*, in the bits-and-gains table assigned during initialization. A Sync vector $\mathbf{s}(t_j^{\text{sc}}) = [s_1(t_j^{\text{sc}}), \dots, s_l(t_j^{\text{sc}}), \dots, s_K(t_j^{\text{sc}})]^T$ is transmitted from DP/CO to CPEs. Accordingly, the received sync vector at CPE-end presents as

$$\begin{aligned} \mathbf{q}(t_j^{\text{sc}}) &= \mu \mathbf{H}_\Sigma \mathbf{G} \mathbf{s}(t_j^{\text{sc}}) + \mathbf{v}_l \mu h_{ll} g_l s_l(t_j^{\text{sc}}) + \mathbf{n} \\ &= \mu \mathbf{H}_\Sigma \mathbf{G} (\mathbf{s}(t_j^{\text{sc}}) + \mathbf{e}(t_j^{\text{sc}})), \end{aligned} \quad (5)$$

assigning $\mathbf{e}(t_j^{\text{sc}}) = \mathbf{G}^{-1} \mathbf{H}_\Sigma^{-1} (\mathbf{v}_l \mu h_{ll} g_l s_l(t_j^{\text{sc}}) + \mathbf{n}) / \mu$. The error samples of sync symbols $\mathbf{e}(t_j^{\text{sc}})$ on victim lines are then fed back to DP/CO.

After sending the sync symbol on scheduled time instants, the transmission on line l goes back to quasi-quiet symbols for all data symbol positions. The transmitter may keep on alternatively sending quasi-quiet symbols and sync symbols on the disorderly leaving line until DP/CO have collected a reasonable number of $\mathbf{e}(t_j^{\text{sc}})$ to do an elegant coupling vector estimation. Stack the error vectors collected without the l -th elements as:

$$\begin{aligned} \mathbf{E} &= \mathbf{I}_{K \setminus l}^{[r]} [\mathbf{e}(t_1^{\text{sc}}), \dots, \mathbf{e}(t_J^{\text{sc}})] \\ &= \mathbf{I}_{K \setminus l}^{[r]} \mathbf{G}^{-1} \mathbf{H}_\Sigma^{-1} \mathbf{v}_l \mu h_{ll} g_l \mathbf{s}_l^T + \mathbf{N}, \end{aligned} \quad (6)$$

where $\mathbf{I}_{K \setminus l}^{[r]}$ is an K -dimension identity matrix excluding the l -th row, $\mathbf{s}_l = [s_l(t_1^{\text{sc}}), \dots, s_l(t_J^{\text{sc}})]^T$, and $\mathbf{N} \in \mathbb{C}^{(K-1) \times J}$ is the equalized additive noise on victim lines for J sync time instants. By “victim lines” is meant the other lines in a vectored group except the disorderly leaving line. The estimation of \mathbf{v}_l can be done by

$$\hat{\mathbf{v}}_l = \frac{\mathcal{M}_l \{ \mathbf{H}_\Sigma \mathbf{G} \} \mathbf{E} (\mathbf{s}_l^H \mathbf{s}_l)^{-1} \mathbf{s}_l^H}{\mu h_{ll}}, \quad \hat{\mathbf{v}}_l \in \mathbb{C}^{(K-1) \times 1}, \quad (7)$$

where $\mathcal{M}_l \{ \cdot \}$ is a dimension reducing function by excluding the i -th column and row.

When the coupling vector \mathbf{v}_l is estimated and the whole channel matrix change is derived accordingly, the DP (or CO) may update the precoder based on the channel matrix change and may shut down the transmission on the leaving line completely.

It should be noted that the same scheme as presented above works and may be applied also for the non-linear Tomlinson-Harashima precoder, which will be used in G.fast phase 2 supporting up to 212 MHz in frequency.

The fast channel estimation described herein is different from the one described in [2]. With a deeper understanding regarding the mechanism what

exactly causes the channel change, the new method explicitly estimates the reflected crosstalk coefficients which cause the channel changes and then calculate the channel change. This is especially important in high frequencies for G.fast use, where the whole channel matrix changes due to a DLE. The previous method described in [2] actually is an approximate of the new method described herein. In low frequencies, the changes in other columns are much smaller than the column associated with the leaving line. Thus, for certain frequencies, e.g. VDSL2 frequency range, the method in [2] works sufficiently well by estimating the dominant column changed and neglecting other columns. However, the changes in other columns get closer in magnitude to the column associated with the leaving line in higher frequency, where the crosstalk level gets closer to the direct channel. In other words, the dominance of the leaving column decreases over frequencies. Therefore, the performance of the pervious method described in [2] degrades over frequencies. The new method significantly improves the previous method in higher frequencies, and is a complete solution, which covers both low and high frequencies.

Hardware Implementations

The techniques and processes described above can be implemented in a network node which is operable to provide vectoring for a group of lines in a DSL system. As previously mentioned, the node may be denoted Vectoring Control Entity, VCE, and may be comprised in a CO or a DP. Fig. 5 is a schematic illustration of an exemplifying embodiment of a VCE 500 in which a method embodying any of the presently described techniques can be implemented. A computer program for controlling the VCE 500 to carry out a method embodying the present invention is stored in a program storage 504, which comprises one or several memory devices. Data used during the performance of a method embodying the present invention may also be stored in the program storage 504, or a separate data storage, which also may comprise one or more memory devices. During performance of a method embodying the present invention, instructions 505, such as program steps may be fetched from the program storage 504 and be executed by processing means 503, such as a Central Processing Unit, CPU, or other processor. Output information resulting from performance of a method embodying the present invention can be stored back in a data storage, or, be sent to an Input/Output (I/O) interface, which includes a network interface for sending and receiving data to and from other network nodes and which may also include a radio transceiver for communicating with one or more terminals. The VCE 500 is associated with the same technical features, objects and advantages as the previously described method embodiments. The VCE is described in brief in order to avoid unnecessary repetition.

The part of the network node 500 which is most affected by the adaptation to the herein described solution is illustrated as an arrangement 501, surrounded by a dashed line. The further functionality 506 illustrated in Fig. 5 may be assumed to carry out regular VCE and/or node functions.

Thus, when an DLE occurs on a line l in a vectored group of DSL lines, and the transmission on line l is, at least partly, continued, the execution of the instructions 505 by the processing means 503 causes the VCE 500 to obtain at least one error sample from CPEs connected to other lines in the vectored group of DSL lines, and to calculate an estimate of the channel coefficients, \mathbf{H}' , changed due to the DLE, based on the at least one error sample. The execution of the instructions further causes the VCE to modify a downstream precoder, based on the channel estimate. The estimate of the channel coefficients is calculated based on the model $\mathbf{H}' = \mathbf{H} + \mathbf{CAH}$, as previously described in detail.

The execution of the instructions may further cause the VCE to configured to continue the transmission of sync symbols on line l after the DLE. As previously described, the transmission in data symbol positions on line l before the DLE comprises a far-end crosstalk precompensation signal and a direct signal. The execution of the instructions may cause the VCE to continue the transmission of the far-end crosstalk precompensation signal after the DLE, and further to transmit the direct signal on line l with reduced power after the DLE, as compared to before the DLE.

The execution of the instructions may further cause the VCE to obtain at least one error sample from the CPE of at least one other line in the vectored group, and further to send at least one error feedback request over the embedded operations channel (eoc) in both VDSL2 and G.fast or over a robust embedded operations channel, ROC, in VDSL2, or over a robust management channel, RMC, in G.fast, in order to collect one or more error samples.

An alternative implementation of the network node 500 is shown in Fig. 6. The VCE 600 or arrangement 601 comprises an obtaining unit 602, configured to obtain at least one error sample from CPEs connected to other lines in the vectored group of DSL lines. The VCE 600 further comprises a calculating unit 604, configured to calculate an estimate of the channel coefficients, \mathbf{H}' , changed due to the DLE, based on the at least one error sample, thus providing a channel estimate. The VCE 600 further comprises a modifying unit 605, configured to modify a downstream precoder, based on the channel estimate. The arrangement 601 could further comprise a determining or detecting unit 602, configured to detect the occurrence of an DLE on a line in the vectored group. Alternatively, this detection could be regarded as a part of the standard functionality 607.

The VCE described above could comprise further units or modules config-

ured for the different method embodiments described herein.

The units or modules in the arrangements in the respective different network node embodiments and wireless device embodiments described above could be implemented *e.g.*, by one or more of: a processor or a microprocessor and adequate software and memory for storing thereof, a Programmable Logic Device (PLD) or other electronic component(s) or processing circuitry configured to perform the actions described above, and illustrated *e.g.*, in Fig. 5. That is, the units or modules in the arrangements in the different nodes described above could be implemented by a combination of analog and digital circuits, and/or one or more processors configured with software and/or firmware, *e.g.*, stored in a memory. One or more of these processors, as well as the other digital hardware, may be included in a single application-specific integrated circuitry, ASIC, or several processors and various digital hardware may be distributed among several separate components, whether individually packaged or assembled into a system-on-a-chip, SoC. The VCE could be implemented as a computer program, *e.g.*, a software module, which is run on a node which is operable to communicate with and/or control at least parts of the DLE system. Such a node may be located locally, near the DSL lines, or remote, such as in a distributed system, *e.g.*, a cloud solution.

When using the word “comprise” or “comprising” it shall be interpreted as non-limiting, *i.e.*, meaning “consist at least of”.

It should also be noted that in some alternate implementations, the functions/acts noted in the blocks may occur out of the order noted in the flowcharts. For example, two blocks shown in succession may in fact be executed substantially concurrently or the blocks may sometimes be executed in the reverse order, depending upon the functionality/acts involved. Moreover, the functionality of a given block of the flowcharts and/or block diagrams may be separated into multiple blocks and/or the functionality of two or more blocks of the flowcharts and/or block diagrams may be at least partially integrated. Finally, other blocks may be added/inserted between the blocks that are illustrated, and/or blocks/operations may be omitted without departing from the scope of inventive concepts. Moreover, although some of the diagrams include arrows on communication paths to show a primary direction of communication, it is to be understood that communication may occur in the opposite direction to the depicted arrows.

Modifications and other embodiments of the disclosed invention will come to mind to one skilled in the art having the benefit of the teachings presented in the foregoing descriptions and the associated drawings. Therefore, it is to be understood that the invention is not to be limited to the specific embodiments disclosed and that modifications and other embodiments are intended to be included within the scope of this disclosure. Although specific terms may be

employed herein, they are used in a generic and descriptive sense only and not for purposes of limitation.

It is to be understood that the choice of interacting units, as well as the naming of the units within this disclosure are only for exemplifying purpose, and nodes suitable to execute any of the methods described above may be configured in a plurality of alternative ways in order to be able to execute the suggested procedure actions.

It should also be noted that the units described in this disclosure are to be regarded as logical entities and not with necessity as separate physical entities.

While the embodiments have been described in terms of several embodiments, it is contemplated that alternatives, modifications, permutations and equivalents thereof will become apparent upon reading of the specifications and study of the drawings. It is therefore intended that the following appended claims include such alternatives, modifications, permutations and equivalents as fall within the scope of the embodiments.

6 Claims

1. A method performed by a Vectoring Control Entity, VCE, for handling Disorderly Leaving Event, DLE, causing Sudden Termination Change, STC, in a Digital Subscriber Line, DSL, system, the method comprising:
when a DLE occurs on a line l in a vectored group of DSL lines, and the transmission on line l is, at least partly, continued:
 - obtaining (104) at least one error sample from Customer Premises Equipments, CPEs, connected to other lines in the vectored group of DSL lines,
 - calculating (108) an estimate of the channel coefficients, \mathbf{H} , changed due to the DLE, based on the at least one error sample, thus providing a channel estimate, and
 - modifying (110) a downstream precoder, based on the channel estimate, such that retraining of the other lines in the vectored group due to the DLE is avoided,
wherein the estimate of the channel coefficients is calculated based on the model $\mathbf{H}' = \mathbf{H} + \mathbf{C}\mathbf{\Lambda}\mathbf{H}$, where
 - \mathbf{C} is a near-end crosstalk coupling matrix for the CPE end of the vectored group;
 - $\mathbf{\Lambda}$ is a diagonal matrix with the reflection coefficients, after the DLE, of the CPE-end of the cables associated with the vectored group;
 - \mathbf{H} is a matrix with the channel coefficients before the DLE; and

\mathbf{H}' is a matrix with the estimated channel coefficients after the DLE.

2. The method according to claim 1, wherein the transmission of sync symbols on line l is continued after the DLE.
3. The method according to claim 1 or 2, wherein the transmission in data symbol positions on line l before the DLE comprises a far-end crosstalk precompensation signal from other lines and a direct signal of line l , and wherein the far-end crosstalk precompensation signal is continued after the DLE, such that the reflection of cross-talk from the other lines remains cancelled at the CPE end of line l .
4. The method according to claim 3 wherein the direct signal transmitted on line l is reduced in power after the DLE, as compared to before the DLE.
5. Method according to any of the preceding claims, further comprising applying one or more of the following for data symbol positions on line l after the DLE:
 - setting a gain scaling factor to zero, or close to zero;
 - setting symbol constellation points to zero, or close to zero, in a symbol encoder.
6. The method according to any of the preceding claims, wherein the transmission in data symbol positions on other lines than line l before the DLE comprises far-end crosstalk precompensation signals, including the precompensated signal from line l , and a direct signal of its own, and wherein the far-end crosstalk precompensation signal from line l is stopped on the other lines, while the other signals are continued after the DLE.
7. The method according to claim 6 wherein the far-end crosstalk precompensation signal from line l on other lines is reduced in power after the DLE, as compared to before the DLE.
8. The method according to any of the preceding claims, wherein the obtaining of error samples comprises sending at least one error feedback request over either the embedded operations channel (eoc) in both VDSL2 and G.fast or a robust embedded operations channel, ROC, in VDSL2, or a robust management channel, RMC, in G.fast.
9. Vectoring Control Entity, VCE, for handling Disorderly Leaving Event, DLE, causing Sudden Termination Change, STC, in a Digital Subscriber Line, DSL, system, the VCE being configured to:

when a DLE occurs on a line l in a vectored group of DSL lines, and the transmission on line l is, at least partly, continued:

- obtain at least one error sample from Customer Premises Equipments, CPEs, connected to other lines in the vectored group of DSL lines,
- calculate an estimate of the channel coefficients, \mathbf{H}' , changed due to the DLE, based on the at least one error sample, thus providing a channel estimate, and
- modify a downstream precoder, based on the channel estimate, such that retraining of the other lines in the vectored group due to the DLE is avoided,

wherein the VCE is further configured to calculate the estimate of the channel coefficients based on the model $\mathbf{H}' = \mathbf{H} + \mathbf{CAH}$, where \mathbf{C} is a near-end crosstalk coupling matrix for the CPE end of the vectored group;

\mathbf{A} is a diagonal matrix with the reflection coefficients, after the DLE, of the CPE-end of the cables associated with the vectored group;

\mathbf{H} is a matrix with the channel coefficients before the DLE; and

\mathbf{H}' is a matrix with the estimated channel coefficients after the DLE.

10. The Vectoring Control Entity, VCE, according to claim 9, being configured to continue the transmission of sync symbols on line l after the DLE.
11. The Vectoring Control Entity, VCE, according to claim 9 or 10, wherein the transmission in data symbol positions on line l before the DLE comprises a far-end crosstalk precompensation signal from other lines and a direct signal of line l , and the VCE is configured to continue the transmission of the far-end crosstalk precompensation signal after the DLE, such that the reflection of cross-talk from the other lines remains cancelled at the CPE end of line l .
12. The Vectoring Control Entity, VCE, according to claim 11, being configured to transmit the direct signal on line l with reduced power after the DLE, as compared to before the DLE.
13. The Vectoring Control Entity, VCE, according to any of claims 9-12, being configured to apply one or more of the following for data symbol positions on line l after the DLE:
 - setting a gain scaling factor to zero, or close to zero;

-setting symbol constellation points to zero, or close to zero, in a symbol encoder.

14. The Vectoring Control Entity, VCE, according to any of claims 9-13 wherein the transmission in data symbol positions on other lines than line l before the DLE comprises far-end crosstalk precompensation signals, including the precompensated signal from line l , and a direct signal of its own, and wherein the VCE is configured to stop the far-end crosstalk precompensation signal from line l on the other lines, while other signals are continued after the DLE.
15. The Vectoring Control Entity, VCE, according to claim 14, being configured to reduce the far-end crosstalk precompensation signal from line l on other lines in power after the DLE, as compared to before the DLE.
16. The Vectoring Control Entity, VCE, according to any of claims 9-15, wherein the obtaining of error samples comprises sending at least one error feedback request over either the embedded operations channel (eoc) in both VDSL2 and G.fast or a robust embedded operations channel, ROC, in VDSL2, or a robust management channel, RMC, in G.fast.
17. Digital Subscriber Line Access Multiplexer comprising a VCE according to any of claims 9-16.

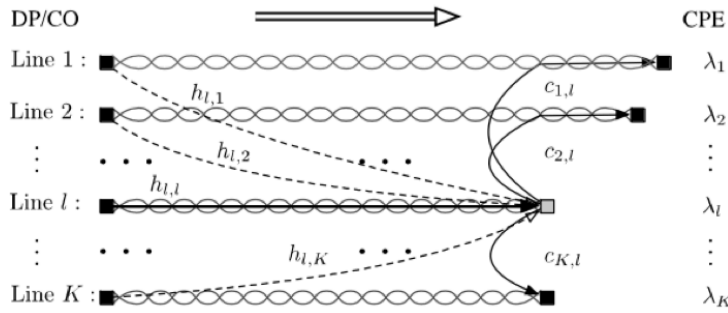


Fig. 1

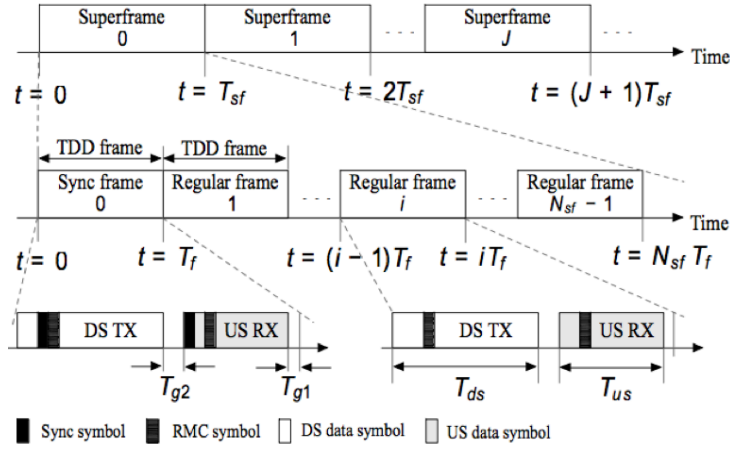


Fig. 2

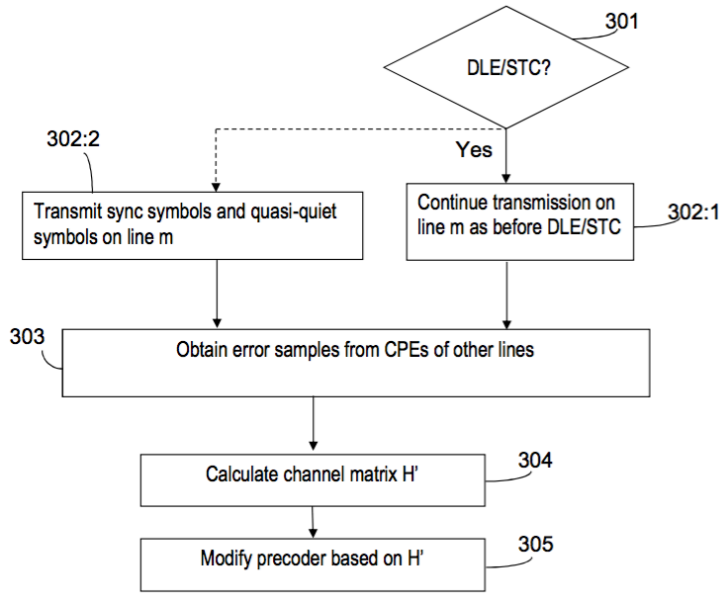


Fig. 3

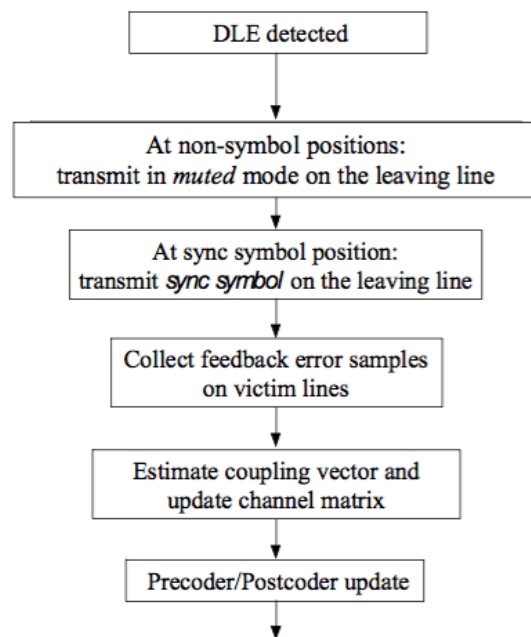


Fig. 4

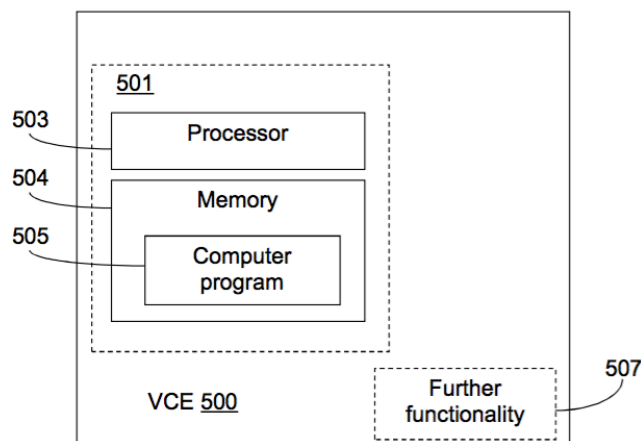


Fig. 5

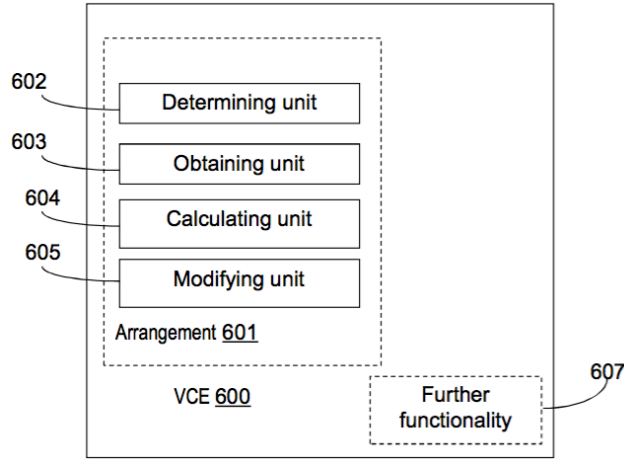


Fig. 6

References

- [1] ITU, "Self-FEXT cancellation (vectoring) for use with VDSL2 transceivers," Recommendation ITU-T G.993.5, April 2010. [Online]. Available: <https://www.itu.int/rec/T-REC-G.993.5/en>
- [2] C. Lu and P.-E. Eriksson, "A Fast Channel Estimation Method for Disorderly Leaving Events in Vectored DSL Systems, in *Proc. 2011 IEEE International Conference on Communications (ICC)*, pp. 1-6, June 2011.
- [3] ITU, "Fast Access to Subscriber Terminals - Physical Layer Specification," Recommendation Draft ITU-T G.9701, 2014. [Online]. Available: <https://www.itu.int/rec/T-REC-G.9701/en>

Paper III

Fast Mitigation of Sudden Termination Changes in Wideband Wireline Systems

Abstract

Vectoring enables cooperative crosstalk mitigation in wideband wireline systems. A sudden termination change within a vectored group alters the entire perceived channel matrix and thus disturbs the vectoring operation since the precoder, which is tuned to the channel before the change, is no longer up to date. Instead of directly dealing with a full-matrix change, we use a model-based approach which greatly reduces the number of parameters. We analyze residual crosstalk and its impact on performance degradation during showtime for both linear and non-linear precoding. As a solution, precoder updating procedures for both precoding systems are presented accounting for a sudden line deactivation or (re)activation in a vectored group. As an alternative to the state-of-the-art methods, the proposed procedures significantly reduce the complexity of channel estimation and precoder updating and minimize the disturbed period for active users.

Based on: Y. Huang, T. Magesacher, C. Lu, and P. Ödling, "Fast Mitigation of Sudden Termination Changes in Wideband Wireline Systems," submitted to *IEEE Transactions on Communications*.

1 Introduction

The rise of networked society makes wireline and wireless communications converge to the same infrastructure, providing ubiquitous and ultra-high speed networks. To serve the massive connectivity and a wide range of real-time applications, the wireline access industry advances towards a fiber-to-the-last-distribution-point paradigm [1]. In this scenario, the hybrid fiber-DSL concept [2–4] exploits shorter copper pairs and wider bandwidth to provide multi-gigabit aggregate bit-rate.

Vectoring [5, 6] enables high speed communication in wideband wireline systems by mitigating crosstalk between lines. With vectoring implemented, the transceivers of a copper pair group co-located at the distribution point (DP) can work cooperatively to cancel out crosstalk. This kind of cooperation relies on accurate channel information. When exploring higher spectrum, new practical issues that may influence end-users' quality of experience are observed. One of them results from a sudden termination change (STC) within a vectored group. A sudden change of the terminating impedance alters the perceived channel coupling conditions and leads to residual crosstalk caused by a disrupted vectoring operation. Previous studies (cf., for example, [7] and the references therein) indicate that serious signal-to-noise ratio (SNR) drops begin to take on for frequencies around 30 MHz and beyond, which are the frequencies used in the emerging G.fast [2] and similar fixed broadband technologies. It manifests a reduced bit-loading (exemplified in Fig. 1) for the other active users in the vectored group. Since nowadays the served applications have a sharply reducing tolerance to service interruptions, it is necessary to retrieve the original performance as soon as possible.

In [8] a procedure is described that allows coordination between transceivers at both DP and customer premise equipment (CPE) ends and acquire information necessary to update the precoder/equalizer before a line leaves and its termination impedance changes. While solving the problem of orderly leaving events, [8] does not address situations where there is no previous intent announced by the leaving transceiver(s), termed disorderly leaving event (DLE). A DLE is a typical scenario leading to an STC. Examples include a power loss, unplugging the connected equipment, etc. In [9], a scheme is proposed for linear precoding systems [10] to make DLEs unnoticeable to active users. Due to the diminished direct channel dominance with increasing frequency, non-linear precoding [11, 12] is also proposed as a candidate for the frequency range above 106 MHz, and therefore should be considered in implementation.

In this paper, we first analyze and quantify the STC influence on showtime lines for both linear and non-linear precoding systems. We extend the interference mitigation scheme proposed in [9] to non-linear precoding systems as well

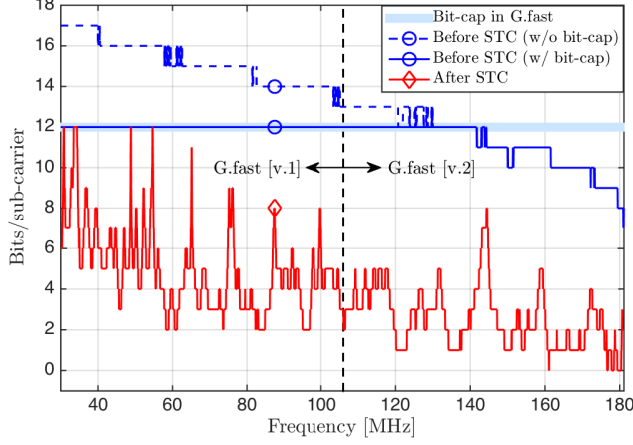


Fig. 1: Bit-loading results on a victim line exemplify the STC influence in a linear precoding system. The results are based on cable channel measurements from 30 MHz to 180 MHz. Assume a transmit PSD of -76 dBm/Hz and a background noise PSD of -150 dBm/Hz over the copper cable. There is a big drop in loaded bits due to an STC no matter bit-cap is applied or not.

as general STC cases including, for example, the reactivation of a line. Based on the parameterized channel estimation method, we propose low complexity precoder updating by avoiding full matrix inversion for linear precoders and full matrix QR-decomposition for non-linear precoders. For STC cases when a line is (re)activated in a vectored group, we also propose a new precoder update procedure which minimizes the disturbing period to the whole vectored group.

The paper is organized as following. In Section 2 a system model is presented to interpret STC, which enables the formulation and analysis of STC disturbance in Section 3. In Section 4, we propose a method with low complexity to quickly mitigate STC interference when a line is deactivated in a vectored group for both linear and non-linear precoding schemes. Section 5 derives the procedure to update precoder when a line is joining a vectored group. Section 6 concludes the work.

Notation: Bold capital letters (*e.g.*, \mathbf{A}) and bold lower-case letters (*e.g.*, \mathbf{a}) denote matrices and column vectors, respectively. $a_{i,j}$ is the element in i -th row and j -th column of \mathbf{A} and a_i is the i -th element of \mathbf{a} . $\mathbf{A}_{\mathcal{I},\mathcal{J}}$ denotes the submatrix of \mathbf{A} constructed by the rows and columns in the index sets \mathcal{I} and \mathcal{J} , respectively. For compactness, $\mathbf{A}_{n \setminus i} \in \mathbb{C}^{(n-1) \times (n-1)}$ denotes the (i, i) minor of \mathbf{A} that deletes the i -th row and column from $\mathbf{A} \in \mathbb{C}^{n \times n}$ (*i.e.*, $\mathbf{A}_{n \setminus i} =$

$\mathbf{A}_{\{1,\dots,n\}\setminus i, \{1,\dots,n\}\setminus i}$ and \mathbf{A}_{-i} denotes the submatrix obtained by deleting the i -th row from \mathbf{A} (i.e., $\mathbf{A}_{-i} = \mathbf{A}_{\{1,\dots,n\}\setminus i, \{1,\dots,n\}}$). a^* denotes the conjugate of a . \mathbf{A}^\top , \mathbf{A}^H , and \mathbf{A}^\dagger denote transpose, Hermitian transpose, and pseudo inverse of \mathbf{A} , respectively. $\boldsymbol{\epsilon}_i$ is an elementary column vector with a 1 on the i -th position and 0s elsewhere. \mathbf{I} denotes the identity matrix.

2 Wireline System Model

2.1 Vectoring Operation

Consider a wideband discrete multi-tone modulation (DMT) system with a group of K twisted pairs connecting the DP to CPEs. Let $\mathbf{H} \in \mathbb{C}^{K \times K}$ denote the frequency-domain channel matrix experienced in downstream direction by transceivers when all CPEs in the group are properly connected (or equivalently, all terminations are perfectly matched). For the sake of simple notation but without loss of generality, the sub-carrier index is omitted. Diagonal and off-diagonal elements of \mathbf{H} denote direct-channel coefficients and far-end crosstalk (FEXT) coupling coefficients, respectively.

Vectoring enables cooperative signal processing to cancel out undesired crosstalk within the group. By using a properly designed precoder for downstream and an equalizer for upstream at the DP, FEXT can be significantly reduced. Specifically in downstream, let $\mathbf{G} = \text{diag}([g_1, g_2, \dots, g_K]) \in \mathbb{R}^{K \times K}$ denote a diagonal matrix, where each element g_i denotes the per-line gain multiplier, including the gain adjuster, frequency-domain spectrum shaping coefficient, power-normalization factor, etc. (see [2]) and let $\bar{\mathbf{x}}(t) = \mathbf{G}\mathbf{x}(t)$ denote the signal after gain scaling. Assume that the cyclic prefix of DMT is not shorter than the impulse responses of the coupling paths. Furthermore, assume that the IFFT of group users is well synchronized. Transmitting the precoded signal $P\{\bar{\mathbf{x}}(t)\} \in \mathbb{C}^{K \times 1}$ at time instant t yields the receive signal $\mathbf{y}(t) \in \mathbb{C}^{K \times 1}$ at the CPE-side given by

$$\mathbf{y}(t) = \mathbf{H}P\{\bar{\mathbf{x}}(t)\} + \mathbf{n}(t),$$

where $P\{\cdot\}$ denotes a precoder designed for \mathbf{H} , and $\mathbf{n}(t) \in \mathbb{C}^{K \times 1}$ denotes the background noise on twisted pairs. Since most derivations in this work consider only a single time instant, we hereinafter omit the time index for brevity unless it is necessary to stress a time dependency.

A properly designed precoder limits the transmit power under the regulated power spectrum density (PSD) mask and mitigates crosstalk such that

$$\mathbf{H}P\{\bar{\mathbf{x}}\} = \boldsymbol{\Sigma}\mathbf{x}, \quad (1)$$

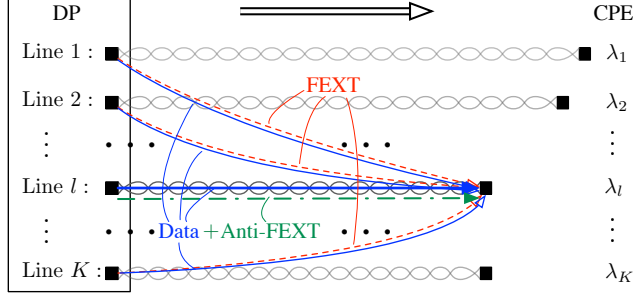


Fig. 2: Downstream vectoring operation for a linear precoding system exemplified on line l . The FEXT (red dashed lines) and anti-FEXT (green dashed-dotted line) signals will cancel out at the l -th termination at the CPE-side. Only the data signal (blue solid lines) is effectively transmitted to the end-user.

where $\mathbf{\Sigma} \in \mathbb{C}^{K \times K}$ is a diagonal matrix. The equalized receive signal is then written as

$$\mathbf{z} = \mathbf{E} \mathbf{H} \mathbf{P} \{\bar{\mathbf{x}}\} + \mathbf{E} \mathbf{n},$$

where $\mathbf{E} = \mathbf{\Sigma}^{-1}$ is a diagonal matrix containing equalizing coefficients at the CPE-side.

Fig. 2 illustrates the principle of vectoring based on the notion of “anti-FEXT”. For the sake of simplicity, we focus on a single line for linear precoding schemes (*i.e.*, $P_o\{\bar{\mathbf{x}}\} = \mathbf{P}\bar{\mathbf{x}}$, where \mathbf{P} denotes the linear precoding matrix). The receive signal at the l -th CPE-end can be written as

$$y_l = \underbrace{h_{l,l} p_{l,l} \bar{x}_l}_{\text{Data via direct path (bold solid blue in Fig. 2)}} + \underbrace{\mathbf{H}_{l,\{1,\dots,K\} \setminus l} \mathbf{P}_{\{1,\dots,K\} \setminus l, l} \bar{x}_l}_{\text{Data via FEXT-paths (thin solid blue in Fig. 2)}} + \underbrace{\mathbf{H}_{l,\{1,\dots,K\} \setminus l} \mathbf{P}_{K \setminus l, l} \bar{\mathbf{x}}_{\{1,\dots,K\} \setminus l}}_{\text{FEXT (dashed red in Fig. 2)}} + \underbrace{h_{l,l} \mathbf{P}_{l,\{1,\dots,K\} \setminus l} \bar{\mathbf{x}}_{\{1,\dots,K\} \setminus l}}_{\text{Anti-FEXT (dashed-dotted green in Fig. 2)}} + \mathbf{n}. \quad (2)$$

The precoder located at the DP knows all FEXT paths ending in line l and generates an “anti-FEXT” signal (dashed-dotted green line) that cancels out the FEXT (dashed red lines) at the CPE so that only the data components arrive. Note that data is not only arriving via line l itself (bold blue line) but also via FEXT coupling paths (thin blue lines) since the other lines are also transmitting their anti-FEXT components to eliminate the FEXT originating from line l . As a result, the vectoring operation transforms the matrix channel into K interference-free channels whose throughput is limited by background

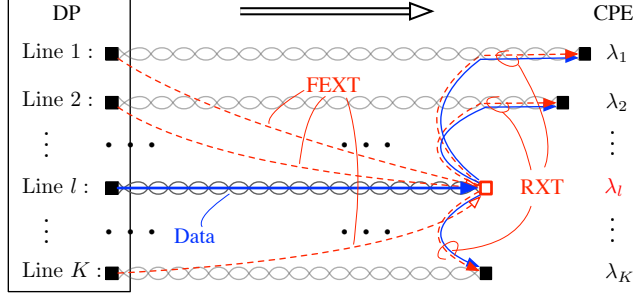


Fig. 3: Downstream RN model. All signals, including data (blue solid lines) and FEXT (red dashed lines), arriving at the mismatched termination l will be reflected and coupled via the NEXT paths, generating residual crosstalk. For a channel matrix, the reflected blue solid lines imply changed direct couplings, and the reflected red dashed lines imply changed FEXT couplings.

noise. The benefit of vectoring, however, is severely degraded by an STC event, as analyzed in the next section.

2.2 Reflected-NEXT (RN) Model

In [13, 14], a FEXT-reflected-NEXT (FRN) model is proposed to characterize the changed coupling condition due to an alien-line impedance mismatch at the CPE-side. The STC case we study in this work is similar—except now the impedance change happens within the vectored group, as illustrated in Fig. 3 before involving any precoding scheme. In this scenario, not only FEXT but also data signals from the direct channel are reflected and coupled via near-end crosstalk (NEXT) paths. Therefore, we term it generally reflected-NEXT (RN) model. Without loss of generality, we illustrate the STC coupling model in downstream on a certain sub-carrier. It applies, *mutatis mutandis*, to upstream.

Let $\mathbf{\Lambda} = \text{diag}([\lambda_1, \lambda_2, \dots, \lambda_K]) \in \mathbb{C}^{K \times K}$ denote a diagonal matrix containing the reflection coefficients λ_i , $i = 1, \dots, K$ for each termination at the CPE-side. Furthermore, let $\mathbf{\Lambda}_o$ and $\mathbf{\Lambda}'$ denote the termination matrices before and after an STC, respectively. The corresponding perceived channel matrices are $\mathbf{H}\{\mathbf{\Lambda}_o\}$ and $\mathbf{H}\{\mathbf{\Lambda}'\}$.

For simplicity, assume for a moment that all vectored lines are initially perfectly terminated ($\mathbf{\Lambda}_o = \mathbf{0}$ and thus $\mathbf{H}\{\mathbf{\Lambda}_o\} = \mathbf{H}$), which corresponds to the state illustrated in Fig. 2. Let $\mathbf{C} \in \mathbb{C}^{K \times K}$ denote the NEXT coupling matrix at the CPE-side for the perfect-termination case. The diagonal entries

of \mathbf{C} , corresponding to the CPE-side echo coefficients, are assumed to be 0. In practice, most often only one diagonal element of $\mathbf{\Lambda}$ will deviate significantly from its original value at a given time instant due to an STC (*i.e.*, mismatch of a single line only). Assume line l exhibits an STC, which in the simplified case is quantified by a reflection coefficient changing from 0 to $|\lambda'_l| \gg 0$. Consequently, $\mathbf{\Lambda}' = \text{diag}([0, \dots, 0, \lambda'_l, 0, \dots, 0])$. The perceived channel matrix after STC becomes

$$\mathbf{H}\{\mathbf{\Lambda}'\} = \mathbf{H}\{\mathbf{\Lambda}_o\} + \mathbf{\Delta},$$

where $\mathbf{\Delta} = \mathbf{C}\mathbf{\Lambda}'\mathbf{H}$ quantifies the deviation from the all-terminated case according to the RN model. Note that the reflected part $\mathbf{C}\mathbf{\Lambda}'$ is actually

$$\mathbf{C}\mathbf{\Lambda}' = [\mathbf{0} \quad \dots \quad \mathbf{0} \quad \mathbf{v}_l \quad \mathbf{0} \quad \dots \quad \mathbf{0}]$$

where

$$\mathbf{v}_l = \lambda'_l [c_{1,l}, \dots, c_{i,l}, \dots, c_{K,l}]^\top. \quad (3)$$

As illustrated in Fig. 3, the RN model suggests that the channel deviation can be written as

$$\mathbf{\Delta} = \mathbf{C}\mathbf{\Lambda}'\mathbf{H} = \mathbf{v}_l \mathbf{H}_{l,\{1,\dots,K\}}, \quad (4)$$

where $\mathbf{H}_{l,\{1,\dots,K\}}$ is just a row vector. Since $\mathbf{\Delta} \neq \mathbf{0}$, the outdated precoding with $P_o\{\cdot\}$ designed for $\mathbf{H}\{\mathbf{\Lambda}_o\} = \mathbf{H}$ yields a perturbed version of \mathbf{z} , denoted by \mathbf{z}' , *i.e.*,

$$\mathbf{z}' = \underbrace{\mathbf{E}\mathbf{H}P_o\{\bar{\mathbf{x}}\} + \mathbf{E}\mathbf{n}}_{\mathbf{z}_d} + \underbrace{\mathbf{E}\mathbf{C}\mathbf{\Lambda}'\mathbf{H}P_o\{\bar{\mathbf{x}}\}}_{\boldsymbol{\xi}}, \quad (5)$$

where \mathbf{z}_d is the desired receive signal obtained with the precoder tuned to the perceived channel $\mathbf{H}\{\mathbf{\Lambda}_o\}$ before the STC and $\boldsymbol{\xi}$ is the residual crosstalk due to the STC. Our target is to update the precoder to mitigate also the residual crosstalk from RN couplings.

In practice, it is nearly impossible to achieve perfect termination of a multi-pair wireline channel in its characteristic matrix impedance. Thus, already before an STC occurs, the termination will in general cause reflected-NEXT components (since $\mathbf{\Lambda}_o \neq \mathbf{0}$) resulting in a perceived channel $\mathbf{H}\{\mathbf{\Lambda}_o\} = \mathbf{H} + \mathbf{C}\mathbf{\Lambda}_o\mathbf{H}$. After an STC from $\mathbf{\Lambda}_o$ to $\mathbf{\Lambda}' = \mathbf{\Lambda}_o + \mathbf{\Lambda}_\delta$, the outdated precoder tuned to $\mathbf{H}\{\mathbf{\Lambda}_o\}$ yields

$$\mathbf{z}' = \underbrace{\mathbf{E}\mathbf{H}\{\mathbf{\Lambda}_o\}P_o\{\bar{\mathbf{x}}\} + \mathbf{E}\mathbf{n}}_{\mathbf{z}_d} + \underbrace{\mathbf{E}\mathbf{C}\mathbf{\Lambda}_\delta\mathbf{H}P_o\{\bar{\mathbf{x}}\}}_{\boldsymbol{\xi}}. \quad (6)$$

In the scenario of single line mismatch at a given time instant, the channel deviation is

$$\mathbf{\Delta} = \mathbf{C}\mathbf{\Lambda}_\delta\mathbf{H} = \mathbf{v}_l^\delta \mathbf{H}_{l,\{1,\dots,K\}},$$

for $\mathbf{v}_l^\delta = (\lambda'_l - \lambda_l) [c_{1,l}, \dots, c_{i,l}, \dots, c_{K,l}]^\top$, where λ_l and λ'_l denote the l -th reflection coefficients before and after the STC, respectively. Since there is no difference in formulating Eqs. (5) and (6), we consider the case where all vectored lines are initially perfectly terminated (*i.e.*, $\mathbf{\Lambda}_o = \mathbf{0}$) in the following discussions to avoid unnecessary confusion.

Apart from the deactivated-line case discussed above, another practically relevant case causing severe performance degradation occurs when a line in vicinity is (re)activated in the vectored group. The only difference from the deactivated-line case is that the outdated precoder $P_o\{\cdot\}$ is tuned to $\mathbf{H}\{\mathbf{\Lambda}_o\} = \mathbf{H} + \mathbf{\Delta}$ and the target channel after STC becomes $\mathbf{H}\{\mathbf{\Lambda}'\} = \mathbf{H}$. Therefore, the model component analysis in Section 3 focuses on the deactivated-line case only.

The residual crosstalk $\boldsymbol{\xi}$ that is not covered by the outdated precoder $P_o\{\cdot\}$ is the main reason for the performance degradation. To mitigate this interference effectively and minimize the disturbing period to active users, we start by decomposing the residual crosstalk.

3 Residual Crosstalk Analysis

The undesirable residual crosstalk $\boldsymbol{\xi}$ in Eq. (5) is dependent on the precoded transmit signal $P_o\{\bar{\mathbf{x}}\}$. For linear and non-linear precoding schemes suggested in [2], we analyze the contributing source(s) of $\boldsymbol{\xi}$ when a line is suddenly deactivated in the vectored group.

3.1 Residual Crosstalk in Linear Precoding Systems

The function $P_o\{\cdot\}$ in linear precoding systems performs linear multiplication in frequency domain. The outdated linear precoder (LP) as in [10] defines $\mathbf{P}_o^L = (\mathbf{H}\{\mathbf{\Lambda}_o\})^{-1} = \mathbf{H}^{-1}$. Note that in this work, the power normalization factor and direct channel gain have already been included in the corresponding multiplier in \mathbf{G}^L , where the data signal after gain scaling is $\bar{\mathbf{x}} = \mathbf{G}^L \mathbf{x}$.

Consider again the case when the l -th termination is deactivated while all other lines are perfectly terminated. The residual crosstalk can be simplified as

$$\begin{aligned} \boldsymbol{\xi}^L &= \mathbf{E} \mathbf{C} \mathbf{\Lambda} \mathbf{H} \mathbf{P}_o^L \bar{\mathbf{x}} = \mathbf{E} \mathbf{v}_l \boldsymbol{\epsilon}_l^\top \bar{\mathbf{x}} \\ &= \mathbf{E} \mathbf{v}_l \bar{x}_l, \end{aligned} \tag{7}$$

where \mathbf{v}_l is defined in Eq. (3) and $\bar{x}_l = g_l^\top x_l$ is the gain-scaled data signal transmitting on line l .

According to Eq. (7), we conclude that the only activating source of the residual crosstalk, given the outdated LP, is the data signal leading to the l -th CPE. In addition, the strength of the residual crosstalk is mainly determined by the effective direct channel gain g_l^L of the deactivating line and the NEXT coupling magnitude included in \mathbf{v}_l .

3.2 Residual Crosstalk in Non-Linear Precoding Systems

When exploring a wider frequency range, for example beyond 100 MHz, the diagonal dominance of the channel declines which reduces the merit of applying LP. Non-linear precoding is suggested as an alternative [2, 15]. Specifically, a Tomlinson-Harashima precoder (THP) is implemented in space domain [11] modifying the transmit signal non-linearly to achieve crosstalk-free transmission without causing transmit power increase.

Performing QR-decomposition on the Hermitian-transpose of the original channel matrix $\mathbf{H}\{\Lambda_o\} = \mathbf{H}$ yields $\mathbf{H}^H = \mathbf{Q}\mathbf{R}$. Equivalently, $\mathbf{H} = \mathbf{R}^H\mathbf{Q}^H$, where \mathbf{Q} is a unitary matrix and \mathbf{R}^H is a lower-triangular matrix. To achieve crosstalk-free transmission, dirty paper coding (DPC) [16] can be used to pre-code the transmit signal as $\mathbf{Q}(\mathbf{R}^H)^{-1}\mathbf{G}^{\text{NL}}\mathbf{x}$ such that $\mathbf{G}^{\text{NL}}\mathbf{x}$ will be received after going through the channel. However, there is an inherent power increase issue in DPC. In practice, THP is used instead, which can be written as

$$P_o^{\text{NL}}\{\bar{\mathbf{x}}\} = \mathbf{Q}\bar{\mathbf{x}}, \quad (8)$$

where $\bar{\mathbf{x}}$ denotes the recursive computation of the inverse $(\mathbf{R}^H)^{-1}$ in combination with a modulo operation on the gain-scaled transmit signal $\bar{\mathbf{x}} = \mathbf{G}^{\text{NL}}\mathbf{x}$:

$$\bar{x}_m = \Gamma \left\{ \frac{1}{r_{m,m}} \bar{x}_m - \langle m > 1 \rangle \sum_{i=1}^{m-1} \frac{r_{i,m}^*}{r_{m,m}} \bar{x}_i \right\}, \quad \text{for } m = 1, \dots, K. \quad (9)$$

The $\langle \cdot \rangle$ produces 1 if the statement inside is true, otherwise produces 0. The non-linear modulo operation on each M -QAM symbol x is defined as

$$\Gamma\{x\} \triangleq x - \sqrt{M}d \left\lfloor \frac{x}{\sqrt{M}d} + \frac{1}{2} + j\frac{1}{2} \right\rfloor,$$

where d is the minimum constellation spacing.

To make the non-linear precoding feasible, the modulo arithmetic $\Gamma\{\cdot\}$ should be employed both at transmitter and receiver. Based on the observation that $\Gamma\{x \pm y\} = \Gamma\{\Gamma\{x\} \pm \Gamma\{y\}\}$, the STC-disturbed receive signal in Eq. (5) becomes

$$\Gamma\{\mathbf{z}'\} = \Gamma\left\{ \Gamma\{\mathbf{z}_d\} + \underbrace{\mathbf{E}\mathbf{C}\mathbf{A}\mathbf{H}P_o^{\text{NL}}\{\bar{\mathbf{x}}\}}_{\boldsymbol{\xi}^{\text{NL}}} \right\},$$

where $\Gamma\{\cdot\}$ denotes modulo operation on each entry of the input vector. The residual crosstalk part can be expanded using Eq. (8) as

$$\begin{aligned}\xi^{\text{NL}} &= \Gamma\left\{\mathbf{E}\mathbf{C}\mathbf{A}\mathbf{H}P_o^{\text{NL}}\{\bar{\mathbf{x}}\}\right\} \\ &= \Gamma\left\{\mathbf{E}\mathbf{v}_l(\mathbf{R}_{\{1,\dots,K\},l})^H\bar{\mathbf{x}}\right\}.\end{aligned}\quad (10)$$

Further expanding Eq. (10) with Eq. (9), we have

$$\begin{aligned}\xi^{\text{NL}} &= \Gamma\left\{\mathbf{E}\mathbf{v}_l\sum_{i=1}^l r_{i,l}^* \bar{x}_i\right\} \\ &= \Gamma\left\{\mathbf{E}\mathbf{v}_l r_{l,l}\left(\sum_{i=1}^{l-1} \frac{r_{i,l}^*}{r_{l,l}} \bar{x}_i + \Gamma\left\{\frac{1}{r_{l,l}} \bar{x}_l - \sum_{i=1}^{l-1} \frac{r_{i,l}^*}{r_{l,l}} \bar{x}_i\right\}\right)\right\} \\ &= \Gamma\{\mathbf{E}\mathbf{v}_l \bar{x}_l\},\end{aligned}\quad (11)$$

since $\Gamma\{ax\} = \Gamma\{a\Gamma\{x\}\}$ where a is a constant. Similarly to the situation in Section 3.1, the residual crosstalk in non-linear precoding systems is driven by the transmitted data signal for the deactivated termination and its strength depends on the l -th effective channel gain and the NEXT couplings. In addition, it is also influenced by the non-linear modulo operation $\Gamma\{\cdot\}$.

3.3 STC Impact on Linear and Non-linear Precoders

In order to analyze the impact of an STC, we focus on a single subcarrier and apply both LP and THP for predefined channel conditions. The results are averaged over a large ensemble of coupling values drawn from distributions whose parameters are aligned with cable measurements. The motivation for explicitly using theoretical channel realizations in this subsection is to separate different impact factors and isolate the effect of discussed coupling magnitudes from possible performance variations due to non-ideal measurements. Also, artificial channel data allows the observation of trends over wider magnitude ranges compared to snapshot channel-measurements.

Since the average NEXT magnitude does not change much for a certain cable setup, we consider the magnitude difference between diagonal and FEXT couplings as the main impact factor, which determines the effective channel gains for LP and THP respectively. Random 3×3 channel matrices are generated such that each entry fulfils preset magnitude value and uniform distributed phase, *i.e.*, $h_{i,j} \sim A_{i,j} \exp(j2\pi\phi_{i,j})$ where $A_{i,j}$ is the coupling magnitude and $\phi_{i,j} \sim \mathcal{U}(0, 1]$. Average receive SNR on victim lines is computed as a comparing

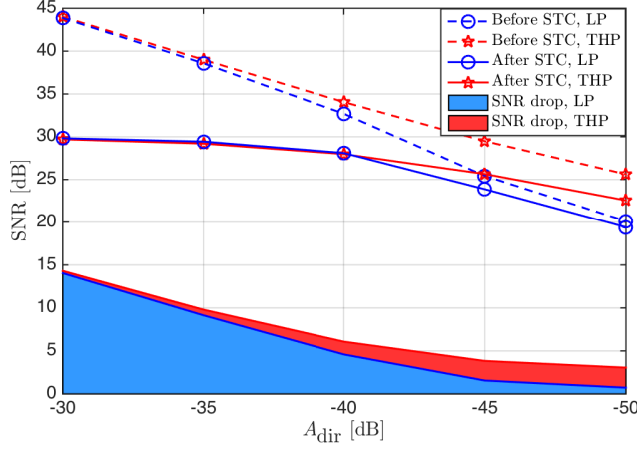


Fig. 4: Impact of STC on one victim line given different diagonal dominant property of the channel, assuming a FEXT coupling of $A_{\text{fext}} = -50$ dB, a NEXT coupling of $A_{\text{next}} = -30$ dB, and a vectoring group size of $K = 3$.

quantity, given a transmit PSD of -76 dBm/Hz, and a background noise level of -150 dBm/Hz.

In Fig. 4, the diagonal dominance of channel matrices degrades along the abscissa axis since the FEXT magnitude is fixed. The right extremity of the axis is the situation that might happen at very high frequencies that the direct and FEXT couplings are at the same magnitude level. We observe that the SNR drop is more obvious for diagonal dominant channels (*i.e.*, $A_{\text{dir}} \gg A_{\text{fext}}$) than for direct-and-FEXT comparable channels (*i.e.*, $A_{\text{dir}} \approx A_{\text{fext}}$). The reason is that the higher values of direct channel gain g_l indicate both higher original SNR levels before STC and higher residual crosstalk power (see Eqs. (7) and (11)) after STC. The SNR drop decreases along with A_{dir} value meaning that the residual crosstalk becomes less disruptive to the original performance. Here we only make relative comparison in Fig. 4, whereas the absolute numbers might be unrepresentative.

As one of the major advantages, THP generally gives higher effective channel gains comparing to the LP when the coupling magnitude of FEXT becomes comparable to that of the direct paths. Since the g_l^{NL} also contributes in generating residual crosstalk, this advantage, on the other hand, makes the non-linear precoding system more vulnerable to the STC problem than the linear precoding system, showing a larger SNR drop in Fig. 4 for the same channel condition.

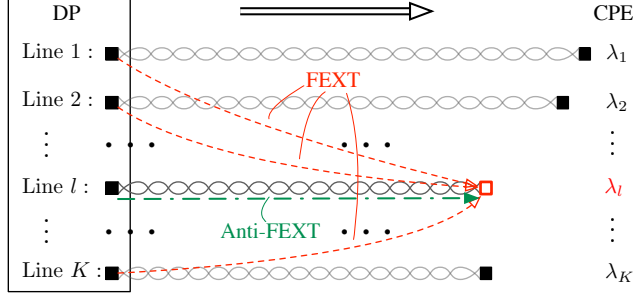


Fig. 5: Silent-mode for residual crosstalk cancellation. Transmit idle symbol which contains pure anti-FEXT signal on the disruptive line l . No signal will be reflected at the mismatched termination. Residual crosstalk is avoided.

3.4 Silent-Mode for Residual Crosstalk Cancellation

Combining Eqs. (7) and (11), the residual crosstalk introduced by a sudden termination deactivating is generally

$$\xi = \begin{cases} \mathbf{E}\mathbf{v}_l g_l^L x_l & \text{for linear precoding,} \\ \Gamma\{\mathbf{E}\mathbf{v}_l g_l^{\text{NL}} x_l\} & \text{for non-linear precoding.} \end{cases} \quad (12)$$

It is observed in Eq. (12) that the only activating source of the residual crosstalk ξ in both precoding schemes is the transmitted signal x_l on the deactivated line via the l -th direct path (with a channel gain of g_l), which is then reflected and couples to other CPEs via \mathbf{v}_l .

To mitigate the residual crosstalk in Eq. (12), [9] proposes that the DP transmits *idle symbols* [2] on the leaving line l by modifying only the l -th multiplier to be $g_l = 0$. Mathematically, the residual crosstalk becomes $\xi = 0$ for both precoding schemes. As sketched in Fig. 5, the main idea is to transmit only the anti-FEXT signal using the outdated precoder $P_o\{\cdot\}$ after an STC. The pure anti-FEXT, generated by feeding all-zero data symbols for line l into the precoder, cancels out FEXT and thus there is no energy arriving at the mismatched termination to cause any reflections and subsequent NEXT into other lines. No precoder update is needed at this stage. It enables an “STC-silent” scenario in the sense that active users remain undisturbed. Thus, we call this kind of transmission mode *silent mode*. As a result, the STC-interfering period to active users is shortened to the time it takes the DP to detect the loss of signal on line l .

Fig. 6 shows that the rate degradation problem introduced in Fig. 1 can be fixed by simply zeroing the multiplier of the l -th line, which would essentially

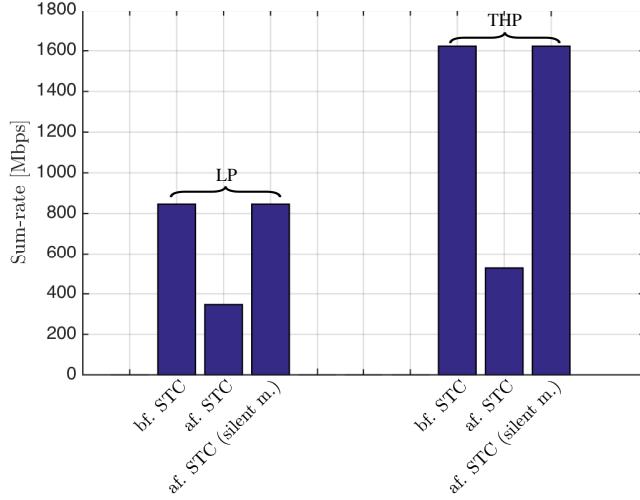


Fig. 6: Sum-rate comparison on one victim line, given a full line transmission with the outdated precoder $P_o\{\cdot\}$. Cable measurements are used for a group size of $K = 3$. The results are calculated over 30 MHz–106 MHz for linear precoding system, and over 30 MHz–180 MHz for non-linear precoding system. A bit cap of 12 bits is assumed.

solve the disrupted-vectoring problem due to STC. However, keeping the analog front-end running to send pure anti-crosstalk signals consumes power. If the deactivated termination leaves for long, it is thus desirable to invoke a further process in order to track the dimension reduced new channel, and update the precoder accordingly.

4 Precoder Update When Deactivating the Disruptive Line

4.1 Parameterized Channel Estimation

Both cable measurements and the RN model in Section 2 indicate that the whole channel matrix except for the l -th row has been changed after an STC. However as interpreted in Eq. (4), the non-sparse channel deviation matrix $\Delta = \mathbf{v}_l \mathbf{H}_{l,\{1,\dots,K\}}$ is actually composed by two vectors, where $\mathbf{H}_{l,\{1,\dots,K\}}$ is already known as part of the original channel $\mathbf{H}\{\Lambda_o\}$. To estimate the new channel matrix $\mathbf{H}\{\Lambda'\}_{K \setminus l} \in \mathbb{C}^{(K-1) \times (K-1)}$ after shutting down the disruptive line, we only need to estimate the vector \mathbf{v}_l of length $K - 1$.

Table 1: Proposed procedure at the DP-side to deactivate a line

Procedure 1: To deactivate a line
if loss of signal (<i>los</i>) is detected on line <i>l</i> then if Upstream then Track received signal power on line <i>l</i> . else if Downstream then repeat On line <i>l</i> : • transmit idle symbol on non-sync-symbol positions; • transmit synchronization symbols on sync-symbol positions; until <i>J</i> error symbols are collected end if Estimate $\hat{\mathbf{v}}_l$ (Eq. (14)); Shut down analog front-end on line <i>l</i> ; Update the precoder as $\hat{\mathbf{P}}^L$ (Eq. (19)) or $\hat{P}^{NL}\{\cdot\}$ (Eq. (21)). end if

In [9], parameterized channel estimation for linear precoding is proposed. To make the whole process unnoticeable to active users, idle symbols and synchronization symbols are alternatively transmitted on the leaving line until the process illustrated in Table 1 is completed.

Firstly, apply silent-mode (see Section 3.4) during data transmission periods to keep active users undisturbed during the channel tracking process. In addition, use synchronization symbols to do an error-based channel estimation. The transmitted synchronization symbol $\mathbf{s}(j) = [s_1(j), \dots, s_l(j), \dots, s_K(j)]^T$ from the DP at the time instant *j* yields

$$\begin{aligned} \mathbf{q}(j) &= \mathbf{\Sigma} \mathbf{s}(j) + \mathbf{v}_l g_l s_l(j) + \mathbf{n}(j) \\ &= \mathbf{\Sigma} (\mathbf{s}(j) + \mathbf{e}(j)), \end{aligned} \quad (13)$$

at CPEs, where $\mathbf{e}(j) = \mathbf{E} (\mathbf{v}_l g_l s_l(j) + \mathbf{n}(j))$ and $\mathbf{E} = \mathbf{\Sigma}^{-1}$ is the equalizing matrix. The synchronization error samples $\mathbf{I}_{-l} \mathbf{e}(j)$ on the victim lines are then fed back to DP.

After *J* synchronization time instants, the DP collects *J* error symbols on the victim lines as

$$\begin{aligned} \mathcal{E} &= \mathbf{I}_{-l} [\mathbf{e}(1), \mathbf{e}(2), \dots, \mathbf{e}(J)] \\ &= \mathbf{I}_{-l} \mathbf{E} \mathbf{v}_l g_l \mathbf{s}_l^T + \mathbf{N}, \end{aligned}$$

where $\mathbf{s}_l = [s_l(1), \dots, s_l(J)]^T$ is the synchronization sequence transmitted on the leaving line *l* at synchronization instants $j = 1, \dots, J$, and $\mathbf{N} \in \mathbb{C}^{(K-1) \times J}$

is the equalized additive noise on victim lines. The contributing reflecting crosstalk coefficients defined in Eq. (3) is estimated by

$$\hat{\mathbf{v}}_l = \boldsymbol{\Sigma}_{K \setminus l} \boldsymbol{\mathcal{E}}(\mathbf{s}_l^T)^\dagger / g_l, \quad \hat{\mathbf{v}}_l \in \mathbb{C}^{(K-1) \times 1}. \quad (14)$$

Although the derivation for Eq. (14) is based on LP, simulation shows that it works for non-linear precoding systems as well. The same procedure as in Table 1 can be used when THP is applied.

During the whole process, DP is still able to track the received signal power on line l , whose transceiver is not turned off immediately. In case of, for example, an STC false alarm, no channel retraining is required and it is faster to get back to the original vectoring operation.

A traditional way to counteract the STC disruption, however, is to shut down line l as soon as possible. As clarified in [9], this is not adequate to cancel out all residual crosstalk. To retrieve the original performance, an additional elementwise estimation for the dimension-reduced new channel $\mathbf{H}\{\boldsymbol{\Lambda}'\}_{K \setminus l}$ using synchronization symbols and pilot sequences may be required. When Hadamard sequences are applied, at least $2^{\log_2(K-1)}$ synchronization symbols are required to estimate $(K-1)^2$ channel elements for each sub-carrier. Since the orthogonality of Hadamard sequence can be degraded by background noise, a multiple of $2^{\log_2(K-1)}$ synchronization symbols may be required to accomplish a desired estimation.

In Fig. 7, computational complexities of the traditional and proposed estimation methods on one sub-carrier are compared by counting the number of involved additions and multiplications. J for the traditional method stands for the number of synchronization symbol groups, where $2^{\log_2(K-1)}$ synchronization symbols are mutually orthogonal in each group. Thus, the actual number of involved synchronization symbols for each estimation is $J \cdot 2^{\log_2(K-1)}$. The number of required synchronization symbols also determines the length of the disturbing period to active users. As a comparison, J in our proposed estimation method is the pure number of synchronization symbols applied as no orthogonality is assumed. Accordingly, there is more freedom to choose the number of synchronization symbols used for estimation. It is clear in Fig. 7 that the parameterized estimation is much simpler than the traditional way, and the advantage becomes more evident as the size of vectored group grows.

A further observation is that in the case of a single line STC, the new channel rightly after the termination mismatch is a rank-1 update of the original channel as

$$\mathbf{H}\{\boldsymbol{\Lambda}'\} = \mathbf{H}\{\boldsymbol{\Lambda}_o\} + \mathbf{v}_l \mathbf{H}_{l, \{1, \dots, K\}}, \quad (15)$$

which implies that the rank of channel deviation $r(\boldsymbol{\Delta}) = 1$. This property facilitates precoder updating in a complexity-efficient way. The simplified pre-

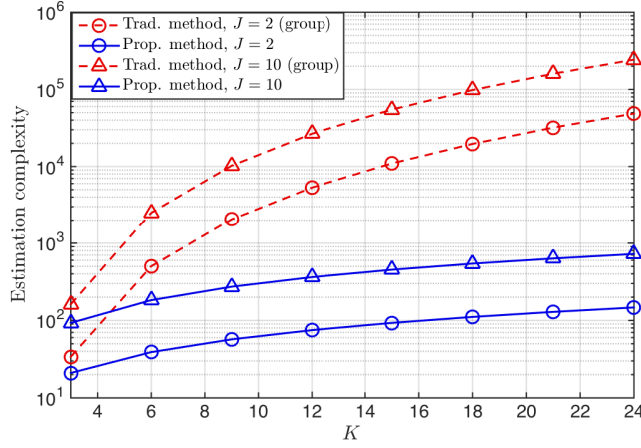


Fig. 7: Comparison of computational complexity for estimating $\mathbf{H}\{\Lambda'\}_{K \setminus l}$ on one sub-carrier.

coder update for both precoding systems will be addressed in the following subsections.

4.2 Linear Precoder (LP) Update

With \mathbf{v}_l estimated, the LP can be updated as the inverse of the new channel matrix $\mathbf{H}\{\Lambda'\}_{K \setminus l}$ according to the RN model, *i.e.*,

$$\hat{\mathbf{P}}_{\text{basic}}^L = (\mathbf{H}_{K \setminus l} + \hat{\mathbf{v}}_l \mathbf{H}_{l, \{1, \dots, K\} \setminus l})^{-1}.$$

As the original \mathbf{H} is not always directly available and full matrix inversion is not the best choice, we perform the precoder updating by utilizing only the outdated precoder \mathbf{P}_o^L and the estimated $\hat{\mathbf{v}}_l$ instead.

Consider that the LP operates for frequencies up to 106 MHz, where the channel matrix is still diagonally dominant. Separating $\mathbf{P}_o^L = \mathbf{P}_\Sigma + \mathbf{P}_\Delta$, where \mathbf{P}_Σ carries the diagonal entries and \mathbf{P}_Δ carries the off-diagonal entries, the original channel matrix \mathbf{H} can be estimated by the first-order inverse approximation as

$$\begin{aligned} \mathbf{H} &= (\mathbf{P}_o^L)^{-1} = ((\mathbf{I} + \mathbf{P}_\Delta \mathbf{P}_\Sigma^{-1}) \mathbf{P}_\Sigma)^{-1} \\ &\approx \mathbf{P}_\Sigma^{-1} (\mathbf{I} - \mathbf{P}_\Delta \mathbf{P}_\Sigma^{-1}), \end{aligned} \quad (16)$$

the l -th row of which, excluding $h_{l,l}$, is then given as

$$\hat{\mathbf{H}}_{l,\{1,\dots,K\}\setminus l} = \frac{-\boldsymbol{\epsilon}_l^T \mathbf{P}_o^L \mathbf{P}_\Sigma^{-1} \mathbf{I}_{-l}^T}{p_{l,l}}. \quad (17)$$

Let \mathbf{M}_σ denote a permutation matrix, *i.e.*,

$$\mathbf{M}_\sigma = [\boldsymbol{\epsilon}_{\sigma(1)} \quad \boldsymbol{\epsilon}_{\sigma(2)} \quad \cdots \quad \boldsymbol{\epsilon}_{\sigma(K)}]^T.$$

With $\sigma_1 = [\{1, \dots, K\} \setminus l, l]$, the channel matrix can be reformed as

$$\mathbf{M}_{\sigma_1} \mathbf{H} \mathbf{M}_{\sigma_1}^T = \begin{bmatrix} \mathbf{H}_{K \setminus l} & \mathbf{H}_{\{1,\dots,K\} \setminus l, l} \\ \mathbf{H}_{l, \{1,\dots,K\} \setminus l} & h_{l,l} \end{bmatrix}.$$

A permuted precoder is obtained correspondingly as

$$\mathbf{P}_\sigma = \mathbf{M}_{\sigma_1} \mathbf{P}_o^L \mathbf{M}_{\sigma_1}^T = \begin{bmatrix} \mathbf{P}_A & \mathbf{p}_B \\ \mathbf{p}_C & p_D \end{bmatrix},$$

where \mathbf{P}_A has the same size as $\mathbf{H}_{K \setminus l}$. A preliminarily updated precoder $\tilde{\mathbf{P}} \in \mathbb{C}^{(K-1) \times (K-1)}$ is then generated by

$$\tilde{\mathbf{P}} = \mathbf{P}_A - \frac{\mathbf{p}_B \mathbf{p}_C}{p_D}, \quad (18)$$

which essentially approximates $(\mathbf{H}_{K \setminus l})^{-1}$.

Using the Sherman-Morrison formula, the LP for $\mathbf{H}\{\boldsymbol{\Lambda}'\}_{K \setminus l}$ can then be updated by using the estimated vector $\hat{\mathbf{v}}_l$ in Eq. (14), the derived row vector $\hat{\mathbf{H}}_{l, \{1,\dots,K\} \setminus l}$ in Eq. (17) and the preliminarily updated precoder $\tilde{\mathbf{P}}$ in Eq. (18), *i.e.*,

$$\hat{\mathbf{P}}^L = \tilde{\mathbf{P}} \left(\mathbf{I} - \frac{\hat{\mathbf{v}}_l \hat{\mathbf{H}}_{l, \{1,\dots,K\} \setminus l} \tilde{\mathbf{P}}}{1 + \hat{\mathbf{H}}_{l, \{1,\dots,K\} \setminus l} \tilde{\mathbf{P}} \hat{\mathbf{v}}_l} \right), \quad \hat{\mathbf{P}}^L \in \mathbb{C}^{(K-1) \times (K-1)} \quad (19)$$

without performing full matrix inversion. In addition, the multiplier matrix \mathbf{G}^L can also be updated accordingly.

4.3 Tomlinson-Harashima Precoder (THP) Update

For a small group number K , updating the THP can be achieved by a new QR-decomposition on the dimension-reduced new channel $\mathbf{H}\{\boldsymbol{\Lambda}'\}_{K \setminus l} = \mathbf{H}\{\boldsymbol{\Lambda}_o\}_{K \setminus l} + \hat{\mathbf{v}}_l \mathbf{H}_{l, \{1,\dots,K\} \setminus l}$. For large K , the computational complexity can be reduced by QR-updates of the original \mathbf{Q} and \mathbf{R} exploiting the property of the Hessenberg matrix and Givens rotations [17].

Let $\mathcal{J}_1 = \mathbf{J}_{K-1}^{(1)} \cdots \mathbf{J}_l^{(1)}$ denote the sequence of Givens rotations which zeros out the extra sub-diagonal entries of $\mathbf{R}\mathbf{I}_{-l}^\top$. $\mathcal{J}_2 = \mathbf{J}_1^{(2)} \cdots \mathbf{J}_{K-1}^{(2)}$ is another Givens rotation sequence such that

$$\mathcal{J}_2 \mathcal{J}_1 \mathbf{Q}^H \boldsymbol{\epsilon}_l = \alpha_1 \boldsymbol{\epsilon}_1,$$

where α_1 is a complex number with $|\alpha_1| = 1$. The preliminary QR-update for the dimension-reduced original channel $\mathbf{H}_{K \setminus l}^H$ can be executed as

$$\begin{aligned} \tilde{\mathbf{R}} &= \mathbf{I}_{-1} \mathcal{J}_2 \mathcal{J}_1 \mathbf{R} \mathbf{I}_{-l}^\top, \\ \tilde{\mathbf{Q}} &= \mathbf{I}_{-1} \mathbf{M}_{\boldsymbol{\sigma}_2} \mathbf{Q} \mathcal{J}_1^H \mathcal{J}_2^H \mathbf{I}_{-1}^\top, \end{aligned} \quad (20)$$

where the permutation order is $\boldsymbol{\sigma}_2 = [l, \{1, \dots, K\} \setminus l]$. Equivalently, we estimate the Hermitian transpose of the dimension-reduced new channel as

$$\begin{aligned} (\mathbf{H}\{\boldsymbol{\Lambda}'\})_{K \setminus l}^H &= \mathbf{H}_{K \setminus l}^H + \mathbf{H}_{l, \{1, \dots, K\} \setminus l}^H \hat{\mathbf{v}}_l^H \\ &= \mathbf{H}_{K \setminus l}^H + \mathbf{Q}_{-l} \mathbf{R}_{\{1, \dots, K\}, l} \hat{\mathbf{v}}_l^H \\ &= \tilde{\mathbf{Q}} \left(\tilde{\mathbf{R}} + \mathbf{u} \hat{\mathbf{v}}_l^H \right), \end{aligned}$$

where $\mathbf{u} = \tilde{\mathbf{Q}}^H \mathbf{Q}_{-l} \mathbf{R}_{\{1, \dots, K\}, l}$. Perform the third Givens rotation sequence $\mathcal{J}_3 = \mathbf{J}_1^{(3)} \cdots \mathbf{J}_{K-2}^{(3)}$ for

$$\mathcal{J}_3 \mathbf{u} = \alpha_2 \boldsymbol{\epsilon}_1,$$

where α_2 is a complex number that $|\alpha_2| = \|\mathbf{u}\|_2$. And also perform the forth Givens rotation sequence $\mathcal{J}_4 = \mathbf{J}_{K-2}^{(4)} \cdots \mathbf{J}_l^{(4)}$ for upper-triangularizing the upper Hessenberg matrix $\mathcal{J}_3 \left(\tilde{\mathbf{R}} + \mathbf{u} \hat{\mathbf{v}}_l^H \right)$. The rank-1 update of Eq. (20) yields

$$\begin{aligned} \hat{\mathbf{R}} &= \mathcal{J}_4 \mathcal{J}_3 \left(\tilde{\mathbf{R}} + \mathbf{u} \hat{\mathbf{v}}_l^H \right), \\ \hat{\mathbf{Q}} &= \tilde{\mathbf{Q}} \mathcal{J}_3^H \mathcal{J}_4^H. \end{aligned}$$

Therefore, the updated non-linear precoding function works as

$$\hat{P}^{\text{NL}}\{\bar{\mathbf{x}}_{K \setminus l}\} = \hat{\mathbf{Q}} \hat{\hat{\mathbf{x}}}, \quad (21)$$

where

$$\hat{\hat{x}}_m = \Gamma \left\{ \frac{1}{\hat{r}_{m,m}} \bar{x}_m - \langle m > 1 \rangle \sum_{i=1}^{m-1} \frac{\hat{r}_{i,m}^*}{\hat{r}_{m,m}} \hat{\hat{x}}_i \right\}, \quad \text{for } m = 1, \dots, K-1.$$

As stated in [17], a new QR-decomposition from scratch needs a factor $\mathcal{O}(K^3)$ flops, whereas the above update procedure can be executed in $\mathcal{O}(K^2)$ flops.

Both methods in Section 4.2 and 4.3 can be extended to general cases when $r(\boldsymbol{\Delta}) \geq 1$.

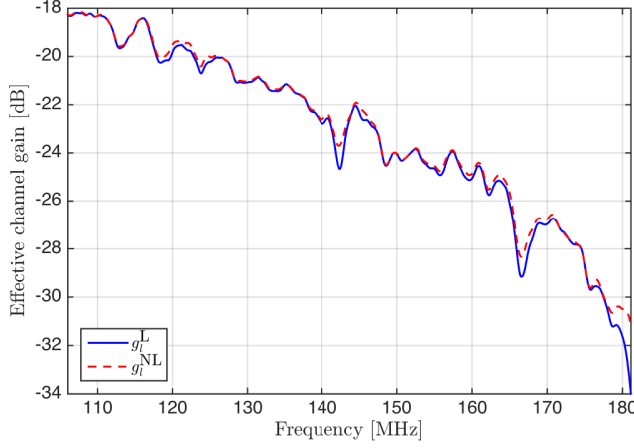


Fig. 8: Effective channel gains on the deactivating line when applying LP and THP respectively to the measured channel.

4.4 Simulation Comparison

In order to evaluate the performance of the proposed precoder update schemes, we measure direct paths and crosstalk paths from a 30-pair, 100 m, 0.5 mm cable [18]. To separate the influence of effective direct channel gain and the effectiveness of the proposed precoder updating methods, 3 pairs from a single binder are chosen such that there is no big difference between g_l^L and g_l^{NL} of the deactivating line even for frequencies from 106 MHz to 180 MHz (see Fig. 8). The measurement points follow a 51.75 kHz sub-carrier spacing, and we consider 3 500 sub-carriers in total, which corresponds to a frequency range up to 180 MHz. The all-terminated case and a deactivating STC-case, where line $l = 3$ is left unterminated, yield two 3×3 matrices $\mathbf{H}\{\mathbf{\Lambda}_o\}$ and $\mathbf{H}\{\mathbf{\Lambda}'\}$ for each sub-carrier, respectively. Note that crosstalk measurements while simultaneously synthesizing an exact open-line termination impedance for the victim line are impossible and a specially tailored measurement setup could at best approximate the scenario. Since the crosstalk coefficients from other lines into the leaving line are of no importance to the precoder update, we thus copy the third row of $\mathbf{H}\{\mathbf{\Lambda}'\}$ from $\mathbf{H}\{\mathbf{\Lambda}_o\}$.

We study the effectiveness of proposed schemes by exploring the entire frequency range up to 180 MHz for both linear and non-linear precoding systems to allow for a fair comparison. Depending on the channel conditions, LP may be the preferred choice for lower frequencies, while THP may be used

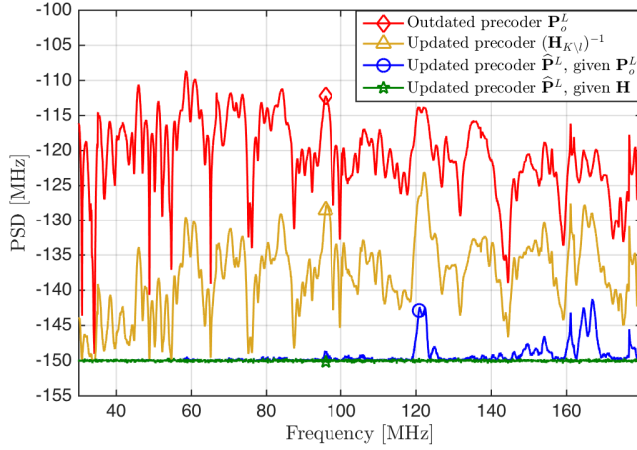


Fig. 9: Residual crosstalk PSD on victim line 2 after an STC for linear precoding systems. Parameterized estimation is performed with $J = 1$.

for higher frequencies where the channel matrix is no longer diagonally dominant. The comparison is made in frequency domain based on the PSD of the resulting residual crosstalk. The simulations are based on system parameters of G.fast [2].

Fig. 9 presents the residual crosstalk PSD on one of the victim lines in the vectored group. By stopping transmission on the leaving line and updating the precoder to $(\mathbf{H}\{\mathbf{\Lambda}_o\}_{K\setminus l})^{-1}$ for the dimension-reduced original channel (*i.e.*, the traditional operation), a reduction in residual crosstalk (from the red diamond-marked curve to the yellow triangle-marked one) is observed. However, the reduced residual crosstalk is still far above background noise level, especially for high frequencies where the crosstalk channel has a coupling level closer to that of the direct channel. Thus, further channel tracking is needed.

In contrast, the resulting residual crosstalk of our proposed operation (blue circle-marked and green star-marked curves) are almost unnoticeable, as they stay quite close to the background noise. Using $J = 1$ synchronization symbol to estimate $\hat{\mathbf{v}}_l$, the updated precoder $\hat{\mathbf{P}}^L$ from Eq. (19) can effectively cover the new channel $\mathbf{H}\{\mathbf{\Lambda}'\}_{K\setminus l}$. In addition, the blue circle-marked curve in Fig. 9 applies the approximation in Eq. (17) to update the precoder directly from the outdated \mathbf{P}_o^L , whereas the green star-marked curve assumes prior knowledge of the original channel $\mathbf{H}\{\mathbf{\Lambda}_o\} = \mathbf{H}$ to be available. The approximation in Eq. (16) becomes less accurate when the frequency increases and the magnitude

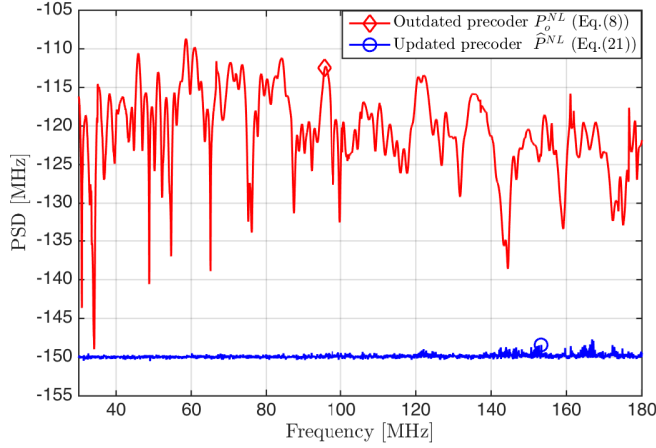


Fig. 10: Residual crosstalk PSD on victim line 2 after an STC for non-linear precoding systems. Parameterized estimation is performed with $J = 1$.

difference between direct and FEXT paths becomes smaller. Consequently, the blue circle-marked curve exhibits a slightly higher residual crosstalk for frequencies around 120 MHz and beyond.

Similarly to the linear precoding system, we can reduce the residual crosstalk in a non-linear precoding system effectively to the background noise level with the proposed method. In Fig. 10, a parameterized estimation of $\hat{\mathbf{v}}_l$ is performed using only $J = 1$ synchronization symbol, and the precoder updating procedure proposed in Section 4.3 is applied.

5 Precoder Update When (Re)Activating an Additional Line

Similar vectoring interruption occurs when a line is activated in the vectored group. It can also be generalized as an STC problem with a termination reflection coefficient changing from non-zero to zero. To differentiate from the STC-case discussed in above sections, we refer to it as activating STC.

If the line is to be reactivated in the vectored group and the channel information, including direct and FEXT couplings and reflecting crosstalk coefficients, are still stored at the DP-side, the precoder update is trivial. Otherwise, it is necessary to estimate all channel coefficients related to the joining line. Because of the ignored reflected-NEXT deviation, a full channel retraining may be

needed when the basic channel discovery routine is not adequate. In the latter case, we propose a fast and effective tracking procedure for the dimension-increased channel condition based on the RN model.

Assume again a vectored group of size K . One neighboring line is joining this group. According to the RN model, the original channel before an activating STC event is composed by two parts, *i.e.*,

$$\bar{\mathbf{H}}\{\Lambda_o\} = \mathbf{H} + \mathbf{v}\mathbf{h}_r^T,$$

where $\mathbf{v} \in \mathbb{C}^{K \times 1}$ denotes a column vector of reflected crosstalk coefficients from the joining termination, and $\mathbf{h}_r^T \in \mathbb{C}^{1 \times K}$ denotes the FEXT from vectored lines into the joining line. The effective channel matrix after an STC becomes

$$\bar{\mathbf{H}}\{\Lambda'\} = \begin{bmatrix} \mathbf{H} & \mathbf{h}_c \\ \mathbf{h}_r^T & h_{K+1} \end{bmatrix}, \quad (22)$$

where h_{K+1} is the new direct channel and $\mathbf{h}_c \in \mathbb{C}^{K \times 1}$ denotes the FEXT channels from the joining line into vectored lines.

Consider a simplified traditional channel discovery procedure [2] with two phases. *Phase-1* estimates the FEXT from the joining line into the vectored lines (*i.e.*, \mathbf{h}_c), updates precoder coefficients to cancel out this crosstalk, and then *phase-2* estimates the FEXT into the joining line (*i.e.*, \mathbf{h}_r^T). However, there has already been a deviation in *phase-1* due to the ignorance of the $\Delta = \mathbf{v}\mathbf{h}_r^T$, which changes the coupling conditions among the original vectored lines as well. The effectiveness of the whole estimation and update procedure is degraded.

Thus, we propose a new channel discovery order, which is detailed for linear precoding systems. A similar updating principle can also be applied in non-linear precoding systems.

5.1 Error-Based Channel Estimation And Precoder Update

The precoder fulfilling vectoring operation diagonalizes the original channel as

$$\bar{\Sigma} = (\mathbf{H} + \mathbf{v}\mathbf{h}_r^T)\bar{\mathbf{P}}\bar{\mathbf{G}},$$

where $\bar{\mathbf{P}} = (\bar{\mathbf{H}}\{\Lambda_o\})^{-1}$ and $\bar{\mathbf{E}} = (\bar{\Sigma})^{-1}$ denotes the corresponding diagonal matrix composed by equalizing coefficients.

When the additional line $K+1$ is activated, its reflection coefficient changes from $|\lambda_{K+1}| \gg 0$ to $\lambda_{K+1} = 0$. The deviation term $\mathbf{v}\mathbf{h}_r^T$ changing from non-zero to zero causes a disturbance to the K original CPEs. To minimize this

Table 2: Proposed channel discovery procedure for a joining line

Procedure 2: To (re)activate a line
<hr/> if Joining request is received for line $K + 1$ then PHASE-1: repeat Transmit quiet symbols for all symbols positions on the joining line. until J_1 received synchronization symbols from all $K + 1$ CPEs are collected. Estimate $\hat{\mathbf{h}}_r^\top$ and $\hat{\mathbf{v}}$ (Eq. (23)). PHASE-2: Update the precoder related to the original vectored group to $\hat{\mathbf{P}}$ (Eq. (24)) repeat On line $K + 1$: • transmit quiet symbols on non-sync-symbol positions; • transmit synchronization symbols on sync-symbol positions; until J_2 received synchronization symbols from all $K + 1$ CPEs are collected. end if Estimate $[\hat{\mathbf{h}}_e^\top, \hat{h}_{K+1}]^\top$ (Eq. (25)); Update the precoder to $\hat{\hat{\mathbf{P}}}$ (Eq. (26)). <hr/>

disruption, we propose a reordered channel discovery procedure summarized in Table 2.

The transceiver unit for the joining line at the DP-side first transmits *quiet symbols* for all symbol positions. The quiet symbol is constructed by setting the constellation point to 0, which results in zero transmit power. Equivalently, the multiplier matrix, precoder and equalizer can be represented as $\bar{\mathbf{G}}_{+0} = \begin{bmatrix} \bar{\mathbf{G}} & \mathbf{0} \\ \mathbf{0}^\top & 0 \end{bmatrix}$, $\bar{\mathbf{P}}_{+0} = \begin{bmatrix} \bar{\mathbf{P}} & \mathbf{0} \\ \mathbf{0}^\top & 0 \end{bmatrix}$, and $\bar{\mathbf{E}}_{+0} = \begin{bmatrix} \bar{\mathbf{E}} & \mathbf{0} \\ \mathbf{0}^\top & 1 \end{bmatrix}$, respectively.

During the synchronization period, we can perform the *phase-1* estimation. Since nothing is essentially sent from the $(K + 1)$ -th transmitter, the received signal at the joining CPE is the pure FEXT from the vectored lines. Mathematically, transmitting a synchronization symbol $\mathbf{s}_o(1) = [s_1(1), \dots, s_K(1)]^\top$ yields

$$q_{K+1}(1) = \mathbf{h}_r^\top \bar{\mathbf{P}} \bar{\mathbf{G}} \mathbf{s}_o(1) + n.$$

at the joining CPE at the first synchronization time instant. The errors oc-

curing at the other active CPEs result from the “disappeared” deviation term $\mathbf{v}\mathbf{h}_r^\top$, *i.e.*,

$$\mathbf{e}_o(1) = -\bar{\mathbf{E}}(\mathbf{v}\mathbf{h}_r^\top \bar{\mathbf{P}}\bar{\mathbf{G}}\mathbf{s}_o(1) + \mathbf{n}).$$

Let J_1 denote the number of synchronization time instants needed to accomplish a *phase-1* estimation. During this period, $\mathbf{S}_{o,J_1} = [\mathbf{s}_o(1), \dots, \mathbf{s}_o(J_1)]$ are transmitted from the K vectored lines. The received error symbols on the joining CPE and the original CPEs are represented by $\mathbf{q}_{K+1,J_1} = [q_{K+1}(1), \dots, q_{K+1}(J_1)]^\top$ and $\mathcal{E}_{o,J_1} = [\mathbf{e}_o(1), \dots, \mathbf{e}_o(J_1)]$, respectively. The channel deviation can be estimated by two vectors as

$$\begin{aligned}\hat{\mathbf{h}}_r^\top &= \mathbf{q}_{K+1,J_1}^\top (\bar{\mathbf{P}}\bar{\mathbf{G}}\mathbf{s}_o)^\dagger, \\ \hat{\mathbf{v}} &= -\bar{\Sigma}\mathcal{E}_{o,J_1}(\hat{\mathbf{h}}_r^\top \bar{\mathbf{P}}\bar{\mathbf{G}}\mathbf{s}_o)^\dagger.\end{aligned}\tag{23}$$

During the next data transmission period, update the first sub-block of the precoder $\bar{\mathbf{P}}_{+0}$ as

$$\tilde{\mathbf{P}} = \bar{\mathbf{P}} \left(\mathbf{I} + \frac{\hat{\mathbf{v}}\hat{\mathbf{h}}_r^\top \bar{\mathbf{P}}}{1 - \hat{\mathbf{h}}_r^\top \bar{\mathbf{P}}\hat{\mathbf{v}}} \right),\tag{24}$$

to eliminate the residual crosstalk from the deviation $-\Delta$. Update the first sub-block of $\bar{\mathbf{G}}_{+0}$ accordingly to be $\tilde{\mathbf{G}}$. The negative influence of the (re)activating event on the original CPEs is eliminated hereafter.

During *phase-2*, start transmitting synchronization symbols on all the $K+1$ lines. Equivalently, the precoder works as $\bar{\mathbf{P}}_{+1} = \begin{bmatrix} \tilde{\mathbf{P}} & \mathbf{0} \\ \mathbf{0}^\top & 1 \end{bmatrix}$, and the multiplier matrix is $\bar{\mathbf{G}}_{+1} = \begin{bmatrix} \tilde{\mathbf{G}} & \mathbf{0} \\ \mathbf{0}^\top & \alpha \end{bmatrix}$ with a power-regulating constant α . Similarly after J_2 synchronization time instants, the received sequence at the joining CPE is

$$\mathbf{q}_{K+1,J_2}^\top = \mathbf{h}_r^\top \tilde{\mathbf{P}}\tilde{\mathbf{G}}\mathbf{s}_{o,J_2} + \alpha h_{K+1} \mathbf{s}_{K+1}^\top + \mathbf{n}^\top,$$

where $\mathbf{s}_{K+1}^\top = [s_{K+1}(1), \dots, s_{K+1}(J_2)]^\top$ is the synchronization sequence transmitting on the joining line during the J_2 time instants. The errors from the first K CPEs are composed by

$$\mathcal{E}_{o,J_2} = \bar{\mathbf{E}}(\alpha \mathbf{h}_c \mathbf{s}_{K+1}^\top + \mathbf{N}).$$

The new direct channel and the third vector can then be estimated by

$$\begin{aligned}\hat{h}_{K+1} &= (\mathbf{q}_{K+1,J_2}^\top - \hat{\mathbf{h}}_r^\top \tilde{\mathbf{P}}\tilde{\mathbf{G}}\mathbf{s}_{o,J_2})(\mathbf{s}_{K+1}^\top)^\dagger / \alpha, \\ \hat{\mathbf{h}}_c &= \bar{\Sigma}\mathcal{E}_{o,J_2}(\mathbf{s}_{K+1}^\top)^\dagger / \alpha.\end{aligned}\tag{25}$$

At this point, the estimation for the dimension increased new channel is completed:

$$\widehat{\mathbf{H}}\{\mathbf{\Lambda}'\} = \begin{bmatrix} \mathbf{H} & \widehat{\mathbf{h}}_c \\ \widehat{\mathbf{h}}_r^T & \widehat{h}_{K+1} \end{bmatrix}.$$

Note that the Shur complement of \mathbf{H} in matrix $\widehat{\mathbf{H}}\{\mathbf{\Lambda}'\}$, *i.e.*,

$$\gamma = \widehat{h}_{K+1} - \widehat{\mathbf{h}}_r^T \widetilde{\mathbf{P}} \widehat{\mathbf{h}}_c,$$

is just a scalar. Also, the Shur complement of \widehat{h}_{K+1} , *i.e.*, $\mathcal{S}_{\widehat{h}} = \mathbf{H} - \widehat{\mathbf{h}}_c \widehat{\mathbf{h}}_r^T / \widehat{h}_{K+1}$, is again a rank-1 update of matrix \mathbf{H} , and therefore,

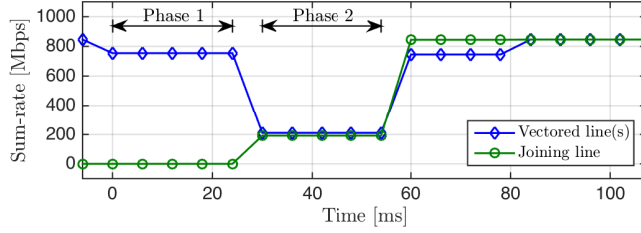
$$\mathcal{S}_{\widehat{h}}^{-1} = \widetilde{\mathbf{P}} \left(\mathbf{I} + \widehat{\mathbf{h}}_c \widehat{\mathbf{h}}_r^T \widetilde{\mathbf{P}} / \gamma \right).$$

No explicit matrix inversion is needed to recalculate the precoder for $\widehat{\mathbf{H}}\{\mathbf{\Lambda}'\}$. We can update the precoder based on previous knowledge of $\widetilde{\mathbf{P}}$ in Eq. (24) with the three estimated vectors as

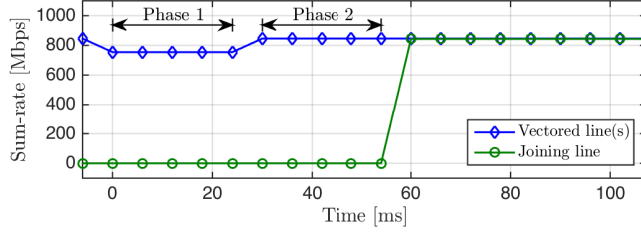
$$\widehat{\mathbf{P}} = \left(\widehat{\mathbf{H}}\{\mathbf{\Lambda}'\} \right)^{-1} = \begin{bmatrix} \mathcal{S}_{\widehat{h}}^{-1} & -\widetilde{\mathbf{P}} \widehat{\mathbf{h}}_c / \gamma \\ -\widehat{\mathbf{h}}_r^T \mathcal{S}_{\widehat{h}}^{-1} / \widehat{h}_{K+1} & 1/\gamma \end{bmatrix}. \quad (26)$$

5.2 Simulation Comparison

The traditional line initializing approach first estimates the crosstalk from the joining line into the vectored lines (*i.e.*, \mathbf{h}_c), followed by the estimation from the vectored lines into the joining line (*i.e.*, \mathbf{h}_r^T). Because of the coupling deviation, which is now recognized as the influence of STC, the *phase-1* estimation does not obtain the actual FEXT from the joining line (see Fig.11a). Although in *phase-2* the precoder is active based on the previous estimation for vectored lines among themselves and for joining lines into the vectored lines, we observe in Fig.11a that the vectored lines still receive strong crosstalk disturbance once the joining line starts transmitting. The disturbed period may be extended since [2] defines a transmission repetition on the joining line in presence of strong crosstalk. Even if \mathbf{h}_c is estimated again after the estimation of \mathbf{h}_r^T in *phase-2*, a full-channel retraining procedure may still be needed to obtain the original sum-rate. In Fig. 11a, a gap is observed between the blue diamond-marked line after *phase-2* and the original sum-rate level before STC, due to the inadequate crosstalk cancellation. Thus, full-channel retraining is performed at around 80 ms to recover the original sum-rate level. During the whole process,



(a) Traditional procedure



(b) Proposed procedure

Fig. 11: Sum-rate over 30 MHz–106 MHz frequencies during the process of new line (re)activation. Activating STC occurs at time 0. Calculations are taken using channel measurements described in Section 4.4.

the vectored lines suffer from a persistent disturbance, which grows with group size.

The proposed procedure, on the other hand, suggests to estimate \mathbf{h}_r^T first. According to the RN model, \mathbf{h}_r^T is part of the attributes that compose of the STC deviation. The errors collected at the original CPEs contribute to both estimating \mathbf{h}_r^T and correcting the crosstalk among the vectored lines after the STC. As shown in Fig.11b, the throughput degradation for the vectored lines is minor within a much shorter period of time compared to that of the traditional procedure in Fig.11a. The vectored lines can recover their original performance once the *phase-1* estimation is completed. Although the starting time for the joining line is delayed a bit, the disturbance to the original active users becomes unnoticeable during the whole line initializing process.

6 Conclusion

An STC caused when a line is abruptly deactivated or (re)activated in a vectored group alters the perceived channel coupling conditions, which leads to significant service degradation for active users in the neighborhood. Based on the RN model, we characterize the changed channel with a vector composed by reflecting crosstalk coefficients and identify the residual crosstalk caused by an STC. The proposed precoder updating procedures for deactivating and (re)activating lines minimize the residual crosstalk disturbance to active users compared to the state-of-the-art methods. In addition, both channel estimation and precoder updating procedures are simplified, lowering complexity and cost for the modems at the DP-side.

References

- [1] P. Ödling, T. Magesacher, S. Höst, P. O. Börjesson, M. Berg, and E. Areizaga, "The Fourth Generation Broadband Concept," *IEEE Communications Magazine*, vol. 47, no. 1, pp. 62-69, January 2009.
- [2] ITU, "Fast Access to Subscriber Terminals - Physical Layer Specification," Recommendation Draft ITU-T G.9701, 2014. [Online]. Available: <https://www.itu.int/rec/T-REC-G.9701/en>
- [3] M. Timmers, M. Guenach, C. Nuzman, and J. Maes, "G.fast: Evolving the Copper Access Network," *IEEE Communications Magazine*, vol. 51, no. 8, pp. 74-79, August 2013.
- [4] W. Coomans, R. Moraes, K. Hooghe, A. Duque, J. Galaro, M. Timmers, A. van Wijngaarden, M. Guenach, and J. Maes, "XG-FAST: Towards 10 Gb/s Copper Access," in *Proc. 2014 GLOBECOM Workshops (GC Wkshps)*, pp. 630-635, December 2014.
- [5] G. Ginis and J. Cioffi, "Vectored Transmission for Digital Subscriber Line Systems," *IEEE Journal on Selected Areas in Communications*, vol. 20, no. 5, pp. 1085-1104, June 2002.
- [6] ITU, "Self-FEXT cancellation (vectoring) for use with VDSL2 transceivers," Recommendation ITU-T G.993.5, April 2010. [Online]. Available: <https://www.itu.int/rec/T-REC-G.993.5/en>
- [7] E. Medeiros, T. Magesacher, P.-E. Eriksson, C. Lu, and P. Ödling, "How Vectoring in G.fast May Cause Neighborhood Wars," in *Proc. 2014 IEEE*

- International Conference on Communications (ICC)*, pp. 3859-3864, June 2014.
- [8] Alcatel-Lucent, "Influence of an Impedance Change on a Leaving Line onto the Direct and Crosstalk Channels of the Active Lines," ITU-T SG15 Contribution 2013-10-Q4-058, October 2013.
 - [9] Y. Huang, T. Magesacher, E. Medeiros, C. Lu, P.-E. Eriksson, and P. Ödling, "Mitigating Disorderly Leaving Events in G.fast," in *Proc. 2015 IEEE International Conference on Communications (ICC)*, pp. 939-944, June 2015.
 - [10] R. Cendrillon, G. Ginis, E. Van den Bogaert, and M. Moonen, "A Near-Optimal Linear Crosstalk Precoder for Downstream VDSL," *IEEE Transactions on Communications*, vol. 55, no. 5, pp. 860-863, May 2007.
 - [11] G. Ginis and J. Cioffi, "A Multi-User Precoding Scheme Achieving Crosstalk Cancellation with Application to DSL Systems", in *Proc. Conference Record of the Thirty-Fourth Asilomar Conference on Signals, Systems and Computers*, vol.2, pp. 1627-1631, October 2000.
 - [12] C. Windpassinger, R. Fischer, T. Vencel and J. Huber, "Precoding in Multiantenna and Multiuser Communications," *IEEE Transactions on Wireless Communications*, vol. 3, no. 4, pp. 1305-1316, July 2004.
 - [13] Futurewei Technologies, "G.fast: SNR Drop and FEXT Channel Variations due to Change of Alien Termination," ITU-T SG15 contribution 2013-10-q4-046, March 2013.
 - [14] E. Medeiros, T. Magesacher, P. Ödling, D. Wei, X. Wang, Q. Li, P.-E. Eriksson, C. Lu, J. Boschma, and B. van den Heuvel, "Modeling Alien-Line Impedance Mismatch in Wideband Vectored Wireline Systems," *IEEE Communications Letters*, vol. 18, no. 9, pp. 1527-1530, September 2014.
 - [15] Alcatel, "G.fast: Comparison of Linear and Non-linear Pre-coding," ITU-T SG15 Contribution 2013-01-Q4-046, January 2013.
 - [16] M. Costa, "Writing on Dirty Paper (Corresp.)," *IEEE Transactions on Information Theory*, vol. 29, no. 3, pp. 439-441, May 1983.
 - [17] Gene H. Golub and Charles F. Van Loan, *Matrix Computations (3rd Ed.)*, Baltimore, MD, USA: Johns Hopkins University Press, 1996.
 - [18] Ericsson AB, *Access Network Pair cable, TEL 312*, 2010. [Online]. Available: <http://goo.gl/4RdCXc>

Paper IV

Rate-Boosting Using Strong Crosstalk in Next Generation Wireline Systems

Abstract

Next-generation wireline systems may exploit frequencies up to several hundred MHz on short lines. Strong crosstalk coupling, comparable to the direct paths, is one of the main channel characteristics at high frequencies. Instead of fully canceling all crosstalk, we utilize strong crosstalk paths to boost data-rate for active users. Two linear precoding schemes, based on maximum ratio combining and convex optimization respectively, are proposed and applied to a common network topology. The precoding schemes exploit constructive crosstalk signals on unused lines or in unused parts of the spectrum on neighboring lines to boost data-rate while still complying with the regulated spectral power limits per line. More than 500 Mbps throughput gain per active user can be achieved compared to state-of-the-art linear precoding.

Based on: Y. Huang, T. Magesacher, E. Medeiros, C. Lu, P.-E. Eriksson, and P. Ödling, "Rate-Boosting Using Strong Crosstalk in Next Generation Wireline Systems," in *Proc. 2015 IEEE Global Communications Conference (GLOBECOM)*, San Diego, USA, December 2015. © 2015 IEEE. Reprinted with permission.

1 Introduction

Data-rate hungry services may soon push current wireline broadband networks to their limit. The fiber-to-the-home (FTTH) concept, which would conceivably satisfy the throughput demand, is still no ubiquitous reality since its installation requires large efforts in both time and money. The migration via a hybrid copper-fiber concept [1] bridges the gap by continuously using the copper wires to support the costly last-mile part. Recent standardization efforts have resulted in the emerging G.fast system [2, 3] capable of supporting in the order of 1 Gbps aggregate net data-rate on copper pairs. In its second version, even higher data-rates can be expected. Future efforts, such as [4–6], aim at providing multi-gigabit access via copper by exploring frequency ranges well beyond 100 MHz.

The first version of G.fast relies on linear precoding [7, 8] to mitigate crosstalk. Linear precoding is a well developed scheme and has been widely implemented in vectored digital subscriber line (DSL) systems for its effectiveness and low-complexity. In order to transmit below the regulated power spectrum density (PSD) mask on each line and each sub-carrier, power normalization is included in the linear precoder which, however, degrades the system performance at very high frequencies [9, 10]. In [11], the choice of the power normalization factor for linear precoding is posed as a linear programming problem, resulting in a moderate increase in delivered data-rate.

In practice, resources are still available for further data-rate boosting without additional hardware cost. For example, as part of the zero-touch philosophy, G.fast equipment could be pre-installed on a bundle basis regardless whether all customers have signed up or not. Thus, there could be more available lines than active users. Furthermore, users sharing the same binder may use either very-high-bit-rate digital subscriber line (VDSL2) [12] equipment or G.fast equipment. The lines of VDSL2 users will be idle for frequencies beyond 35 MHz [13]. In both cases, idle lines are available and already connected to transceiver equipment at the distribution point (DP).

In this paper, we exploit strong crosstalk from idle lines in a constructive way to boost the data-rate of active users (see Fig. 1), while mitigating destructive crosstalk among active users and fully obeying the spectral power limits. The supporting lines can be unused lines or lines with unused spectrum in the cable, which allows for permanent boosting. Alternatively, lines connecting users that are temporarily idle or have no data to transmit at the moment can be used for peak-rate boosting. Two linear precoding schemes are introduced in the downstream direction. The first method is maximum ratio combining (MRC), which is frequently used in wireless multiple-input-single-output transmission to maximize the delivered energy to the active users. In order to

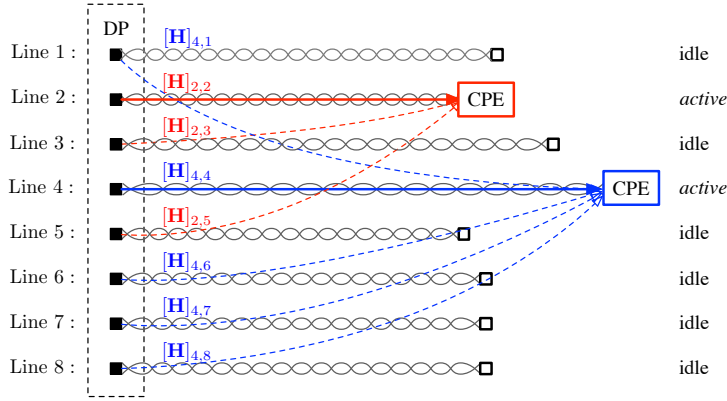


Fig. 1: Example scenario with two active CPEs and six idle lines contributing constructive FEXT. Line 2, 3 and 5 are chosen to support the CPE-2, and the other lines within the group are chosen to support CPE-4.

further exploit the rate-boosting potential via cooperative linear precoding, we formulate a convex feasibility problem resulting in the second precoder, which shows significant throughput gain at high frequencies.

2 Channel Characteristics at High Frequencies

In DSL systems, single line performance is defined as the throughput in an end-to-end transmission over a certain line with a fixed background-noise level. It can be viewed as an upper bound of the throughput on that line since no other interference or transmit power constraint is considered. Crosstalk among copper wires within a binder, classified into near-end crosstalk (NEXT) and far-end crosstalk (FEXT), is an inherent wireline channel property. In order to approach the single line performance for each line in the group, crosstalk cancellation is needed. NEXT can be mitigated by using duplexing methods such as frequency-division duplexing (FDD) or time-division duplex (TDD), whereas FEXT can be mitigated by vectoring [14], as indicated in the VDSL2 [15] and G.fast [2] standards.

In the downstream direction, which is our main focus in this paper, a precoder in the DP enables cooperative data transmission. Consider a vectored group of size N . Let $\mathcal{N} = \{1, \dots, N\}$ denote the set of line indices in the vectored group. Also, let $\mathbf{H} \in \mathbb{C}^{N \times N}$ denote the frequency domain channel matrix of the vectored group on a certain sub-carrier. The prevailing idea to

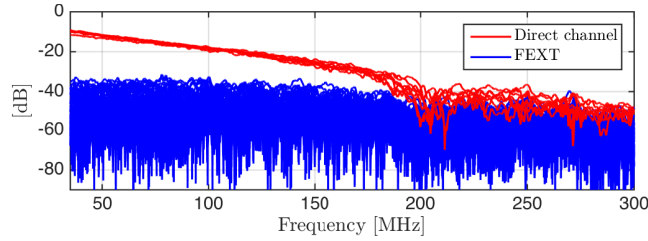
cancel out crosstalk is to use a linear precoder which diagonalizes the channel matrix [8]. Mathematically, the nearly optimal linear precoder $\mathbf{P} \in \mathbb{C}^{N \times N}$ is given by

$$\mathbf{P} = 1/\mu \mathbf{H}^{-1} \mathbf{H}_\Sigma,$$

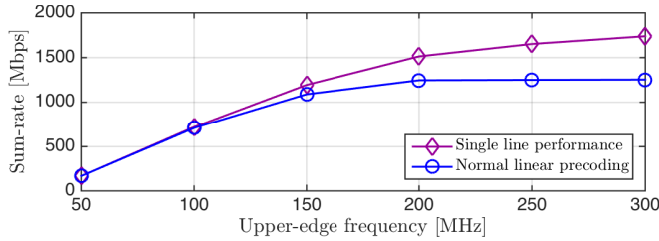
where \mathbf{H}_Σ is a diagonal matrix carrying the diagonal elements of \mathbf{H} . The scalar μ is defined to make the overall precoded signal comply with the transmit power constraint, *i.e.*,

$$\mu = \max_{i \in \mathcal{N}} \left\| [\mathbf{H}^{-1} \mathbf{H}_\Sigma]_{\text{row } i} \right\|_2. \quad (1)$$

When the frequency range is extended, new channel characteristics are observed. To demonstrate this, we take measurements for direct paths and FEXT paths from a 30 pairs, 100 m, 0.5 mm cable [16]. In this case study, 8 pairs are randomly chosen from a single binder. A sub-carrier spacing of 51.75 kHz has been used. Channel measurements are taken from 35 MHz up to 300 MHz (see Fig. 2a). The choice of 35 MHz yields a generous spectral margin with respect to the VDSL2 30 MHz profile. It can be observed that the FEXT becomes



(a) Channel measurements



(b) Accumulated bit-rate in the band from 35 MHz to upper-edge frequency

Fig. 2: Channel measurements and average accumulated bit-rate per line for an 8-line vectored group.

comparable to the direct channel as the frequency increases. As a consequence, the column-wise diagonal dominant (CWDD) property, which is the foundation of the near-optimal linear precoder, begins to diminish. Its influence on the system performance is illustrated in Fig. 2b.

In Fig. 2b, the average sum-rate for the 8 lines is shown versus available bandwidth, which is defined as upper-edge frequency minus 35 MHz. Although the bandwidth keeps increasing, the sum-rate of the linear precoding system diverges gradually from the single line performance and converges to a saturation level. By utilizing the strong crosstalk from idle pairs, however, it is possible to boost the rate beyond this saturation level.

3 Maximum Ratio Combining (MRC) Precoding Scheme for Rate-Boosting

3.1 Group-MRC precoder

Consider a scenario with K active users out of N vectored lines. A simplified example with $N = 8$ and $K = 2$ is sketched in Fig. 1.

Let $\mathbf{H}_{\text{sub}} \in \mathbb{C}^{K \times N}$ denote the channel paths ending in the active customer premise equipment (CPE). The signal $\mathbf{r} \in \mathbb{C}^{K \times 1}$ received by the active users is given by $\mathbf{r} = \mathbf{H}_{\text{sub}}\mathbf{s} + \mathbf{n}$, where $\mathbf{s} \in \mathbb{C}^{N \times 1}$ is the transmit signal and $\mathbf{n} \in \mathbb{C}^{K \times 1}$ denotes noise. We are looking for a “good” precoder $\mathbf{P}_{\text{sub}} \in \mathbb{C}^{N \times K}$ yielding $\mathbf{s} = \mathbf{P}_{\text{sub}}\mathbf{x}$, where $\mathbf{x} \in \mathbb{C}^{K \times 1}$ are the symbols to be transmitted, such that the active CPEs get a higher receive signal-to-noise ratio (SNR) compared to vectoring using only the active lines. In order to cancel the destructive crosstalk among the active users, we also want $\mathbf{H}_{\text{sub}}\mathbf{P}_{\text{sub}} = \mathbf{D}$, where $\mathbf{D} \in \mathbb{R}^{K \times K}$ is a diagonal matrix.

We apply the concept of MRC to the precoded signals with the goal of rate-boosting via crosstalk. If all N twisted pairs are available to support CPE no. k (*i.e.*, $K = 1$), the effective channel is the k -th row of \mathbf{H} , denoted as $\mathbf{h}_k^T = [\mathbf{H}]_{k1}, \dots, [\mathbf{H}]_{kN}$. Also notice that each element of \mathbf{h}_k^T represents channel attenuation, where $\|\mathbf{h}_k^T\|_1^2$ is larger than $\|\mathbf{h}_k^T\|_2^2$. Thus, to maximize the receive SNR and therefore boost the bit-rate, assign the precoder to be a column vector as

$$\mathbf{p}_k = \frac{1}{\mu} \begin{bmatrix} \frac{[\mathbf{H}]_{k1}^*}{|[\mathbf{H}]_{k1}|} & \dots & \frac{[\mathbf{H}]_{kN}^*}{|[\mathbf{H}]_{kN}|} \end{bmatrix}^T,$$

where μ is the normalization factor defined similarly as in Eq. (1). The precoded signals from different transmitters are added up coherently, yielding a received

signal at the active CPE given by

$$r_k = \mathbf{h}_k^T \mathbf{p}_k x_k + n = 1/\mu \sum_{i=1}^N |[\mathbf{H}]_{ki}| x_k + n. \quad (2)$$

In the general case of $K > 1$, group-MRC can be performed. The i -th column of \mathbf{H}_{sub} represents the channel paths originating from transmitter i . For each transmitter, there should be only one targeted receiver. Therefore, a grouping metric is needed to determine the group of “supporting” line(s) assigned to each active user. Assume for the i -th column of \mathbf{H}_{sub} , $[\mathbf{H}_{\text{sub}}]_{l_i i}$ is chosen to be the supporting path from transmitter i . Accordingly, assign an $N \times K$ MRC precoder matrix \mathbf{P}_{MRC} whose entries are composed by

$$[\mathbf{P}_{\text{MRC}}]_{ij} = \begin{cases} \frac{[\mathbf{H}_{\text{sub}}]_{ji}^*}{|[\mathbf{H}_{\text{sub}}]_{ji}|} & \text{if } j = l_i, \\ 0 & \text{otherwise.} \end{cases} \quad (3)$$

Also include the second precoder matrix

$$\mathbf{P}_{\text{D}} = (\mathbf{H}_{\text{sub}} \mathbf{P}_{\text{MRC}})^{-1} (\mathbf{H}_{\text{sub}} \mathbf{P}_{\text{MRC}})_{\Sigma}$$

to cancel the destructive crosstalk among the active users. Together with the power scaling factor μ , the overall precoder can be written as

$$\mathbf{P}_{\text{sub}} = 1/\mu \mathbf{P}_{\text{MRC}} \mathbf{P}_{\text{D}}$$

where $\mu = \max_{i \in \mathcal{N}} \|[\mathbf{P}_{\text{MRC}} \mathbf{P}_{\text{D}}]_{\text{row } i}\|_2$.

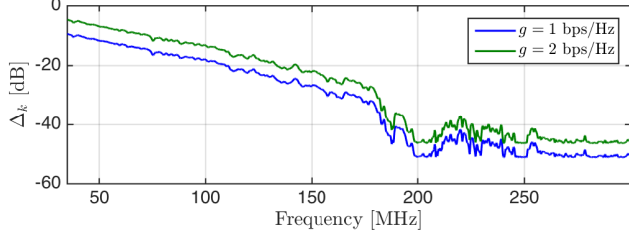
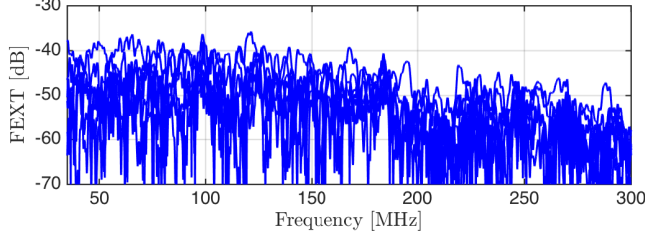
3.2 Data-rate performance

With the MRC of the precoded signal, we can realize an equivalent channel

$$\boldsymbol{\rho}_{\text{MRC}} = \text{diag}(\mathbf{H}_{\text{sub}} \mathbf{P}_{\text{sub}}), \quad \boldsymbol{\rho}_{\text{MRC}} \in \mathbb{R}^{K \times 1}$$

to the active users. To quantify the rate-boosting contribution from the resulting channel, we calculate the increased spectrum efficiency compared to a reference linear precoding system, whose precoded equivalent channel is denoted by $\boldsymbol{\gamma}$. The reference can be the single line performance, normal linear-precoding performance or any other control group. Given a certain $\boldsymbol{\gamma}$ and transmit power P_{tx} , we can calculate the spectrum efficiency gain on line k as

$$\begin{aligned} g([\boldsymbol{\gamma}]_k, P_{\text{tx}}) &= \log_2 \left(1 + \frac{P_{\text{tx}} |[\boldsymbol{\rho}_{\text{MRC}}]_k|^2}{\sigma^2 \Gamma} \right) - \log_2 \left(1 + \frac{P_{\text{tx}} |[\boldsymbol{\gamma}]_k|^2}{\sigma^2 \Gamma} \right) \\ &= \log_2 \left(1 + \frac{\Delta_k \cdot P_{\text{tx}}}{\sigma^2 \Gamma + P_{\text{tx}} |[\boldsymbol{\gamma}]_k|^2} \right), \end{aligned} \quad (4)$$

(a) Theoretical requirement on Δ_k (Eq. (5))

(b) FEXT coupling ending in CPE-2

Fig. 3: Comparison between the theoretical requirement on Δ_k to gain a desired g from the normal linear precoder performance and actual FEXT coupling level available to support the gain.

where σ^2 is the background noise power and Γ is the reserved SNR gap. Here we define a parameter $\Delta_k = |[\boldsymbol{\rho}_{\text{MRC}}]_k|^2 - |[\boldsymbol{\gamma}]_k|^2$, which denotes the increased channel gain obtained by constructive FEXT on line k . Equivalently, we can expect that the required boosting in channel gain for a certain spectrum efficiency gain should be

$$\Delta_k [\text{dB}] = \log_{10}(2^g - 1) + c_k, \quad (5)$$

where $c_k = \log_{10}\left(\left(\sigma^2\Gamma + P_{\text{tx}}|[\boldsymbol{\gamma}]_k|^2\right)/P_{\text{tx}}\right)$ is a constant on a certain sub-carrier of line k .

Taking line 2 of our measurements as an example, assume $P_{\text{tx}} = -76$ dBm/Hz, $\sigma^2 = -140$ dBm/Hz and $\Gamma = 9.8$ dB. In Fig. 3a, we show the theoretical requirement on Δ_k to increase the spectrum efficiency from the normal linear precoder performance by $g = 1$ bps/Hz and $g = 2$ bps/Hz at different frequencies. For other values of g , the curve shifts in vertical direction with a term of $\log_{10}(2^g - 1)$.

Fig. 3a reveals that MRC of constructive FEXT to boost data-rate requires

much higher Δ_k at lower frequencies than at higher frequencies. In Fig. 3b, it is shown that the available FEXT coupling at lower frequencies, however, is not that much stronger than the FEXT level of higher frequencies, which significantly limits the potential gain we can extract from the lower part of the frequency range. For frequencies above 150 MHz, it seems more likely to achieve the additional power requirement Δ_k . Therefore, we would rather focus on and explore the right-hand side of the frequency axis and utilize the strong crosstalk to achieve rate-boosting. Hereinafter, we refer to the frequency ranges above and below 150 MHz as high-frequency range and low-frequency range, respectively.

To show the rate-boosting result with a practical channel setup, we consider a grouping criterion based on the magnitude of crosstalk couplings, *i.e.*,

$$l_i = \arg \max_l |[\mathbf{H}_{\text{sub}}]_{li}|^2, \quad (6)$$

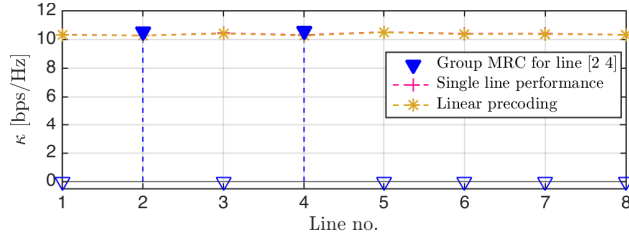
and construct \mathbf{P}_{MRC} as in Eq. (3). In our experimental setup, the copper pairs are short and have equal lengths. The corresponding FEXT coupling coefficients are therefore similar in magnitude level. This implies that the maximum power of Eq. (6) for different i will not always concentrate on the same l . It enables an “even-share” grouping scheme where the number of supporting lines for each active user is on average the same over the studied frequencies. Based on the measurements described in Section 2, Fig. 4 presents the average spectrum efficiency of the group-MRC method for both low-frequency and high-frequency range. Considering a bit cap $\bar{b} = 12$ bits, the average spectrum efficiency κ for each line is calculated as

$$\kappa = \frac{\sum_{i=1}^{N_{\text{tone}}} \min\{\bar{b}, \log_2(1 + SNR/\Gamma)\}}{N_{\text{tone}}}, \quad (7)$$

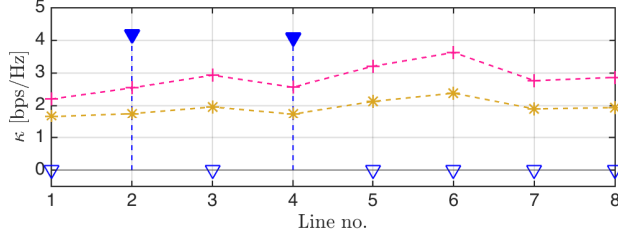
where N_{tone} is the number of sub-carriers involved and SNR is the receive signal-to-noise power ratio.

According to Fig. 4a, the gain in spectrum efficiency is barely noticeable in the low-frequency range since the crosstalk paths are not strong enough to contribute, which is consistent with the conclusion in Fig. 3. In the high-frequency range (see Fig. 4b), the group-MRC shows more than 2 bps/Hz spectrum efficiency gain on average compared to its linear-precoding counterpart.

When comparing the performance of the group-MRC precoder to the normal linear precoder on each sub-carrier, however, we notice that the MRC scheme is not always a good solution for rate-boosting. In Fig. 5, there are negative gains at some sub-carriers, where the MRC precoder delivers a lower data-rate to active users than the normal linear precoder. This disadvantage of the MRC precoder becomes more notable when the number of available idle



(a) 35 MHz–150 MHz



(b) 150 MHz–300 MHz

Fig. 4: Spectrum efficiency comparison for group-MRC precoding with the grouping scheme defined in Eq. (6) for different frequency ranges.

lines decreases, or equivalently, K increases (comparing Fig. 5a with Fig. 5b). The reduced effective channel gain results partly from the normalization factor μ . As μ equals to the maximum norm-2 of the precoder's row-vectors, simply multiplying with $1/\mu$ may cause a large penalty in the resulting channel gain of the MRC precoder. Furthermore, the rate-boosting performance of the MRC precoder depends largely on the chosen grouping metric. As shown in Fig. 5, the metric chosen in Eq. (6) does not give a “fair” boosting to active users at most sub-carriers.

4 Optimized Precoding Scheme for Rate-Boosting

As discussed above, the MRC precoder does not guarantee that we can always achieve the optimal utilization of available idle pairs. Therefore, further investigation on the rate-boosting possibility in a general case is desired. We formulate this as an optimization problem, where the objective is to find a linear precoder \mathbf{P}_{opt} giving an equivalent channel

$$\mathbf{\Theta} = \mathbf{H}_{\text{sub}} \mathbf{P}_{\text{opt}}, \quad (8)$$

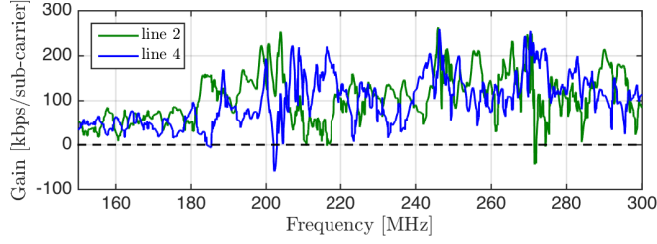
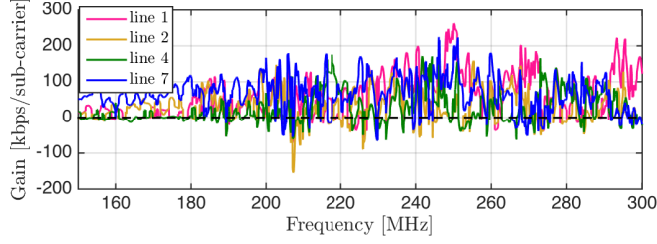

 (a) Active users $K = 2$ ($N = 8$)

 (b) Active users $K = 4$ ($N = 8$)

Fig. 5: Bit-rate gain of the group-MRC precoder over 150 MHz–300 MHz, compared to the normal linear precoder.

subject to the following constraints:

Channel gain By optimally utilizing the available constructive FEXT, the equivalent channel with a linear precoder results in $\boldsymbol{\rho}_{\text{opt}} = \text{diag}(\mathbf{H}_{\text{sub}}\mathbf{P}_{\text{opt}})$, and can deliver a data-rate as high as possible to active users given a certain channel environment.

Residual crosstalk It is not necessary to have the off-diagonal entries of the effective channel $\boldsymbol{\Theta}$ to be strictly 0, which is the main objective of the traditional linear precoder. Instead, residual crosstalk can be allowed as long as its maximum power is lower than a small number ϵ^2 . In order not to decrease the receive SNR, we confine ϵ^2 to be lower than the background noise level.

Transmit power To fulfil the transmit power constraint, the precoder should have its row vector power confined by $\|\mathbf{P}_{\text{opt}}\|_{l,1\dots K} \leq 1$, for $l = 1, \dots, N$.

The objective together with the three constraints result in a feasibility problem. Let \otimes stand for the Kronecker product, and $\text{vec}(\cdot)$ operate on a matrix to

stack the columns of the matrix to be a long column vector. We can rewrite the equivalent channel in Eq. (8) as $\mathbf{A}\mathbf{p} = \boldsymbol{\theta}$, where $\mathbf{A} = \mathbf{I}_K \otimes \mathbf{H}_{\text{sub}} \in \mathbb{C}^{K^2 \times KN}$, $\mathbf{p} = \text{vec}(\mathbf{P}_{\text{opt}}) \in \mathbb{C}^{KN \times 1}$, and $\boldsymbol{\theta} = \text{vec}(\boldsymbol{\Theta}) \in \mathbb{C}^{K^2 \times 1}$. The related feasibility problem with convex constraints [17] can be written as

$$\begin{aligned} \mathbf{p}_{\text{opt}} = \quad & \text{find} \quad \mathbf{p} \\ & \text{subject to} \quad \mathbf{E}_d \mathbf{A} \mathbf{p} = \boldsymbol{\rho}_{\text{opt}} \\ & \quad \max |\mathbf{E}_d^c \mathbf{A} \mathbf{p}| \leq \epsilon \\ & \quad \|\mathbf{E}_{r,l} \mathbf{p}\|_2 \leq 1 \quad \text{for } l = 1, \dots, N. \end{aligned} \quad (9)$$

Here we define three versions of the matrix \mathbf{E} such that $\mathbf{E} \text{vec}(\mathbf{X})$ results in a vector composed by specific entries of the original matrix \mathbf{X} . $\mathbf{E}_d \in \mathbb{R}^{K \times K^2}$ is defined to extract the diagonal entries such as $\mathbf{E}_d(\mathbf{A}\mathbf{p}) = \text{diag}(\mathbf{H}_{\text{sub}} \mathbf{P}_{\text{opt}})$, *i.e.*,

$$[\mathbf{E}_d]_{ij} = \begin{cases} 1 & \text{if } j = (i-1)K + i, \\ 0 & \text{otherwise.} \end{cases}$$

$\mathbf{E}_d^c \in \mathbb{R}^{K(K-1) \times K^2}$ is defined to extract the off-diagonal entries in a similar manner, *i.e.*,

$$[\mathbf{E}_d^c]_{ij} = \begin{cases} 1 & \text{if } j = i + \lfloor (i-1)/K \rfloor + 1, \\ 0 & \text{otherwise.} \end{cases}$$

Finally, $\mathbf{E}_{r,l} \in \mathbb{R}^{K \times KN}$ extracts the l -th row of the matrix as $\mathbf{E}_{r,l} \mathbf{p} = [\mathbf{P}_{\text{opt}}]_{l,1 \dots K}$, *i.e.*,

$$[\mathbf{E}_{r,l}]_{ij} = \begin{cases} 1 & \text{if } j = (i-1)N + l, \\ 0 & \text{otherwise.} \end{cases}$$

The last two constraints in Eq. (9) generate a fixed region around the optimal solution. The main source that influences the feasibility of the optimization problem lies in the first function, which is affine. If we are too aggressive in achieving gain and set too high values for the desired $\boldsymbol{\rho}_{\text{opt}}$, the optimization problem in Eq. (9) will become unfeasible. Therefore, to approach the highest possible $\boldsymbol{\rho}_{\text{opt}}$ and still fulfil the other two constraints, we propose a feasibility-based iterative method as described in Table 1.

As our final goal is to provide the active users with a boosted data-rate, we set the main iteration-driving parameter to be g , as defined in Eq. (4), which represents a spectrum efficiency gain on a certain sub-carrier compared to a reference performance. The gains for all K active users compose a vector \mathbf{g} . Again, let $\boldsymbol{\gamma}$ denote the equivalent channel of the reference performance. Define a scalar parameter $\beta_1 = -\sigma^2 \Gamma / P_{\text{tx}}$, which is constant over the whole frequency range, and a vector parameter $\boldsymbol{\beta}_2 = |\boldsymbol{\gamma}|^2 - \beta_1$, which keeps constant on a certain

Table 1: Proposed iteration for optimizing a rate-boosting precoder

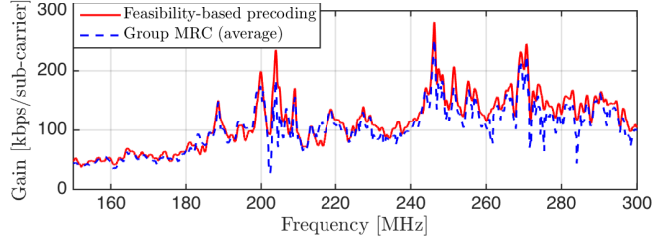
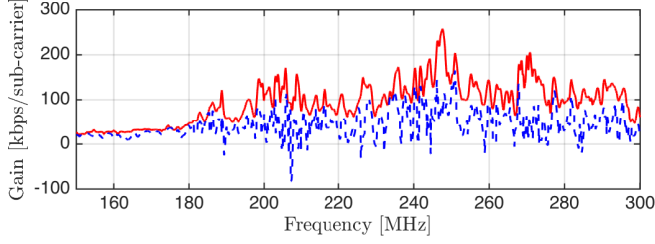
On sub-carrier t :
Initialize
<ul style="list-style-type: none"> • Set gain step size as Δ_g; • Set basic gain for each line $\mathbf{g} = \mathbf{g}_0$; • Set parameters $\beta_1 = -\sigma^2\Gamma/P_{\text{tx}}$, $\beta_2 = \gamma - \beta_1$; • $\rho_{\text{opt}}^2 = 2^{\mathbf{g}} \odot \beta_2 + \beta_1$; • Set feasible = 1.
while feasible = 1 do
<ul style="list-style-type: none"> • Solve optimization problem in Eq. (9); if Failed then – feasible = 0; end if • if feasible = 1 then – Reshape \mathbf{p}_{opt} to \mathbf{P}_{opt}; – Update $\mathbf{g} = \mathbf{g} + \Delta_g$; – Update $\rho_{\text{opt}}^2 = 2^{\mathbf{g}} \odot \beta_2 + \beta_1$; end if
end while

sub-carrier. Together with these parameters, we can calculate the desired ρ_{opt} using the expected \mathbf{g} as

$$\rho_{\text{opt}} = (2^{\mathbf{g}} \odot \beta_2 + \beta_1)^{1/2},$$

where \odot denotes the Hadamard product and the power is taken elementwisely. Starting with a conservative gain setting \mathbf{g}_0 and increasing the gain gradually with a step size Δ_g , we will reach a ρ_{opt} after j iterations that makes the whole setup unfeasible. The optimized precoder vector \mathbf{p}_{opt} obtained as the result of iteration $j - 1$ gives the maximum possible ρ_{opt} . The starting points in \mathbf{g}_0 are determined by the original and expected data-rate for the active users. For example, the spectrum efficiency on line 2 and 4 are originally 2 bps/Hz and 4 bps/Hz at a certain sub-carrier, and aim for a boosting result of 3 bps/Hz and 5 bps/Hz, respectively. A possible choice for initialization can be $\mathbf{g}_0 = [2, 4]^T$, and setting the same Δ_g for both lines.

In the following simulations, we choose the normal linear precoding performance as the baseline. Fig. 6 compares the rate-boosting results between the group-MRC method applying the grouping metric in Eq. (6) and the feasibility-based optimization method summarized in Table 1. We focus on the frequency range between 150 MHz and 300 MHz, where strong crosstalk dominates. For

(a) Active users $K = 2$ ($N = 8$)(b) Active users $K = 4$ ($N = 8$)**Fig. 6:** Data-rate gain at studied frequencies with different number of active users.

each sub-carrier, the increased bit-rate compared to the throughput of normal linear precoding is calculated. For the feasibility-based optimization method, the curves for active users are identical since we choose the even-gain strategy in the iterative process. For the group-MRC method, the average increase over the targeted lines is presented.

In Fig. 6, we observe that the optimized precoder has a curve that is generally higher than the group-MRC curve, which means that the simple metric given by Eq. (6) does not fully explore the rate-boosting ability from the constructive FEXT paths. The advantage of the optimized precoder is more obvious when the number of available idle lines for each active user decreases. Most importantly, the optimized precoder will never yield a negative gain as the MRC method does. The superior performance of the optimized precoder is rooted mainly in the following three aspects. First, the normalization factor μ limits the possible power gain of the MRC method. Second, the vectoring precoder \mathbf{P}_D that is included in the group-MRC precoder sets a strict requirement in canceling crosstalk. The purpose of \mathbf{P}_D is to diagonalize the channel matrix and generate zero-valued off-diagonal entries for $\mathbf{H}_{\text{sub}}\mathbf{P}_{\text{sub}}$. In fact, as also implemented in the optimized precoder, we only need to limit the power of those

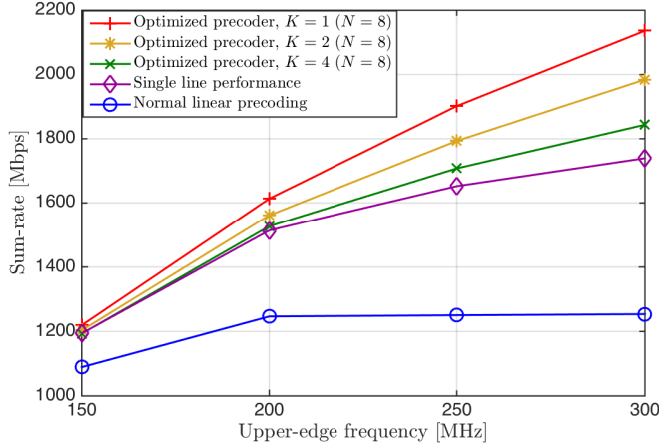


Fig. 7: Accumulated average sum-rate per user versus available bandwidth (35 MHz to upper-edge frequency).

entries to be lower than the background noise level so that the related precoder design constraint gets relaxed. Third, the grouping-metric depends highly on frequency and on channel conditions. It is hard to group the idle lines in an optimal way to perform rate-boosting, since the FEXT varies strongly both over frequency and over lines. The optimized precoder, on the other hand, provides a target-oriented solution without limitation from any specific grouping scheme.

In Fig. 7, we trace back to the problem raised in Section 2, specifically in Fig. 2b. Again, the average sum-rate over active users is calculated. For the case of $K = 1$, where 7 idle lines are available to support rate-boosting, the basic MRC precoding in Eq. (2) is performed. For the cases of $K = 2$ and $K = 4$, the optimized precoding scheme is applied. It is clear that by utilizing strong crosstalk from idle lines in the vicinity, the linear precoder can break through the saturation level at high frequencies and provide the active users with significant data-rate gain. In the simulation starting from 35 MHz and ending in 300 MHz, we can achieve 589.61 Mbps sum-rate gain per active user compared to the normal linear precoder when 4 idle lines are available for $K = 4$ active users; we gain 729.41 Mbps per user when 6 idle lines are available for $K = 2$ active users; and we gain 882.79 Mbps per user when 7 idle lines are available for $K = 1$ active user.

5 Conclusion

In the next generation wireline systems, the achievable data-rate with linear precoding saturates gradually after a certain frequency (*e.g.*, 150 MHz for our measured channel). To break through this saturation level, we propose rate-boosting for active end-users, utilizing strong crosstalk at high frequencies from idle twisted pairs within the same vectored group. Group-MRC precoding exhibits a substantial data-rate improvement depending on the number of supporting lines. In order to further enhance the performance, we present an optimization-based solution. Compared to standard linear precoding, more than 500 Mbps data-rate gain per active user can be achieved when exploiting bands up to 300 MHz.

References

- [1] P. Ödling, T. Magesacher, S. Höst, P. O. Börjesson, M. Berg, and E. Areizaga, "The Fourth Generation Broadband Concept," *IEEE Communications Magazine*, vol. 47, no. 1, pp. 62-69, January 2009.
- [2] ITU, "Fast Access to Subscriber Terminals - Physical Layer Specification," Recommendation Draft ITU-T G.9701, 2014. [Online]. Available: <https://www.itu.int/rec/T-REC-G.9701/en>
- [3] M. Timmers, M. Guenach, C. Nuzman, and J. Maes, "G.fast: Evolving the Copper Access Network," *IEEE Communications Magazine*, vol. 51, no. 8, pp. 74-79, August 2013.
- [4] W. Coomans, R. Moraes, K. Hooghe, A. Duque, J. Galaro, M. Timmers, A. van Wijngaarden, M. Guenach, and J. Maes, "XG-FAST: Towards 10 Gb/s Copper Access," in *Proc. 2014 GLOBECOM Workshops (GC Wkshps)*, pp. 630-635, December 2014.
- [5] Celtic-Plus, "Multi-Gigabit Access via Copper, <http://goo.gl/cBuoLA> (date visited: March 23, 2015), March 2015.
- [6] 4GBB, "The Initiator of G.fast - A Paradigm Shift in Access Technology, www.4gbb.eu (date visited: Mar. 23, 2015).
- [7] R. Cendrillon, G. Ginis, E. Van den Bogaert, and M. Moonen, "A Near-Optimal Linear Crosstalk Canceler for Upstream VDSL," *IEEE Transactions on Signal Processing*, vol. 54, no. 18, pp. 3136-3146, 2006.

- [8] R. Cendrillon, G. Ginis, E. Van den Bogaert, and M. Moonen, "A Near-Optimal Linear Crosstalk Precoder for Downstream VDSL," *IEEE Transactions on Communications*, vol. 55, no. 5, pp. 860-863, May 2007.
- [9] Lantiq, "G.fast: G.fast Performance over KPN Cable," ITU-T SG15 Contribution 338, July 2013. [Online]. Available: <http://goo.gl/qnA9DN>
- [10] Alcatel, "G.fast: Comparison of Linear and Non-linear Pre-coding," ITU-T SG15 Contribution 2013-01-Q4-046, January 2013.
- [11] F. Müller, C. Lu, P.-E. Eriksson, S. Höst, and A. Klautau, "Optimizing Power Normalization for G.fast Linear Precoder by Linear Programming," in *Proc. 2014 IEEE International Conference on Communications (ICC)*, pp. 4160-4165, June 2014.
- [12] ITU, "Very high speed digital subscriber line transceivers 2 (VDSL2)," Recommendation ITU-T G.993.2, December 2011. [Online]. Available: <https://www.itu.int/rec/T-REC-G.993.2-201112-I/en>
- [13] D. Wei, A. Fazlollahi, G. Long, and E. Wang, "G.fast for FTTdp: Enabling Gigabit Copper Access," in *Proc. 2014 GLOBECOM Workshops (GC Wkshps)*, pp. 668-673, December 2014.
- [14] G. Ginis and J. Cioffi, "Vectored Transmission for Digital Subscriber Line Systems," *IEEE Journal on Selected Areas in Communications*, vol. 20, no. 5, pp. 1085-1104, June 2002.
- [15] ITU, "Self-FEXT cancellation (vectoring) for use with VDSL2 transceivers," Recommendation ITU-T G.993.5, April 2010. [Online]. Available: <https://www.itu.int/rec/T-REC-G.993.5/en>
- [16] Ericsson AB, *Access Network Pair cable, TEL 312*, 2010. [Online]. Available: <http://goo.gl/4RdCXc>
- [17] S. Boyd and L. Vandenberghe, *Convex Optimization*. Cambridge University Press, 2014.

Paper V

Enabling DSL and Radio on the Same Copper Pair

Abstract

To increase indoor coverage for mobile services, we propose a residential small cell infrastructure making use of the existing copper plant. The system is cabinet-based, collocated with VDSL2 and uses small pieces of spectrum next to VDSL2. Inspired by the Ericsson Radio Dot System, it challenges the femtocell paradigm offering full macro functionality in the small cells. An interesting service potential is offered albeit the added mobile traffic capacity is moderate as it is limited by the copper fronthaul.

Based on: Y. Huang, E. Medeiros, S. Höst, T. Magesacher, P.-E. Eriksson, C. Lu, P. Ödling, and P. O. Börjesson, “Enabling DSL and Radio on the Same Copper Pair,” in *Proc. 2015 IEEE International Conference on Communications (ICC)*, London, U.K., pp. 1031–1035, June 2015. © 2015 IEEE. Reprinted with permission.

1 Introduction

The copper access network plays a key role in the evolutionary process of delivering broadband services [1]. Relaying radio signals over high-quality copper cables, as demonstrated by the system introduced in [2], can provide full macro-cell functionality to indoor small cells fed over cables. While [2] focuses on indoor-enterprise environments using standard LAN cables, we pose the question whether it could be used to realize a vision of connected homes exploiting the edge of the access network. Given the increased interest in residential small cells in standardisation bodies and the increasing market uptake of femtocells, the concepts presented in [2] could be extended to the public switched telephone network (PSTN), representing a valuable market opportunity for operators.

The amount of attention given to residential small cells is increasing fast. This is partly fuelled by increasing capacity demands calling for a densification of the cellular networks and insights into the cost of doing so [3]. Estimations in [4, 5] hint that between 70 % and 90 % of the traffic in the mobile networks is generated indoors, and it is suggested that the homes are natural new sites for small cells. But the drive towards small cells is also coming from changes in how we live and how we construct our dwellings. Thick fire-safe concrete walls increasingly block radio waves as we move our systems higher up in frequency. New window types with high energy insulation often have a built-in thin metal layer sealing off the interior both thermally and electromagnetically. Achieving indoor coverage becomes increasingly difficult without placing an antenna inside the home.

The main approach to get an antenna inside the home today is by deploying a femtocell. Here we go deeper into the Radio Dot System [2] idea presented by Ericsson. Instead of using standard LAN cables, we focus on twisted pairs in the PSTN copper plant, using the spectrum above VDSL2 17 MHz profiles but below G.fast (the next generation DSL) and maintaining so low interfering signal levels that these and other legacy systems remain unaffected at large. Thus, we argue that the extended concept is realistic and deployable, albeit it requires similar augmentation of the regulatory regimes like any new DSL system would. We perform the spectrum planning by optimizing for capacity in a typical plant topology and show that decent bit rates can be delivered. In [6] and [7], an alternative femtocell architecture is investigated. It superimposes the radio signal on the lower part of VDSL2 spectrum, starting from 100 kHz, and performs compound MIMO processing over air and cable channels. Although benefiting from lower cable attenuation, directly usage of VDSL2 spectrum makes this system suffer from inevitable VDSL2 interference, and vice versa.

In this paper we intend to develop a realistic and deployable system architecture that is collocated with VDSL2 in the cabinets of the telephony copper

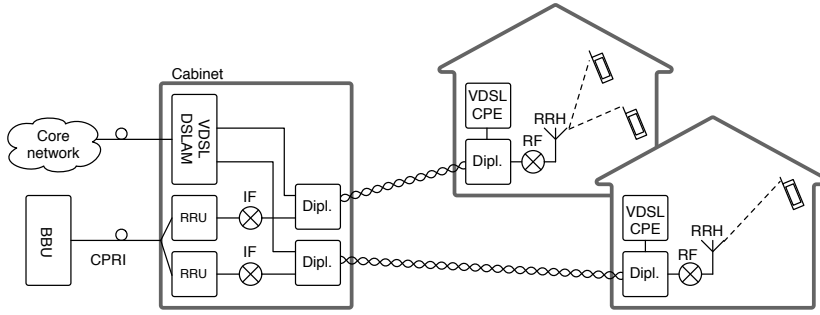


Fig. 1: A schematic for the proposed radio-over-copper system. Notice the co-location of DSL equipment and remote radio units in the cabinet.

network. We extend the concept presented in [2] by evaluating its feasibility over regular telephony cables, using the spectra between VDSL2 [8] and G.fast [9]. Disregarding the losses in the radio channel, the available capacity in the copper loop is evaluated at the chosen band. We optimize the placement of downlink and uplink bands to avoid interfering with legacy systems, and as a result determine the maximum loop lengths over which radio signals can be deployed.

The paper is organized as follows. In Section 2, the system concept is introduced. In Section 3, achievable throughput and coexistence are investigated. Section 4 presents a case study with gap-band optimization and Section 5 concludes the work.

2 Why and Where

The system topology considered in this paper is depicted in Fig. 1. We have a location such as a home connected with telephony wiring feeding radio equipment in turn accessing an indoor radio channel. A traditional femtocell architecture terminates the copper line with some flavor of DSL, say VDSL2, backhauling the femtocell traffic over a bitstream connection. Suppose that we now want to deliver an analog fronthaul service over the copper but in parallel to VDSL2 rather than using it as backhaul. Is it possible and if so what capacity do we release? These are the questions we attempt to answer with this paper.

In Fig. 1 the baseband unit (BBU) is located centralized in the network, and the radio signal is sent out to the remote radio unit (RRU) digitally with *e.g.*, CPRI [10] using a fiber connection. The RRU in this setup is typically

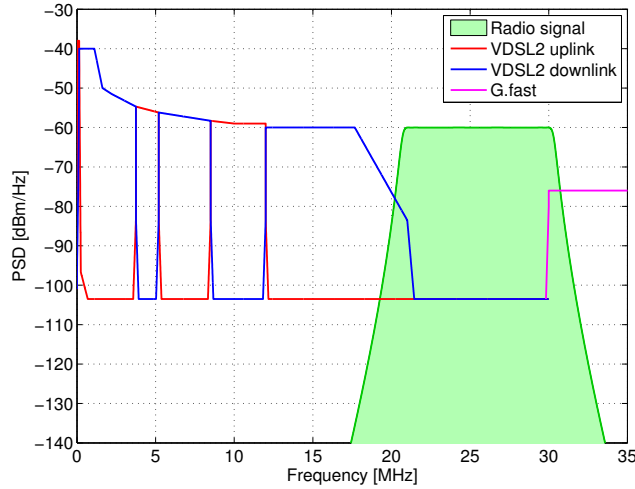


Fig. 2: Bandplans for VDSL2, G.fast and the band of interest for the proposed radio-over-copper system, pictured as a green shaded area.

co-located with the VDSL2 digital subscriber line access multiplexer (DSLAM) in the cabinet. In the downlink direction, the radio signal is up-converted to the band above the VDSL2 signal. A diplexer (Dipl. in the figure) combines the VDSL2 signal and the radio signal on the twisted pair. At the customer premises a second diplexer splits the signals for the VDSL2 customer premises equipment (CPE) and the remote radio head (RRH). Shifting the radio signal up in frequency to the required band gives indoor mobile coverage. A similar procedure occurs in the uplink direction, where the RRH down-converts the radio signal to adequate frequencies in the copper loop. After transmission through the twisted pair, the analog radio signal is sampled at the RRU.

The frequency range we intend to make use of is shown in Fig. 2. The leftmost part of the figure shows the various up- and downlink bands of VDSL2 and the right part shows one of the possible options for the starting frequency of G.fast (30 MHz). This particular spectrum plan was defined by ITU [11] and is typical for what can be expected in many countries. Although VDSL2 30 MHz profiles have been standardized for years, their market penetration in western countries is much lower compared to their 17 MHz counterparts. Therefore, in this paper we target unused spectra between 17 MHz and 30 MHz.

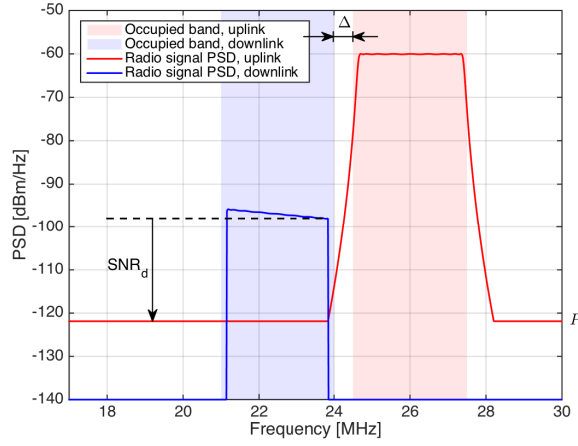
The focus of this work is on spectrum planning and throughput evaluation. Several related issues are left for further study. First, we do not consider crosstalk originating from VDSL2 or G.fast users in neighboring lines. The

band we intend to use lies spectrally between VDSL2 and G.fast. Thus, there is only crosstalk of leakage signals at the band edges. Second, we assume that there is no crosstalk in the VDSL2-G.fast gap band from other radio-over-copper systems—that is, we limit our focus to scenarios with a single radio-over-copper system in the last-drop cable. This assumption is reasonable because the crosstalk between radio-over-copper systems could be dealt with by crosstalk cancellation schemes similar to those used in VDSL2 and G.fast. Third, we do not consider the impact of electromagnetic compatibility. In order to limit unwanted radio egress, we keep the transmit power spectrum density (PSD) in the band of interest between -60 dBm/Hz and -80 dBm/Hz. This choice of transmit PSD is compatible with the limiting PSD masks defined for 30 MHz VDSL2 profiles. Consequently, the egress noise generated by the proposed system would be comparable to that caused by a standard-compliant 30 MHz VDSL2 system. However, analog radio-over-copper transmission remains vulnerable to radio ingress. Interference that is picked up by the copper pair in the gap band directly affects the signal quality, both in downlink and uplink direction. The coexistence analysis presented in the following sections is merely a first step in assessing the feasibility of an analog radio-over-copper system hosting a radio signal between VDSL2 and G.fast.

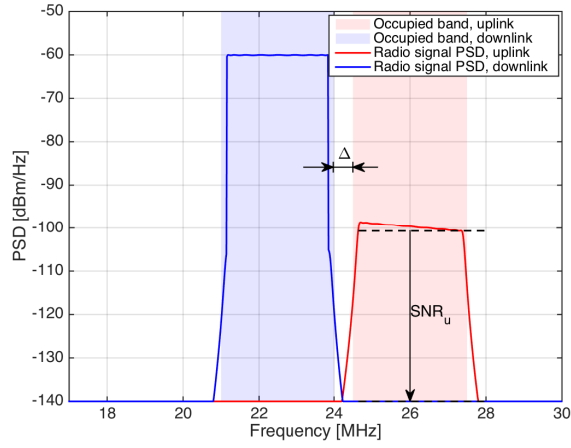
3 Coexistence and Capacity

In our system analysis, we begin by placing the downlink band for the radio signal starting at 21 MHz. Assume the VDSL2 system uses a bandplan occupying frequencies up to 17 MHz (*e.g.*, the FDD bandplan 998ADE17 [8]). Appropriate signal separation through the diplexers pushes the out-of-band leakage from VDSL2 right to the noise floor of the radio signal, and vice versa. The VDSL2 bandplan 998ADE17 shown in Fig. 2 ends with a downlink band in 12–17 MHz. The diplexer filters separating the signals will work on similar power levels, since both are either attenuated (on the RRH side) or un-attenuated (on the RRU side). The alternative to start with the uplink for the radio signal results in an unbalance of amplitudes, which requires substantially more attenuation in the stop band of the filters.

The narrowest bandwidths used in a modern mobile communication system, such as LTE [12], are 1.4 MHz, 3 MHz and 5 MHz, each having a built-in guard band. Unfortunately, two of the 5 MHz bands do not fit into our intended spectrum span from 21 MHz to 30 MHz and two 1.4 MHz bands yield a perhaps less than impressive capacity. Thus we focus on fitting two of the 3 MHz bands. This gives a single parameter to be optimized for the resulting capacity, namely the starting frequency of the 3 MHz uplink band.



(a) RRH side



(b) RRU side

Fig. 3: Mutual interference between uplink and downlink radio signals in the copper cable.

3.1 Downlink

Fig. 3 depicts a schematic bandplan. The downlink signal is notably attenuated after transmission over the copper cable (cf. blue spectrum in Fig. 3a). The

sloped shape of the in-band downlink spectrum is due to the low-pass properties of the cable where the attenuation grows with frequency. This sloped shape will be corrected by an equalizer at the RRH, since the PSD of the transmit signal at the antenna should be flat. At the RRH side of the copper line, the uplink signal is un-attenuated and thus much stronger than the downlink signal. The spectrum (red in Fig. 3a) is stronger and flat over the utilized band. However, the out-of-band leakage, *e.g.*, resulting from the insufficiently suppressed air channel interference, into the downlink signal can be severe if the guard band is not sufficient. After equalization of the downlink signal, the uplink spectrum (red) leaking into the downlink region (blue) will act as in-band interference, which is much stronger than the cable noise.

Let SNR_d denote the downlink signal-to-noise ratio (SNR) defined as the minimum ratio between the downlink signal PSD level and the out-of-band leakage PSD level P from the uplink signal. The level P encountered in a system depends strongly on implementation details. In a real system, P will rather vary over frequency than remain constant over our band of interest. However, from an analysis-perspective, a frequency-flat upper-bound leakage level P is sufficient since higher SNR levels over parts of the downlink band cannot be exploited by our analog relay scheme. In general, a larger gap-band Δ between downlink and uplink yields a lower interference level P and thus higher SNR_d , since the out-of-band leakage of uplink is supposed to be fading out. From an optimization perspective, it is thus rewarding to push the starting frequency of the uplink band upwards in frequency.

We start evaluating the proposed scheme by calculating the peak bit rate supported by the downlink radio link with a single antenna. We then calculate the SNR_d after transmission over the copper loop, while varying the loop length and assuming different levels of leakage between uplink and downlink signals. The objective is to find the reach over which the system could be deployed, given some implementation losses due to band placement. We utilize the BT-CAD55 [13] cable model, since it is representative for copper cables deployed in the field.

Assuming an allowed symbol error rate¹ of 10^{-6} the SNR gap becomes $\Gamma \approx 9$ dB [14]. Then the bit rate supported by the copper channel in either direction can be obtained by

$$R_b = B(1 - \beta) \log_2(1 + 10^{(\text{SNR} - \Gamma)/10}) \quad (1)$$

where B denotes the transmission bandwidth and β is the fraction of B reserved for the built-in guard-bands, yielding the effective bandwidth $W = B(1 - \beta)$.

¹Note that the symbol error rate is an upper bound for the bit error rate.

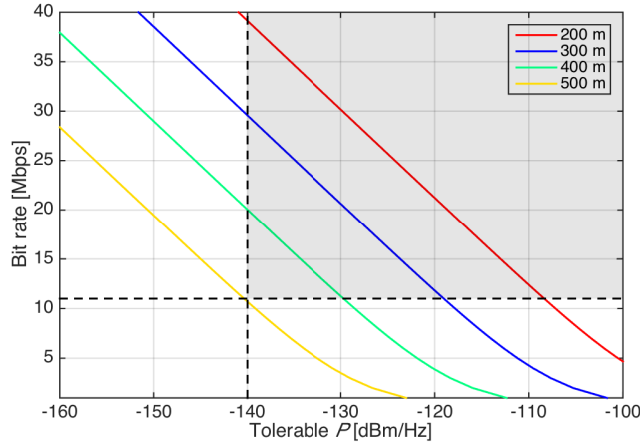


Fig. 4: Bit rate supported by the copper channel for downlink radio signal over the BT-CAD55 cable model, assuming a certain interference from uplink leakage.

A radio signal with 3 MHz bandwidth and $\bar{R}_b^{[d]} = 11$ Mbps downlink peak bit rate is used as a reference.

To enable radio transmission without performance degradation, R_b , the bit rate supported by the copper channel should not be lower than $\bar{R}_b^{[d]}$. Fig. 4 presents the relation between R_b at the far-end of the copper pair and the uplink leakage PSD level P . Given different loop lengths, the insertion loss for the copper cable BT-CAD55 was calculated as in [13]. The background noise on the copper pair limits the noise-plus-interference level inside the downlink band to -140 dBm/Hz. Thus, the grey area in Fig. 4 represents the feasible region for downlink radio transmission over the BT-CAD55 test-loop.

3.2 Uplink

At the RRU side of the copper cable the situation is mirrored as the uplink band is attenuated and the downlink out-of-band leakage causes interference (see Fig. 3b). The achievable rate R_b in uplink direction versus downlink leakage PSD is very similar to the results presented in Fig. 4. However, there is one more effect. The uplink signal will be more attenuated the further up in frequency it is placed. Furthermore, the interference to and from G.fast services increases as the upper edge of the uplink band moves towards 30 MHz. From an optimization perspective, there exists a trade-off between increased

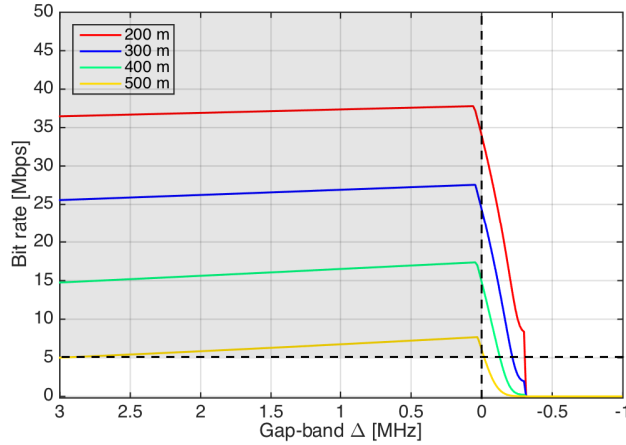


Fig. 5: Bit rates supported by the copper channel for uplink radio signal over the BT-CAD55 model, assuming a certain gap-band Δ .

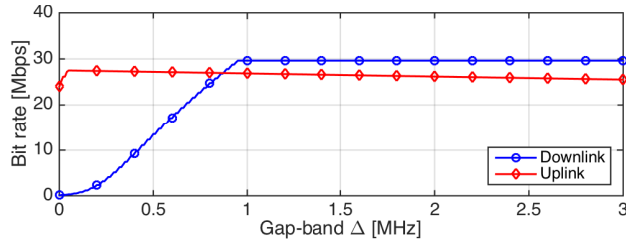
attenuation and larger gap-band.

Clearly, we would like to stay away from the future G.fast band starting at 30 MHz for the sake of both services, but we do not include any specific level of interference in the derivation at this point. The G.fast out-of-band noise decreases very sharply and would not have an impact on the results at least in this direction.

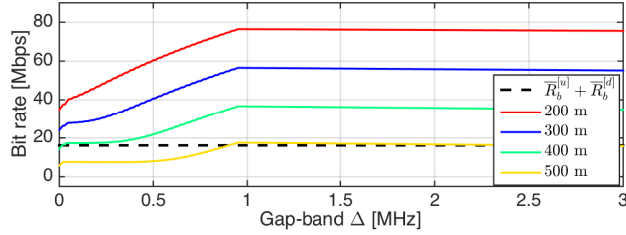
Let Δ denote the gap-band between uplink and downlink. Assume that at the near-end of the copper cable, the baseband downlink radio signal is shifted to the adequate copper frequencies, but does not go through any power amplifier, resulting in a sharply declining PSD at the band edges. The well behaved downlink radio signal results in negligible out-of-band emissions. Typically, the maximum uplink bit rate is $\bar{R}_b^{[u]} = 5$ Mbps. Using this value as a reference and varying Δ , we obtain the uplink feasible region shown in Fig. 5. Combining the feasible regions in both directions, we observe that the system could be deployed almost 500 meters away from the cabinet for the BT-CAD55 cable.

4 Band Placement with Fixed Filter Structure

In this section we evaluate the impact of band placement given a certain fixed diplexer structure. For this case study, we use the spectra shown in Fig. 3. Applying the same methodology as before, we vary Δ , cable length, transmit



(a) Bit rates in both directions over 300 m copper pair.



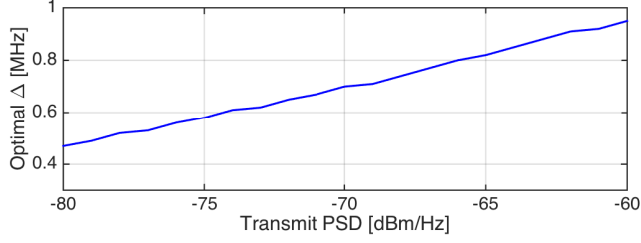
(b) Aggregate bit rates.

Fig. 6: Supported bit rates for the radio signal over BT-CAD55 copper pair, when the transmit PSD is -60 dBm/Hz.

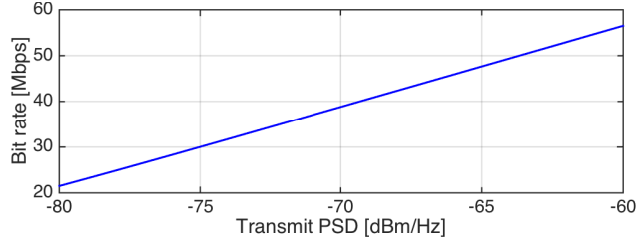
PSD, and cable type while using the peak radio signalling bit rates as a lower-bound threshold for feasibility.

In Fig. 6a the available bit rates over the copper channel for downlink and uplink directions are shown as a function of the gap-band Δ . We chose a 300 meters BT-CAD55 copper pair to obtain a representative attenuation level. The downlink band is positioned at 21–24 MHz, while the uplink band moves depending on Δ . For small Δ , the interference between the two bands can be substantial. As Δ grows, mutual interference fades and there is a frequency point where the downlink band is not interfered anymore, or the interference power level becomes lower than the background noise on the twisted pair. Beyond this frequency point, the bit rate remains constant, *e.g.*, in Fig. 6a typically after $\Delta = 0.95$ MHz. For the uplink band, signal attenuation increases for larger values of Δ , consequently causing a decrease in bit rates.

The aggregate bit rates are presented in Fig. 6b, assuming a transmit PSD of -60 dBm/Hz in both directions. As expected, the aggregate bit rate peaks for $\Delta = 0.95$ MHz. At this point, mutual interference reaches the background noise level, and the uplink band is located as close to downlink as possible. At the optimal gap-band setting, the upper edge of uplink stops before 28 MHz, leaving



(a) Relation between transmit PSD and optimal Δ .



(b) Aggregate bit rates when the optimal Δ is applied.

Fig. 7: Influence of allowed transmit PSD on the band placement, assuming a fixed filter structure in the RRH.

a comfortable gap between the proposed system and future G.fast services.

The maximum transmit power also affects optimal gap-band setting, as evidenced in Fig. 7a. For a fixed filter structure with a particular side-lobe suppression capability, higher in-band transmit power implies increased out-of-band leakage. Therefore, a wider gap-band is required. Lower transmit power allows for shorter gap-bands, but the drop in receive SNR might not justify that choice (see Fig. 7b). High transmit-power levels, however, may cause undesirable leakage into neighboring systems on the same copper pair as well as crosstalk.

The cable channel will not severely affect the total SNR of the combined copper and air channel as long as the available bit rate for the copper segment is well above the peak rate for the air interface. Using this reasoning we evaluate possible deployment distances. In this study case, besides BT-CAD55, we employ two other cables models, ETSI90 and ETSI32, representing high and low quality cables, respectively. The results are collected in Fig. 8, where the aggregate bit rate is shown as a function of cable length, assuming $\Delta = 0.95$ MHz, a transmit PSD of -60 dBm/Hz, and the same fixed filter structure for all cables.

For the BT-CAD55 cable, a length close to 500 meters approaches the air

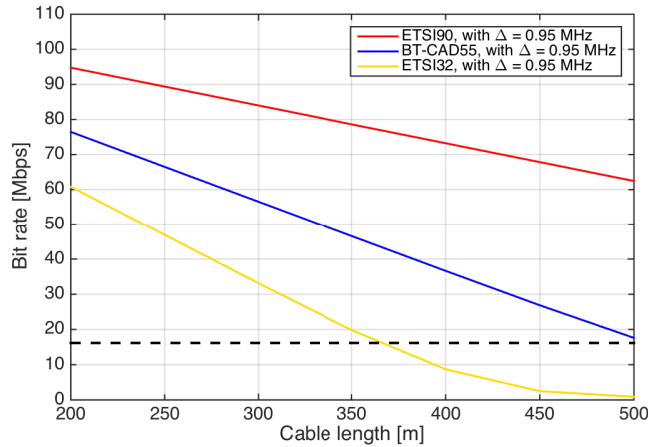


Fig. 8: Achievable aggregate bit rates over the copper channel using the optimal gap-band setting, when the transmit PSD is -60 dBm/Hz.

interface peak rate. For the low quality cable the same limit is at about 360 meters while the high quality cable has a substantial margin even at 500 meters. We conclude that it is possible to transmit analog radio signals for modern communication systems over the telephony copper lines connecting the end user in ranges of at least 350 meters. For medium quality cables this measure is close to 500 meters and for high quality well above 500 meters.

5 Conclusion

Small cells seem to be the next solution to the ever growing capacity demand in mobile networks, which is fuelled by the development of more and more sophisticated services and mobile terminals as well as a growing number of users. Relaying the radio signal over the existing copper access network may provide a valuable contribution to solving both the backhaul bottleneck and placing small cells right where they are needed. We argue that a cabinet-based system is realistic in terms of coexistence with wireline systems and we show that the capacity it delivers is significant. The added capacity is sufficient to deliver decent mobile services to most homes given a typical European topology of the PSTN network. Peak capacity is limited by the copper fronthaul bandwidth but average capacity per user is good as these residential small cell naturally has few users.

References

- [1] P. Ödling, T. Magesacher, S. Höst, P. O. Börjesson, M. Berg, and E. Areizaga, "The Fourth Generation Broadband Concept," *IEEE Communications Magazine*, vol. 47, no. 1, pp. 62-69, January 2009.
- [2] C. Lu, M. Berg, E. Trojer, P.-E. Eriksson, K. Laraqui, O. V. Tidblad, and H. Almeida, "Connecting the dots: small cells shape up for high-performance indoor radio," *Ericsson Review*, vol. 91, December 2014. [Online]. Available: <http://goo.gl/YvdY5N>
- [3] Ericsson AB, "Ericsson Mobility Report: On the pulse of the networked society," whitepaper, 2014. [Online]. Available: <http://goo.gl/QjdGbn>
- [4] Mobidia, "Understanding the Role of Managed Public Wi-Fi in Today's Smartphone User Experience: A Global Analysis of Smartphone Usage Trends Across Cellular and Private and Public Wi-Fi Networks," whitepaper, 2013. [Online]. Available: <http://goo.gl/rCOfr4>
- [5] Cisco, "The Zettabyte Era: Trends and Analysis," whitepaper, 2014. [Online]. Available: <http://goo.gl/p7KX4a>
- [6] J. Gambini and U. Spagnolini, "Radio over Telephone Lines in Femto-cell Systems," in *Proc. 2010 IEEE 21st International Symposium on Personal Indoor and Mobile Radio Communications (PIMRC)*, pp. 1544-1549, September 2010.
- [7] J. Gambini and U. Spagnolini, "Wireless over Cable for Femtocell Systems," in *IEEE Communications Magazine*, pp. 716-720, vol. 51, no. 5, pp. 178-185, May 2013.
- [8] ITU, "Very high speed digital subscriber line transceivers 2 (VDSL2)," Recommendation ITU-T G.993.2, December 2011. [Online]. Available: <https://www.itu.int/rec/T-REC-G.993.2-201112-I/en>
- [9] ITU, "Fast Access to Subscriber Terminals - Physical Layer Specification," Recommendation Draft ITU-T G.9701, 2014. [Online]. Available: <https://www.itu.int/rec/T-REC-G.9701/en>
- [10] Ericsson AB, Huawei Technologies, NEC Corporation, NSN and Alcatel-Lucent, "Common public radio interface Specification V6.0," Publicly available specification, 2013. [Online]. Available: <http://www.cpri.info/spec.html>

- [11] ITU, “Fast access to subscriber terminals (FAST) Power spectral density specification,” Recommendation Draft ITU-T G.9700, April 2014. [Online]. Available: <https://www.itu.int/rec/T-REC-G.9700/en>
- [12] 3GPP, “LTE; Evolved Universal Terrestrial Radio Access (E-UTRA); Base Station (BS) radio transmission and reception,” Tech. Rep. 2011.
- [13] D. Acatauassu, S. Höst, C. Lu, M. Berg, A. Klautau, and P. O. Börjesson, “Simple and Causal Copper Cable Model Suitable for G.fast Frequencies,” *IEEE Transactions on Communications*, vol. 62, no. 11, pp. 4040-4051, November 2014.
- [14] J. G. Proakis, *Digital Communications*, 4th ed. Mc Graw Hill, ISBN 0-07-232111-3, 2001.

Paper VI

LTE over Copper – Potential and Limitations

Abstract

The densification of mobile networks in order to meet increased capacity demands is ongoing, needed and costly. A few papers have been published based on the insight that the fixed broadband networks offer a multitude of sites, for instance our homes, for potential small cell deployment providing backhaul capacity and power without site costs. However, in order to reach economical large-scale benefits, we explore the case when radio systems are deployed in coexistence with DSL. In this paper, we establish the feasibility of such a concept under constraints invoked by state-of-the-art and emerging systems (3GPP, VDSL2 and G.fast) and make statements about the required architecture. We also point out that the enthusiasm of previously published results should be lowered a notch.

Based on: Y. Huang, E. Medeiros, N. Fonseca, S. Höst, T. Magesacher, P.-E. Eriksson, C. Lu, P. Ödling, and P. O. Börjesson, “LTE over Copper – Potential and Limitations,” in *Proc. IEEE 26th Annual International Symposium on Personal, Indoor and Mobile Radio Communications (PIMRC)*, Hong Kong, China, September 2015. © 2015 IEEE. Reprinted with permission.

1 Introduction

The explosive growth of connected smart devices forces operators to invest constantly in improving the capacity of mobile radio networks. Currently, the main approach for addressing the demands is to deploy closely spaced macro base stations. With 4G deployments reaching maturity and the telecom industry starting their research on candidate solutions for 5G, small cells are promoted as an important enabler for higher capacity.

In the papers [1, 2] Gambini *et al.* proposed the reuse of copper lines for the deployment of femtocells based on amplify-and-forward devices. In [3], Lu *et al.* present a solution for increased indoor radio performance. Their system benefits from transparent remote radio heads (RRHs) and shared baseband processors to achieve full coordination between small cells and the macro layer, eliminating the main drawback of femtocells.

In [4] we have evaluated the feasibility of co-deploying fronthaul for modern radio access network together with traditional digital subscriber line (DSL) services, reusing the cabinet infrastructure already in place. Our results suggest that mobile networks with moderate capacity could be deployed over copper without disturbing legacy fixed-access technologies.

In this paper we utilize the basic architecture described in [4] to deploy LTE for small cells over residential unshielded copper loops. Our interest is to investigate the implications of 3GPP compliance on an implementation that down/up converts LTE signals to intermediate frequency (IF) over the copper loops, as illustrated in Fig. 1. Based on the requirements we present design guidelines for an RRH and estimates for how distant these systems could be deployed from the street cabinet.

2 System Architecture

We consider a distributed base station architecture as described in [4] where the cell processing is functionally split among three entities. Baseband processors perform digital signal processing on baseband LTE signals. In downlink direction the baseband signals are up-converted to IF (labeled in Fig. 1) at a remote radio unit (RRU) deployed in colocation with DSL equipment in street cabinets. After IF conversion, the LTE signals are transmitted over a copper pair (represented in Fig. 1) to an RRH, converted to the appropriate radio frequency (RF) and then sent to the user equipment (UE) over the air. In the uplink direction, the radio signal received at the RRH is down-converted to IF, transmitted to the RRU, and finally converted to baseband for receiver processing.

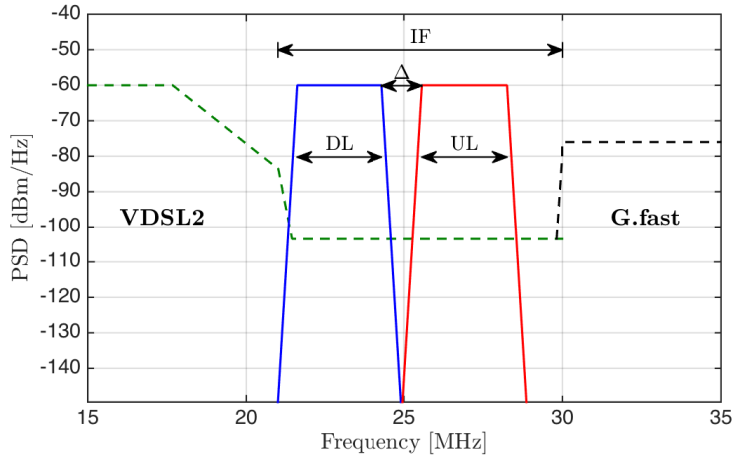


Fig. 1: Bandplan adopted in this paper. The LTE signal is placed between VDSL2 and G.fast systems for coexistence. The dashed lines represent the limit PSD masks for the DSL systems. The frequencies between 17 MHz and 30 MHz are not used by VDSL2 17 MHz profiles or G.fast.

To coexist with VDSL2 and G.fast systems, the target IF band is placed between 21 MHz and 30 MHz, which restricts the available bandwidth for LTE signals to be 3 MHz. The resulting bandplan is presented in Fig. 1, with the downlink LTE band placed between 21 MHz and 24 MHz, a gap-band of $\Delta = 0.95$ MHz, and the uplink signal extending to 28 MHz. As reported in [4], for a maximum transmit power spectrum density (PSD) of $S = -60$ dBm/Hz over the copper pair, the proposed system can be deployed up to 500 meters away from street cabinets.

In Fig. 2 we present a model for the RRH considered in this work. The upper and the lower signal branches, which contain the processing elements for the LTE downlink (DL) and the LTE uplink (UL) path, are connected to the twisted pair via a hybrid coupler. On the opposite side they connect to an RF front-end. The hybrid coupler used in the RRH is not perfect, exhibiting non-negligible trans-hybrid loss [5], denoted as L_{hybrid} . The leakage from uplink to downlink inside the RRH may cause in-band interference and/or out-of-band noise that need to be dealt with in order to avoid performance degradation.

Invoking the requirements imposed by 3GPP regulations and a typical indoor propagation scenario, feasible quantities for the overall in-band amplification G and out-of-band rejection L at the RRH can be derived for uplink and downlink, respectively. Here we perform a “black-box” study without suggest-

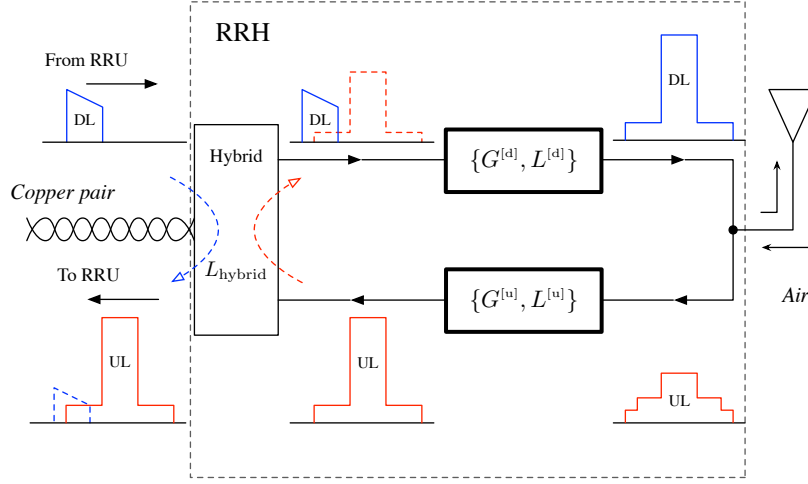


Fig. 2: Model for the RRH. For each direction in-band gain and out-of-band rejection are the parameters. Leakage from uplink to downlink due to an imperfect hybrid is represented by the red dashed arrow.

ing a specific arrangement of amplifiers and filters. Superscripts [u] and [d] are used to distinguish between uplink and downlink, respectively.

The choice of in-band gains depends on the required transmit power over copper and air channels such that the necessary signal-to-noise ratio (SNR) is achieved. In order to avoid mutual interference and also coexist with other wireless systems that operate on adjacent channels, out-of-band rejections are derived according to spectrum emission mask (SEM) and adjacent channel selectivity (ACS) in uplink direction and required adjacent channel leakage power ratio (ACLR) in downlink direction, respectively.

3 Uplink Path

3.1 In-band Signal Amplification $G^{[u]}$

For the uplink direction, we start by estimating the receive power at the RRH antenna. Here we employ the indoor transmission path-loss model [6], which assumes that base station and UE are located in the same building. We calculate the air channel path-loss for a typical residential scenario as

$$L_{\text{air}} [\text{dB}] = 20 \log_{10} f_c + \alpha \log_{10} r + L_f - 28, \quad (1)$$

for a carrier frequency f_c [MHz], a propagation distance r [m] and an indoor environment characterized by distance power loss coefficient α and floor penetration loss factor L_f [dB]. The path-loss L_{air} increases with the distance r between RRH antenna and UE.

For a 3 MHz LTE signal, the uplink peak bit-rate is $\tilde{R}_u = 7.5$ Mbps. The receive SNR at the RRU required to support the peak rate after copper transmission is

$$\widetilde{\text{SNR}}^{[u]} [\text{dB}] = 10 \log_{10} \left(2^{(\tilde{R}_u/B_c)-1} \right) + \Gamma, \quad (2)$$

where $B_c = 2.7$ MHz is the transmission bandwidth configuration [7] and $\Gamma = 9$ dB is reserved to cover implementation losses. Since the maximum output power of the UE is 23 dBm [8], the maximum receive power at the RRH antenna connector is given by $P_{\text{rx,ant}}^{[u]} [\text{dBm}] = 23 - L_{\text{air}}$. Considering thermal noise as the only noise source for the air channel transmission, we can derive the receive SNR at the RRH antenna connector for a certain L_{air} , denoted $\text{SNR}_{\text{air}}^{[u]}$. In this work, we assume that the uplink noise figure in the RRH is 0 dB. The uplink SNR before copper transmission then stays the same as $\text{SNR}_{\text{air}}^{[u]}$. To deliver $\widetilde{\text{SNR}}^{[u]}$ to the RRU, the related SNR required for copper transmission is calculated in linear scale as

$$\text{SNR}_{\text{Cu}}^{[u]} = \frac{\text{SNR}_{\text{air}}^{[u]} \cdot \widetilde{\text{SNR}}^{[u]}}{\text{SNR}_{\text{air}}^{[u]} - \widetilde{\text{SNR}}^{[u]}}. \quad (3)$$

For a given cable type, the channel attenuation L_{Cu} is a monotonically increasing function with respect to both frequency f and cable length d . Let $\mathcal{F}^{[u]}$ denote the IFs occupied by each uplink LTE subcarrier as shown in Fig. 1. To derive the in-band SNR, we use the sub-carrier that experiences the worst case attenuation as a reference. Given the cable noise PSD of $N = -150$ dBm/Hz and using Eq. (3) in dB-scale, the uplink transmit power over the copper should be

$$P_{\text{tx,Cu}}^{[u]} [\text{dBm}] \geq \text{SNR}_{\text{Cu}}^{[u]} + (N + 10 \log_{10} B) + \max_{f \in \mathcal{F}^{[u]}} L_{\text{Cu}}(f, d). \quad (4)$$

Assuming a maximum transmit PSD over the copper as $S_{\text{max}} = -60$ dBm/Hz, one can also estimate the preliminary maximum distance over which such RRH could be deployed from the cabinet for $(P_{\text{tx,Cu}}^{[u]} - \log_{10} B) \leq S_{\text{max}}$.

The necessary amplification in uplink direction can then be calculated as

$$G^{[u]} [\text{dB}] = P_{\text{tx,Cu}}^{[u]} - P_{\text{rx,ant}}^{[u]}. \quad (5)$$

Equivalently, the maximum deployable cable length d fulfilling Eq. (4) can be estimated given a certain available $G^{[u]}$.

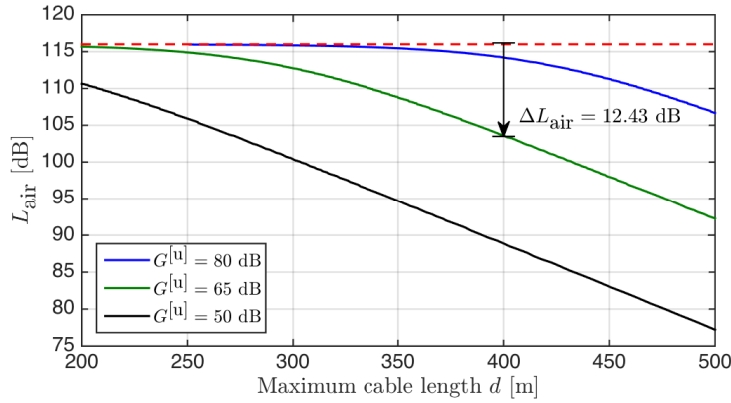


Fig. 3: The three solid curves represent the relationship between deployment distance and the tolerable path-loss in the air for a fixed $G^{[u]}$. The red dashed line represents the initial maximum acceptable path-loss for the LTE uplink peak bit-rate. The ΔL_{air} increases with cable length as exemplified by the arrow around 400 meters.

In Fig. 3 we present the relationship between maximum cable length d (distance between cabinet and RRH deployment site) and the maximum path-loss that the system can endure while still providing the LTE uplink peak bit-rate. For our target deployment scenario, an indoor residential environment at 1.8 GHz, typical values for α and L_f in Eq. (1) are 28 and 10 dB respectively. Notice that to deploy long cables there will be a decrease in the maximum acceptable path-loss corresponding to the gaps between solid lines and the red dashed line in Fig. 3. We refer to this gap as ΔL_{air} . The ΔL_{air} varies for the same deployed cable length with different $G^{[u]}$ available. The cable attenuation used to obtain these curves is calculated using the BT-CAD55 model, commonly employed to estimate capacity in DSL system design [9].

3.2 Out-of-band Rejection $L^{[u]}$

As sketched in the signal flow depicted in Fig. 2, after air channel transmission, the received signal at the RRH may contain, besides the signal of interest, out-of-band components $\text{OOB}_{\text{ant}}^{[u]}$ at the antenna connector. Passing through the amplifying element(s) at the RRH, those out-of-band components experience the same gain as the in-band uplink signal. Although this causes no trouble for the uplink transmission in itself, the out-of-band noise may lower the quality of the downlink signal due to the hybrid leakage. With less than 3 MHz gap-band between downlink and uplink in the copper channel, any neighboring

interference captured by the RRH antenna will leak via the hybrid coupler and overlap with the signal in the downlink processing path.

To guarantee the quality of the in-band signal transmission in downlink direction, the error vector magnitude (EVM) of transmitted signals should be lower than the limits listed in Table 6.5.2-1 in [7]. EVM is defined as

$$\text{EVM} = \sqrt{\frac{1}{K} \frac{\|\mathbf{y} - \mathbf{x}\|_2^2}{P_0}} \cdot 100\%,$$

where \mathbf{x} and \mathbf{y} denote the constellation symbols at the RRU and RRH antenna connector respectively, K is the number of involved symbols, and P_0 is the average power of the modulation scheme used. This quantity can also be translated to an in-band SNR requirement in the downlink direction given by $\widetilde{\text{SNR}}^{[d]} \approx 1/\text{EVM}^2$. Accordingly, the minimum $\widetilde{\text{SNR}}^{[d]}$ is around 15.14 dB for QPSK, 18.06 dB for 16-QAM, and 21.98 dB for 64-QAM. These parameters suggest that a general minimum value of $\widetilde{\text{SNR}}^{[d]} = 21.98$ dB should be guaranteed.

Since it is difficult to mitigate the resulting in-band interference in the downlink path, we should suppress out-of-band emission already in the uplink processing to a level such that the downlink EVM requirement is not violated. Considering the trans-hybrid attenuation L_{hybrid} , the permissible uplink out-of-band emission at the copper connecting port is

$$\text{OOB}_{\text{Cu}}^{[u]} [\text{dBm}] = P_{\text{rx,Cu}}^{[d]} - \widetilde{\text{SNR}}^{[d]} + L_{\text{hybrid}}. \quad (6)$$

Here $P_{\text{rx,Cu}}^{[d]}$ is the signal power reaching the RRH after transmission over the copper channel, *i.e.*,

$$P_{\text{rx,Cu}}^{[d]} [\text{dBm}] = S - \max_{f \in \mathcal{F}^{[d]}} L_{\text{Cu}}(f) + \log_{10} B. \quad (7)$$

Eq. (6) implies a rejection requirement at the RRH given by

$$L^{[u]} [\text{dB}] = P_{\text{tx,Cu}}^{[u]} - \widetilde{\text{SNR}}^{[u]} - \text{OOB}_{\text{Cu}}^{[u]}, \quad (8)$$

where $\widetilde{\text{SNR}}^{[u]}$ is the power ratio between the uplink in-band signal and the maximum out-of-band component that overlaps with the downlink in-band signal.

To properly illustrate the influence of specific 3GPP requirements for the uplink out-of-band rejection we differentiate between two situations:

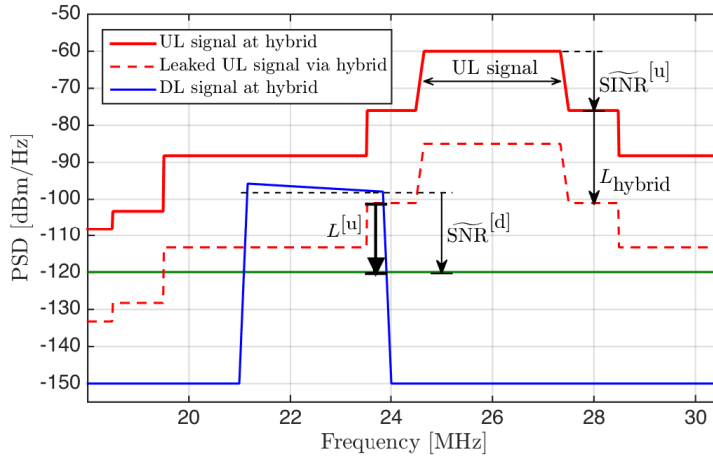


Fig. 4: Leakage of uplink out-of-band emissions into the downlink signal. The red solid curve represents the received uplink signal after amplification at the RRH. The dashed curve represents the leakage PSD if no filtering is performed. The green solid curve represents the acceptable noise floor for downlink peak bit-rates. Calculated for 300 meters of BT-CAD55.

RRH Without An Alien System Nearby

3GPP imposes SEM and spurious emission limits for the UE transmitter [8], which restrict the out-of-band spectral emissions. Assuming that a UE transmits at the worst case PSD mask according to those requirements, the signal received at the RRH after amplification is represented by the red solid curve in Fig. 4. If no filtering is performed, the uplink signal of interest plus its out-of-band components leak via the hybrid resulting in in-band interference to the downlink signal. Since the gap-band reserved between uplink and downlink over copper transmission is small, the leakage imposes a requirement on $L^{[u]}$ as indicated by the arrow in Fig. 4.

RRH With An Alien System Nearby

3GPP also defines an ACS [7] metric in the uplink to coexist with other systems that operate in adjacent channels. It forces the base station receiver to be able to cope with high levels of interference from neighboring channels, which are within the receiver's operating band. This happens for example when a nearby terminal transmits with very high power to reach a distant macro-cell outside

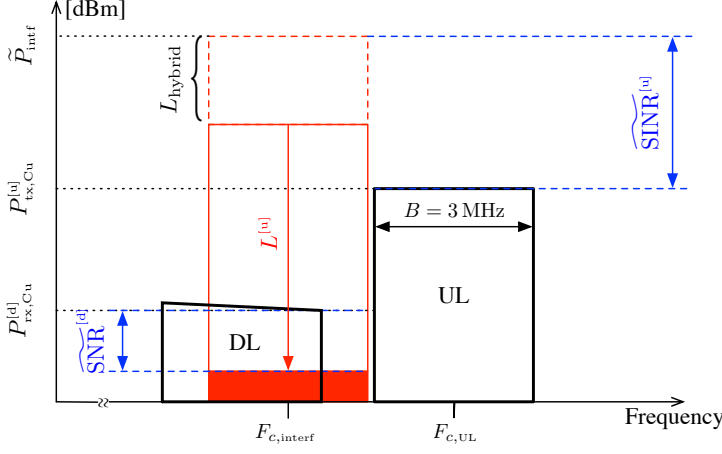


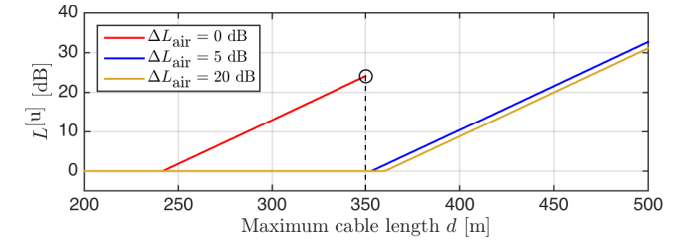
Fig. 5: ACS requirement implications. A neighboring uplink transmission, represented as tall red rectangle must be suppressed to the solid red box in order to avoid drowning the downlink band. The uplink interference is captured at the RRH antenna and may overwhelm the downlink signal via the hybrid if no filtering is performed.

the building (*i.e.*, from another operator). The requirement suggests that an interference with a mean power of $\tilde{P}_{\text{intf}} = 28$ dBm should be supported. When the interference from a nearby system is received and amplified it may impact downlink transmission as depicted in Fig. 5.

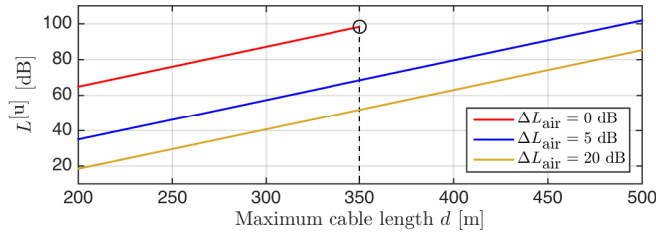
In Fig. 6 we present the relationship between the required out-of-band rejection $L^{[u]}$ and cable length d , with and without alien interference in adjacent channels, for a certain acceptable ΔL_{air} , assuming a trans-hybrid loss of $L_{\text{hybrid}} = 25$ dB [10]. In Fig. 6a, we consider the situation when the highest out-of-band emission below the SEM happens to partially overlap with the downlink in-band signal. Fig. 6b estimates the required $L^{[u]}$ in presence of the worst alien interference that ACS suggests.

4 Downlink Path

For the downlink branch, the EVM requirement described in Section 3.2 also limits the preliminary maximum deployment distance of the proposed system. Given a fixed transmit PSD from the RRU as $S = -60$ dBm/Hz and a background noise PSD of -150 dBm/Hz, the received SNR at the RRH decreases when using longer cables. At the largest deployment distance, the cable should



(a) Without alien system ($\widetilde{\text{SINR}}^{[u]} = 16$ dB, $\widetilde{\text{SNR}}^{[d]} = 21.98$ dB)



(b) With alien system ($\widetilde{P}_{\text{intf}} = 28$ dBm, $\widetilde{\text{SNR}}^{[d]} = 15.14$ dB)

Fig. 6: Required uplink out-of-band rejection $L^{[u]}$ for different cable lengths. Each solid curve is calculated for an acceptable ΔL_{air} . The red curve is interrupted when the maximum transmit PSD is reached.

deliver $\widetilde{\text{SNR}}^{[d]} = 21.98$ dB to the RRH in the downlink direction.

For a home base station with a single antenna, 3GPP stipulates a maximum transmit power $\widetilde{P}_{\text{tx,ant}}^{[d]} = 20$ dBm [7], which requires an in-band signal amplification of

$$G^{[d]} \text{ [dB]} = \widetilde{P}_{\text{tx,ant}}^{[d]} - P_{\text{rx,Cu}}^{[d]}, \quad (9)$$

where $P_{\text{rx,Cu}}^{[d]}$ is the received power in downlink after copper transmission as calculated in Eq.(7).

Also in [7], 3GPP establishes that base stations should suppress adjacent channel signal leakage before passing the signal to the antenna. This requirement, known as ACLR, asks for either an adjacent channel leakage power of -50 dBm/MHz or a 45 dB attenuation compared to the in-band signal power. The less stringent number of the two is considered the limit. For our proposed RRH, the ACLR requirement leads to a total leakage power limit over the neighboring channel of around $\widetilde{\text{OOB}}_{\text{ant}}^{[d]} = -25$ dBm.

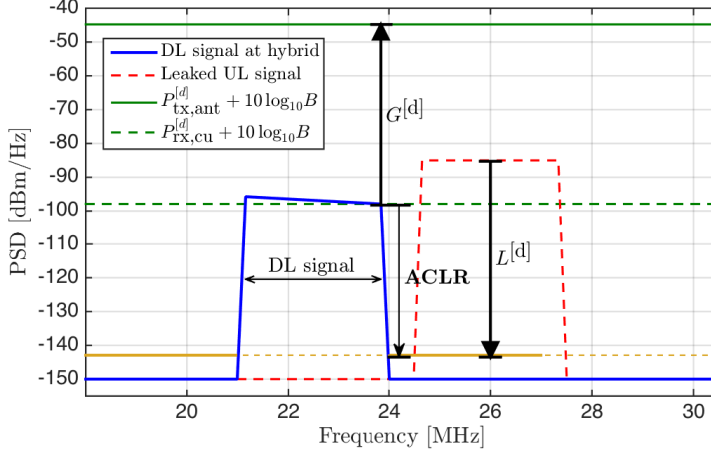


Fig. 7: PSDs of 300meters BT-CAD55 model in the downlink branch, after the hybrid coupler and before filtering. The signal of interest is the left lobe. The band to the right is the upstream signal coupled through the hybrid and should be suppressed to the ACLR level given in yellow.

If the uplink signal leaks into downlink transmission via the hybrid coupler, a big portion of the leakage can be transmitted to the antenna, disrupting neighboring bands. An example of this can be seen in Fig. 7, assuming the uplink out-of-band interference has been in good control. The effective leaked power from the uplink signal can be calculated as

$$\text{OOB}_{\text{Cu}}^{[\text{d}]} [\text{dBm}] = P_{\text{tx,Cu}}^{[\text{u}]} - L_{\text{hybrid}},$$

To fulfil the ACLR requirement, the downlink out-of-band rejection must be

$$L^{[\text{d}]} [\text{dB}] = \text{OOB}_{\text{Cu}}^{[\text{d}]} + G^{[\text{d}]} - \widetilde{\text{OOB}}_{\text{ant}}^{[\text{d}]}, \quad (10)$$

assuming that out-of-band interference at adjacent channels experiences the same amplification as the in-band signal.

As indicated in Eq. (7), the cable attenuation determines the amount of power received at the RRH. To obtain a flat transmit PSD at the antenna connector, each value of $P_{\text{rx,Cu}}^{[\text{d}]}$ leads to a required $G^{[\text{d}]}$. This is illustrated in Fig. 8a for different cable lengths. Also, the uplink signal is amplified before the hybrid, which in turn causes the increase of undesirable leakage through the hybrid. In order to fulfil the ACLR requirement, we must obey the downlink out-of-band rejection requirements depicted in Fig. 8b.

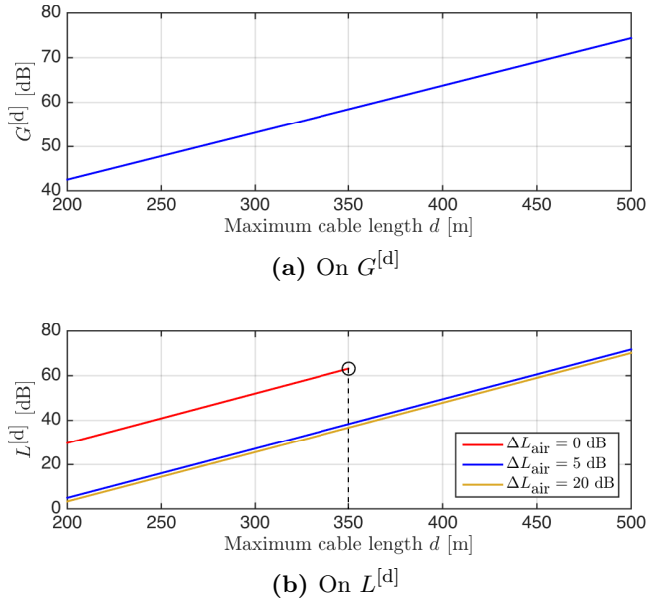


Fig. 8: Influence of cable attenuation on RRH design parameters for downlink direction.

5 Design Implications

By jointly considering the discussed 3GPP requirements and using the described methodology, one can obtain the desired values for total in-band gain and out-of-band rejection required at the RRH. As an example, we list three different designs in Table 1. The bold numbers in each row represent target values, which are prioritized and kept fixed.

For the first row, the acceptable ΔL_{air} is set to 0. This results in a deployment distance of around 350 meters, but very high $G^{[u]}$ and $L^{[u]}$. If alien systems are not a concern, the values in parenthesis should be considered for $L^{[u]}$. In the second row, we are aiming for a deployment distance of 400 meters with an acceptable ΔL_{air} of 5 dB. The requirements for $L^{[u]}$, $G^{[u]}$ and $L^{[d]}$ are relaxed due to the permissible ΔL_{air} , but the value for $G^{[d]}$ increases because of the increased cable length. In the last row, we start by fixing reasonable values for filtering and amplifying components, which limit the deployment reach to around 310 meters without increasing ΔL_{air} significantly.

Table 1: Parameter values for different design objectives

ΔL_{air} [dB]	$L^{[u]}$ [dB]	$G^{[u]}$ [dB]	$L^{[d]}$ [dB]	$G^{[d]}$ [dB]	d [m]
0	98.30 (24.14)	80	63.16	58.45	350
5	79.62 (10.46)	74	49.48	63.76	400
5	60	65	60	65	310

6 Conclusion

Although our results in [4] suggest that modern OFDM-based radio systems could be deployed over copper up to 500 m, once 3GPP requirements are taken into consideration we observe absurdly stringent filtering and amplifying demands in Fig. 3, 6b and 8a, and also limited deployment distance if we do not compromise on radio reach. For as small a gap-band as assumed here, fulfilling 3GPP requirements practically prohibits fully analog implementations, such as the one presented in [1] and [4]. However, with digital filtering in the RRH and reasonable small cell assumptions, we conclude that LTE over copper lines is a technically viable concept. A myriad of small cells could be added to the mobile networks using the existing fixed infrastructure as a base without offending the technical foundations of current standards and regulations.

References

- [1] J. Gambini and U. Spagnolini, "Radio over Telephone Lines in Femto-cell Systems," in *Proc. 2010 IEEE 21st International Symposium on Personal Indoor and Mobile Radio Communications (PIMRC)*, pp. 1544-1549, September 2010.
- [2] J. Gambini and U. Spagnolini, "Wireless over Cable for Femtocell Systems," in *IEEE Communications Magazine*, pp. 716-720, vol. 51, no. 5, pp. 178-185, May 2013.
- [3] C. Lu, M. Berg, E. Trojer, P.-E. Eriksson, K. Laraqui, O. V. Tidblad, and H. Almeida, "Connecting the dots: small cells shape up for high-performance indoor radio," *Ericsson Review*, vol. 91, December 2014. [Online]. Available: <http://goo.gl/YvdY5N>
- [4] Y. Huang, E. Medeiros, S. Höst, T. Magesacher, P.-E. Eriksson, C. Lu, P. Ödling, and P. O. Börjesson, "Enabling DSL and Radio on the Same Copper Pair," in *Proc. 2015 IEEE International Conference on Communications (ICC)*, pp. 1031-1035, June 2015.

- [5] T.-C. Lee and B. Razavi, “A 125-MHz Mixed-Signal Echo Canceller for Gigabit Ethernet on Copper Wire,” *IEEE Journal of Solid-State Circuits*, vol. 36, no. 3, pp. 366-373, March 2001.
- [6] ITU-R, “Propagation Data And Prediction Methods for the Planning of Indoor Radio Communication Systems And Radio Local Area Networks in the Frequency Range 900 MHz to 100 GHz,” International Telecommunication Union (ITU), Recommendation P.1238-7, February 2012. [Online]. Available: <http://goo.gl/ZMIY7E>
- [7] 3GPP, “Evolved Universal Terrestrial Radio Access (E-UTRA); Base Station (BS) radio transmission and reception,” 3rd Generation Partnership Project (3GPP), TS 36.104 V12.6.0, November 2014. [Online]. Available: <http://goo.gl/SCislQ>
- [8] 3GPP, “Evolved Universal Terrestrial Radio Access (E-UTRA); User Equipment (UE) radio transmission and reception,” 3rd Generation Partnership Project (3GPP), TS 36.101 V12.5.0, November 2014. [Online]. Available: <http://goo.gl/1PRPLV>
- [9] D. Acatauassu, S. Höst, C. Lu, M. Berg, A. Klautau, and P.O. Börjesson, “Simple and Causal Copper Cable Model Suitable for G.fast Frequencies,” *IEEE Transactions on Communications*, vol. 62, no. 11, pp. 4040-4051, November 2014.
- [10] Pulse, “Hybrid VDSL Transformer for Use with Infineon VDSL 2-Band, 4-Band and 10Base-S Chipsets,” datasheet, 2003.

Paper VII

Time-Domain Precoding for LTE-over-Copper Systems

Abstract

Crosstalk cancellation is a crucial issue for traditional digital subscriber line systems. For LTE-over-copper systems, however, the need for crosstalk cancellation varies depending on the analog fronthauling architecture and its parameters. A crosstalk handler that is decoupled as much as possible from the rest of the system architecture is thus preferred. Therefore, we propose a time-domain precoding scheme specifically in downstream direction to separate the precoding unit from the LTE signal flow, and perform crosstalk cancellation in an on-demand manner. Estimation of all direct and crosstalk paths is assisted by LTE cell-specific reference signals. The time-domain precoder transforms the interference channel into a crosstalk-free channel with identical direct paths, which allows for low-complexity inter-symbol interference mitigation. We evaluate the concept in terms of signal-to-noise ratio provided for LTE signals using measured wireline channel data.

Based on: Y. Huang, E. Medeiros, T. Magesacher, S. Höst, C. Lu, P.-E. Eriksson, P. Ödling, and P. O. Börjesson, "Time-Domain Precoding for LTE-over-Copper Systems," submitted to *2016 IEEE International Conference on Communications (ICC)*, Kuala Lumpur, Malaysia.

1 Introduction

Small cells are promoted as an important enabler for high capacity indoor radio. However, fronthauling and backhauling that connect small cells to the core network turn out to be challenging due to the deploying locations and set-up cost per user. Reusing fixed broadband networks in this regard can be an economic solution to achieve the small cell densification.

In [1], a femto-wireless-over-cable architecture is proposed to reuse cable infrastructure for femtocell deployment. It cascades cable and air channels together to implement compound MIMO processing, which requires mobile end-users to be aware of the cable related architecture. In [2], the macro network extension and densification are combined together with specific indoor small cell solutions that use fronthauling over structured LAN cables. In our previous work [3,4], the coexistence of LTE analog fronthaul and digital subscriber line (DSL) systems is investigated considering a longer deploying distance—up to 300 meters from the street cabinet to the customer premises, with existing telephone wires.

A challenge of using the existing unshielded copper-based infrastructure is the crosstalk from the neighboring pairs due to electromagnetic coupling (as illustrated in Fig.1). To make the infrastructure between remote radio unit (RRU) and remote radio head (RRH) transparent to mobile end-users, crosstalk cancellation should be employed if the interference is noticeable. In the prevailing DSL systems such as VDSL2 [5], vectoring [6] is implemented to mitigate crosstalk. It applies precoding in downstream and joint equalizing in upstream, where the channel estimation and crosstalk cancellation techniques are typically implemented in frequency-domain.

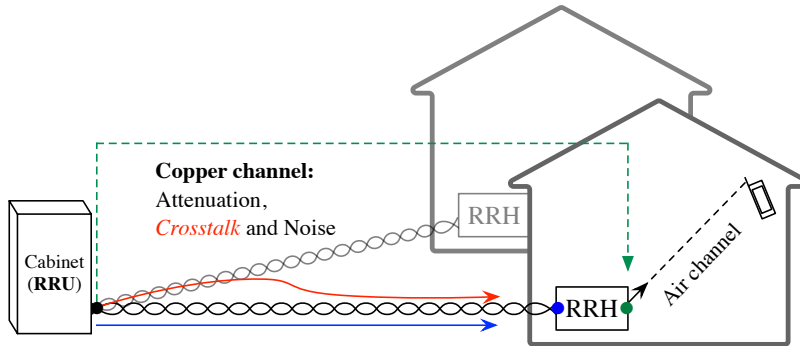


Fig. 1: LoC systematic sketch in the downstream direction.

Compared to the air channel, the copper-pair channel is more stable in time and has much higher signal-to-noise ratio (SNR). Crosstalk which was harmful to DSL signals may not be that detrimental to LTE signals, as the latter are designed to cope with more severe situations in the air channel. Depending on the cable quality, the frequency band used over copper, and also the processing components inside the RRH, the need for crosstalk cancellation in LTE-over-copper (LoC) systems varies. The crosstalk cancellation unit should be more flexible in the sense that it can be easily turned off/on without noticeably interrupting the original LTE signal flow. Moreover, the generated LTE signal from the RRU is typically a time-domain signal, and thus implementing crosstalk cancellation also in time-domain is an appealing solution.

In [7], a time-domain precoding method is proposed for DSL systems based on fractionally-spaced filtering. It performs SNR-based coupling estimation and parameter-based multi-filter updating. Since it concerns a scenario with several DSL access multiplexers (DSLAMs), the algorithm complexity becomes unnecessarily high for our case.

In this work, we focus on precoding in downstream direction to cancel out far-end crosstalk (FEXT) for LoC systems. The proposed precoding unit operates in parallel to the original LTE signal flow as interpreted in Section 2. A channel impulse response (CIR) estimation method for all direct and FEXT paths is proposed in Section 3 by taking advantage of LTE cell-specific reference signals (CRSs). Time-domain precoding for crosstalk cancellation and intersymbol interference (ISI) mitigation is presented and analyzed in Section 4.

2 Precoding Architecture

At the RRU-side, signals are loaded on copper pairs with adequate transmit power for distant copper transmission. We consider a transmit power spectrum density (PSD) of $P_{tx} = -60$ dBm/Hz and a background noise of $N_{bg} = -140$ dBm/Hz, which results in an initial transmit $\text{SNR}_{init} = 80$ dB. At the antenna connector of the RRH (*i.e.*, the right-hand-side of the RRH in Fig. 1), a minimum error vector magnitude (EVM) requirement for LTE signals should be achieved as defined in [8] and also discussed in [4]. Translating into SNR values, it demands around $\text{SNR}_{target} = 15.14$ dB for QPSK, $\text{SNR}_{target} = 18.06$ dB for 16-QAM, and $\text{SNR}_{target} = 21.98$ dB for 64-QAM. From 80 dB on one end to around 20 dB on the other end, a large SNR margin is available for the copper transmission and the implementation of the RRH.

If the FEXT over copper pairs can be covered by this SNR margin, no extra effort for crosstalk cancellation is needed. Otherwise, a precoder should be involved at the RRU-side. The tolerable FEXT magnitude depends on,

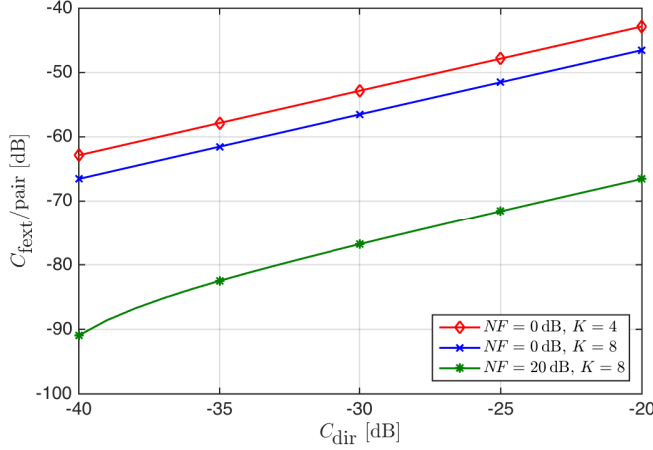


Fig. 2: Tolerable FEXT magnitude per copper pair for different system scenarios. $\text{SNR}_{\text{target}} = 18.06$ dB for 16-QAM is used as an example. A transmit PSD of -60 dBm/Hz and background noise of -140 dBm/Hz are assumed for the copper channel.

among other factors, the cable type, the frequency band where LTE signals are loaded, and the SNR-impacting components within the RRH. While the cable type and applied frequency determine the insertion loss of direct paths (denoted by C_{dir}), the components inside RRH yield an overall noise figure value (denoted by NF). Consider that K RRHs share the same cable binder. To reach a certain $\text{SNR}_{\text{target}}$ for the EVM requirement, the average tolerable FEXT magnitude C_{fext} from each involved pair can be estimated as

$$C_{\text{fext/pair}} = \frac{1}{K-1} \left(\frac{C_{\text{dir}}}{\text{SNR}_{\text{target}} \cdot NF} - \frac{1}{\text{SNR}_{\text{init}}} \right), \quad (1)$$

by counting every variable in linear scale. Fig. 2 illustrates how different variables in Eq. (1) affect the upper limit of the tolerable FEXT. For example for $K = 4$, if the RRH generates $NF = 0$ dB and the direct channel insertion loss is around -25 dB, no precoding is needed as long as the average FEXT from neighboring pairs is below -50 dB. The upper limit per pair reduces for a larger group size (*e.g.*, $K = 8$), which is equivalent to having more interfering sources. A noisier RRH environment with higher NF value also lowers the tolerable FEXT level as the SNR margin left for copper transmission shrinks.

Since the RRU delivers LTE signals in time-domain, we propose a time-domain precoding scheme for LoC systems as illustrated in Fig. 3. Pre-

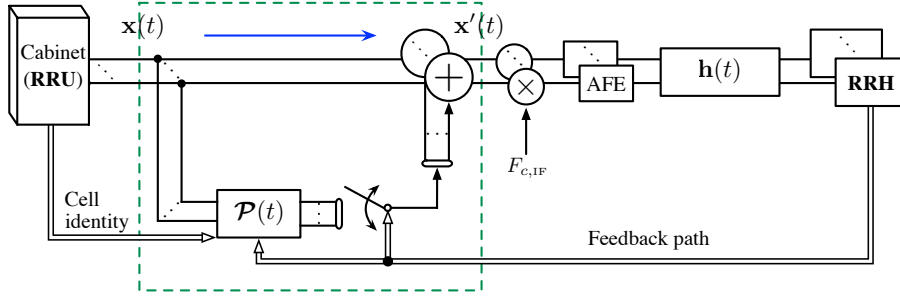


Fig. 3: Time-domain precoding architecture for LoC systems. The precoding unit can be easily turned off/on by de-/activating additive time-domain signals without any processing block located in the LTE path.

compensated signals are generated by the precoder and added directly to LTE signals when crosstalk cancellation is favorable. Because the precoding unit is parallel to the signal path, it can be easily turned off/on based on demand without unnecessarily interrupting the original LTE signal flow.

3 Time-Domain Channel Estimation

When precoding for crosstalk cancellation is necessary, we first need to acquire prior knowledge of CIRs for all direct and FEXT paths. In this work, we propose an error-based CIR estimation assisted by CRSs [9] of the carried LTE signal.

3.1 LTE Cell-Specific Reference Signal (CRS) Alignment

The smallest LTE frame structure unit is the Resource Element (RE). It represents one OFDM symbol in time on one sub-carrier in frequency (see the small squares in Fig. 4). Along the time axis, 7 OFDM symbols with normal customer premise (CP) compose one slot, 2 slots compose one subframe, and 10 subframes compose one frame. A two-dimensional grid containing 1 slot in time-domain and 12 consecutive sub-carriers in frequency-domain is termed Resource Block (RB). A 3 MHz LTE signal, for example, has $N_{rb} = 15$ RBs corresponding to 180 sub-carriers in frequency-domain.

In each slot there are 2 CRS-containing OFDM symbols, numbered 0 and 4 on the left-hand-side of Fig. 4. For symbol-0, there is one reference symbol (black square in Fig. 4) on every 6 sub-carriers. On symbol-4, the reference-symbol positions shift by 3 sub-carriers. The following slots use the same

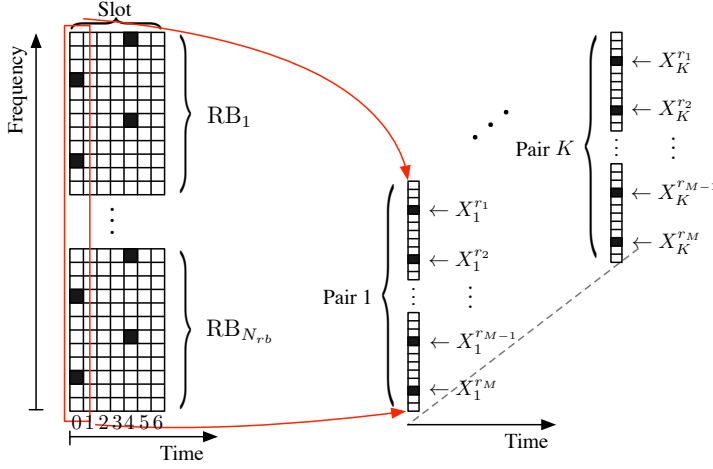


Fig. 4: Illustration of CRS-aided channel estimation. Each small square represents one RE. Each black square represents one reference symbol.

CRS mapping scheme, which forms a diamond mapping pattern to monitor more channel variations in frequency-domain. When applied to estimating the copper channel which is essentially time-invariant, this kind of mapping pattern approximates to having one pilot on every 3 sub-carriers.

There are 504 different CRS sequences defined for LTE, where each sequence corresponds to one of 504 different physical-layer cell identities. Let $N_{\text{ID}}^{\text{cell}}$ denote a certain cell identity. A cell-specific frequency shift of $[N_{\text{ID}}^{\text{cell}} \bmod 6]$ is applied to determine the reference-symbol positioning on the sub-carriers. Equivalently, there are only 6 possible mapping patterns that jointly cover all 504 different cell identities.

Accordingly, the baseband unit can control the CRS positioning by assigning a specific cell identity to each RRH/cell. In turn, we are essentially informed of the reference symbols and their mapping pattern contained in the coming LTE signal by knowing its cell identity. For an RRH group sharing the same cable binder, we can make their CRS mapping identical (as illustrated on the right-hand-side of Fig. 4) by assigning their cell identity to be an integer multiple of 6 apart [10]. For example, let cell identities to be $[2, 8, 14, 26]$ for $K = 4$.

Note that small cells supported by the LoC system have low output power and are deployed in environments with high path-loss (*e.g.*, due to walls). Therefore the above reference signal alignment will not diminish pilot effec-

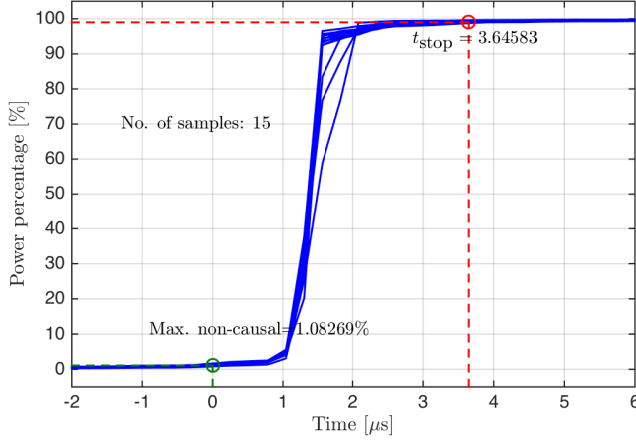


Fig. 5: Energy-based time-domain CIR truncation. t_{stop} marks the time stamp for the maximum channel spread that contains 99% CIR power among the 16 (for $K = 4$) paths.

tiveness due to neighboring cell interference in the air.

3.2 Estimation of Copper Channel Impulse Responses (CIRs)

Assume that the side information of cell identity is available. Consider the case where LTE signals transmitting on a group of K pairs share the same CRS mapping structure. Let \mathbf{F}_N denote an $N \times N$ discrete Fourier transform (DFT) matrix and \mathbf{F}_L is the first L columns of \mathbf{F}_N , where N and L denote the DFT size and the CIR length, respectively.

The implication above that $L < N$ is generally valid in our work. To demonstrate this, we use measured frequency-domain data to simulate direct and FEXT couplings of a 30-pair, 300-meter, 0.5 mm cable [11] with 15 kHz sub-carrier spacing (same as LTE signals). $K = 4$ pairs are randomly picked from the same binder. We choose the band between 21 MHz and 24 MHz (as suggested in [3]), which can fit a 3 MHz LTE signal, as an example. Transforming all K^2 measured paths into time-domain with $N = 256$, Fig. 5 shows that $L = 15$ is the maximum time-domain tap number containing 99% CIR power. We consider a channel spread of $L = 15$ for all K^2 paths in this work.

The channel path from transmitter i to the j -th RRH can be represented

by

$$\mathbf{H}_{j,i} = \mathbf{F}_L \mathbf{h}_{j,i},$$

where $\mathbf{H}_{j,i} = [H_{j,i}^1, \dots, H_{j,i}^{r_1}, \dots, H_{j,i}^{r_M}, \dots, H_{j,i}^N]^T$ (including zero-padding if the number of sub-carriers is smaller than the DFT size N) denotes the frequency-domain channel representation and $\mathbf{h}_{j,i} = [h_{j,i}(0), \dots, h_{j,i}(L-1)]^T$ denotes the time-domain CIR, respectively. Within one CRS-containing OFDM symbol as exemplified in Fig. 4, let $\mathbf{X}_i = [X_i^{r_1}, \dots, X_i^{r_M}]^T$ denote the reference symbols transmitted on pair i , where M is the number of reference symbols in one OFDM symbol, and $\mathcal{R} = [r_1, \dots, r_M]^T$ denotes the set of sub-carrier indices which are loaded with reference symbols. For a group of K RRHs/cells, transmission over copper pairs on a reference-symbol sub-carrier r_i can be modelled as

$$\begin{aligned} \underbrace{\begin{bmatrix} Y_1^{r_i} \\ \vdots \\ Y_K^{r_i} \end{bmatrix}}_{\mathbf{Y}^{r_i}} &= \begin{bmatrix} H_{1,1}^{r_i} & \cdots & H_{1,K}^{r_i} \\ \vdots & \ddots & \vdots \\ H_{K,1}^{r_i} & \cdots & H_{K,K}^{r_i} \end{bmatrix} \begin{bmatrix} X_1^{r_i} \\ \vdots \\ X_K^{r_i} \end{bmatrix} + \mathbf{N} \\ &= \begin{bmatrix} \mathbf{F}_L^{r_i} \mathbf{h}_{1,1} & \cdots & \mathbf{F}_L^{r_i} \mathbf{h}_{1,K} \\ \vdots & \ddots & \vdots \\ \mathbf{F}_L^{r_i} \mathbf{h}_{K,1} & \cdots & \mathbf{F}_L^{r_i} \mathbf{h}_{K,K} \end{bmatrix} \begin{bmatrix} X_1^{r_i} \\ \vdots \\ X_K^{r_i} \end{bmatrix} + \mathbf{N} \\ &= \underbrace{\begin{bmatrix} \mathbf{I}_K \otimes X_1^{r_i} \mathbf{F}_L^{r_i} & \cdots & \mathbf{I}_K \otimes X_K^{r_i} \mathbf{F}_L^{r_i} \end{bmatrix}}_{\mathbf{A}^{r_i}} \underbrace{\begin{bmatrix} \mathbf{h}_{1,1} \\ \vdots \\ \mathbf{h}_{K,1} \\ \vdots \\ \mathbf{h}_{K,K} \end{bmatrix}}_{\mathbf{h}} + \mathbf{N}, \end{aligned} \quad (2)$$

where $\mathbf{F}_L^{r_i}$ denotes the r_i -th row of \mathbf{F}_L , \mathbf{N} denotes the background noise, \mathbf{I}_K denotes a $K \times K$ identity matrix, \otimes denotes Kronecker product, and \mathbf{Y}^{r_i} denotes the receive signal on subcarrier r_i at the RRH-side.

Observe in Eq.(2) that the unknown vector \mathbf{h} is frequency independent, which connects the reference-symbol related matrix \mathbf{A}^{r_i} to the receive signal \mathbf{Y}^{r_i} on each reference-symbol sub-carrier r_i . Stacking and interleaving all the information collected from the M reference-symbol sub-carriers yield

$$\underbrace{\begin{bmatrix} \mathbf{Y}_1^T & \cdots & \mathbf{Y}_K^T \end{bmatrix}^T}_{\mathbf{y}} = \underbrace{\begin{bmatrix} \mathbf{A}_1 & \cdots & \mathbf{A}_K \end{bmatrix}}_{\mathbf{A}} \mathbf{h} + \mathbf{N}, \quad (3)$$

where $\mathbf{Y}_i = [Y_i^{r_1}, \dots, Y_i^{r_M}]^T$ and

$$\mathbf{A}_i = \mathbf{I}_K \otimes \begin{bmatrix} X_i^{r_1} \mathbf{F}_L^{r_1} \\ \vdots \\ X_i^{r_M} \mathbf{F}_L^{r_M} \end{bmatrix}.$$

To make the rank of \mathbf{A} in Eq. (3) equal the dimension of its column space and also to average out the noise influence, we extend \mathbf{y} and \mathbf{A} vertically by stacking more \mathbf{Y}_i and \mathbf{A}_i from the following CRS-containing OFDM symbols in Eq. (3). The K^2 CIRs, which are stacked in one column vector \mathbf{h} can be estimated by

$$\hat{\mathbf{h}} = (\mathbf{A}^H \mathbf{A})^{-1} \mathbf{A}^H \mathbf{y}. \quad (4)$$

Since the CRS related matrix \mathbf{A} in Eq. (4) can be directly generated from the corresponding cell identity and \mathbf{y} is fed back from RRHs, the whole estimation process can be accomplished without interrupting the LTE signal flow.

4 Time-Domain Precoding

The proposed time-domain precoder includes two functional parts: crosstalk cancellation and ISI mitigation.

4.1 Crosstalk Cancellation

With \mathbf{h} estimated in Eq. (4), we can reconstruct it into the direct-and-FEXT-path format as

$$\mathcal{H} = \begin{bmatrix} \hat{\mathbf{h}}_{1,1} & \cdots & \hat{\mathbf{h}}_{1,K} \\ \vdots & \ddots & \vdots \\ \hat{\mathbf{h}}_{K,1} & \cdots & \hat{\mathbf{h}}_{K,K} \end{bmatrix},$$

where each entry $\mathbf{h}_{j,i}$ denotes a length- L time-domain impulse response from the i -th transmitter to the j -th receiver.

Similar to the normal two-dimensional matrix case, it is shown in [12] that the following relation exists for \mathcal{H} :

$$\mathcal{H} * \text{adj}(\mathcal{H}) = \det(\mathcal{H}) * \mathcal{I}, \quad (5)$$

where $*$ denotes the convolutional operator and \mathcal{I} is a diagonal matrix with each diagonal entry being a Dirac delta function δ . Similar to the Leibniz

formula for the determinant of a two-dimensional matrix, $\det(\mathbf{H})$ in Eq. (5) is defined by

$$\det(\mathbf{H}) = \sum_{\sigma \in S_K} \text{sgn}(\sigma) \prod_{i=1}^K \mathbf{h}_{i, \sigma_i},$$

where \prod^* denotes a series of convolution instead of multiplication, σ is one permutation vector out of the permutation group S_K , and $\text{sgn}(\cdot)$ is the sign function of the permutation vector σ . The permutation group S_K contains all possible permutations based on vector $[1, \dots, K]$. Each entry of the adjoint matrix is defined accordingly as

$$[\text{adj}(\mathbf{H})]_{i,j} = (-1)^{i+j} \det(\mathbf{H}_{(j,i)}), \quad (6)$$

where $\mathbf{H}_{(j,i)}$ denotes the (j, i) minor of \mathbf{H} that deletes j -th row and i -th column from \mathbf{H} .

Assign the time-domain diagonalizing precoder to be $\mathbf{P}_D = \text{adj}(\mathbf{H})$. Disregarding the transmit power limitation for now, the receive signal in time-domain becomes

$$\begin{aligned} \mathbf{Y} &= \mathbf{H} * \mathbf{P}_D * \mathbf{X} + \mathbf{N} \\ &= \det(\mathbf{H}) * \mathbf{I} * \mathbf{X} + \mathbf{N}, \end{aligned} \quad (7)$$

where $\mathbf{X} = [\mathbf{x}_1, \dots, \mathbf{x}_K]^T$, and \mathbf{x}_i denotes the time-domain LTE signal transmitted on pair i . The receive signal $\mathbf{Y} = [\mathbf{y}_1, \dots, \mathbf{y}_K]^T$ and background noise \mathbf{N} are defined similarly.

Note that $\det(\mathbf{H})$ in Eq. (7) is *one* CIR with length $KL - (K - 1)$. The term $\det(\mathbf{H}) * \mathbf{I}$ implies that the effective channel after precoding has *identical* CIR on every direct path, while FEXT is zeroed out. The \mathbf{P}_D implemented to generate results in Fig. 6 is constructed based on the estimated CIRs using Eq. (4) with 10 slots of CRS. It is observed that the effective direct CIRs (see black circle-marked lines in Fig. 6) fall into the same pattern and the FEXT paths (blue square-marked lines) are effectively suppressed to much lower power levels compared to the original FEXT paths (red triangle-marked lines).

4.2 Inter-Symbol Interference (ISI) Mitigation

One outcome of the precoding scheme in Section 4.1 is that the direct channel spread is extended from L to $KL - (K - 1)$ (also shown in Fig. 6 when comparing the yellow diamond-marked lines to the black circle-marked lines). The short version of LTE CP duration is $4.6875 \mu\text{s}$, whereas 90% of indoor delay spread is below 500 ns (see Table 5 in [13]). It implies that at least 85% of the LTE

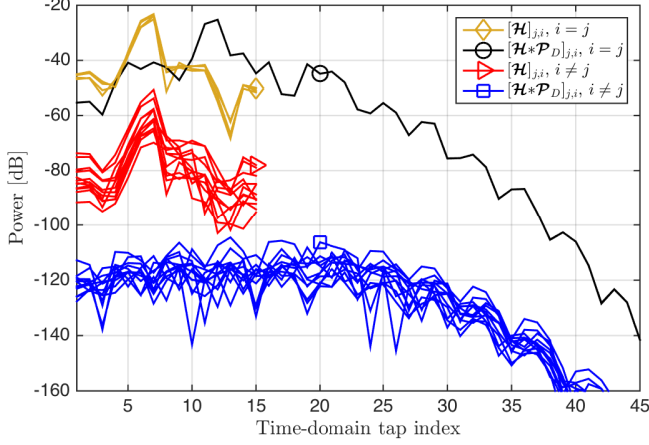


Fig. 6: Equivalent CIRs before and after performing the time-domain diagonalizing precoding. Matrix entries with $i = j$ indicate direct paths, while entries with $i \neq j$ indicate FEXT paths.

CP length can be consumed by transmitting over copper pairs. If the effective copper channel spread after applying \mathcal{P}_D is longer than this CP portion, it is worthwhile introducing further spread confining filter(s) in the precoder to mitigate ISI.

As the time-domain channel representation is a finite impulse response (FIR), full equalization aiming for a Dirac delta function will require an infinite impulse response (IIR) filter. In practice, we compromise by only confining the direct channel spread to be shorter than the reserved CP length for copper transmission. In [14], an optimal shortening filter is proposed which maximizes the shortening SNR (SSNR). Since all K direct paths are the same after applying \mathcal{P}_D , it is sufficient to design a single shortening filter.

Let \mathbf{w} denote the impulse response shortening filter (IRSF) with a desired length L_{IRSF} . Let \mathbf{H}_{conv} denote the convolutional matrix of $\det(\mathcal{H})$ and let \mathbf{h}_{prec} denote the effective direct CIR after implementing the time-domain precoding, *i.e.*,

$$\mathbf{h}_{\text{prec}} = \det(\mathcal{H}) * \mathbf{w} = \mathbf{H}_{\text{conv}} \mathbf{w}.$$

With a certain amount of delay Δ considered and a shortened CIR length of L_{target} targeted, the objective part of \mathbf{h}_{prec} that has effective CIR values is given by

$$\mathbf{h}_{\text{eff}} = \mathbf{Z}_{\text{eff}} \mathbf{h}_{\text{prec}} = \mathbf{H}_{\text{eff}} \mathbf{w},$$

Table 1: Maximum SSNR shortening impulse response filter

	$L_{\text{target}} \geq L_{\text{IRSF}}$	$L_{\text{target}} < L_{\text{IRSF}}$
Eigen-decomp.	$\mathbf{B} = \mathbf{Q}\mathbf{\Sigma}\mathbf{Q}^H$	$\mathbf{B} = [\mathbf{U} \quad \mathbf{V}] \begin{bmatrix} \mathbf{\Sigma} & \mathbf{0} \\ \mathbf{0} & \mathbf{0} \end{bmatrix} \begin{bmatrix} \mathbf{U}^H \\ \mathbf{V}^H \end{bmatrix}$
\mathbf{D}	$(\sqrt{\mathbf{B}})^{-1} \mathbf{C} (\sqrt{\mathbf{B}}^H)^{-1}$	$(\mathbf{\Lambda}^H - \mathbf{\Lambda}^H \mathbf{O}^H) \mathbf{C} (\mathbf{\Lambda} - \mathbf{O} \mathbf{\Lambda})$ for $\mathbf{O} = \mathbf{V}(\mathbf{V}^H \mathbf{C} \mathbf{V})^{-1} \mathbf{V}^H \mathbf{C}$, and $\mathbf{\Lambda} = \mathbf{U}(\sqrt{\mathbf{\Sigma}})^{-1}$.
\mathbf{q}_{\min}	Eigenvector of the minimum eigenvalue λ_{\min} of \mathbf{D} .	
\mathbf{w}_{opt}	$(\sqrt{\mathbf{B}})^{-1} \mathbf{q}_{\min}$	$(\mathbf{I} - \mathbf{O}) \mathbf{\Lambda} \mathbf{q}_{\min}$

where $\mathbf{H}_{\text{eff}} = \mathbf{Z}_{\text{eff}} \mathbf{H}_{\text{conv}}$ and

$$\mathbf{Z}_{\text{eff}} = \begin{bmatrix} \mathbf{0}_{L_{\text{target}} \times (\Delta-1)} & \mathbf{I}_{L_{\text{target}}} & \mathbf{0}_{L_{\text{target}} \times (KL-K+L_{\text{target}}-\Delta)} \end{bmatrix}$$

is a matrix that picks the rows $\mathcal{T} = [\Delta, \dots, \Delta + L_{\text{target}} - 1]$ from a matrix/vector. Similarly, the rest of \mathbf{h}_{prec} is denoted by

$$\mathbf{h}_{\text{rest}} = \mathbf{Z}_{\text{rest}} \mathbf{h}_{\text{prec}} = \mathbf{H}_{\text{rest}} \mathbf{w},$$

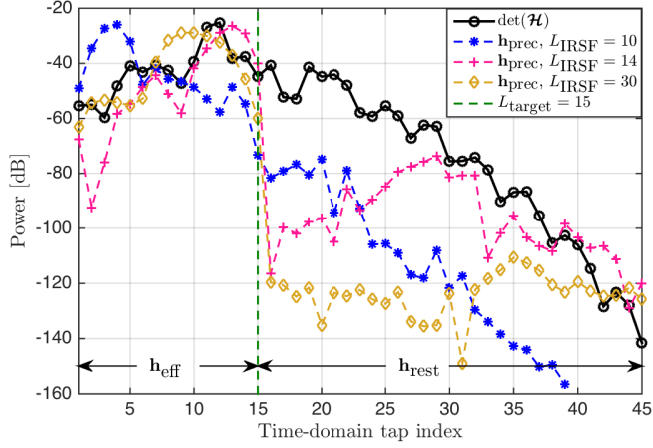
where $\mathbf{H}_{\text{rest}} = \mathbf{Z}_{\text{rest}} \mathbf{H}_{\text{conv}}$ and \mathbf{Z}_{rest} picks the rows $[1, \dots, KL - K + L_{\text{target}} - 1] \setminus \mathcal{T}$ from a matrix/vector. Accordingly, the energy in-and-outside the chunk of interest is formulated respectively as

$$\begin{aligned} \mathbf{h}_{\text{eff}}^H \mathbf{h}_{\text{eff}} &= \mathbf{w}^H \mathbf{H}_{\text{eff}}^H \mathbf{H}_{\text{eff}} \mathbf{w} = \mathbf{w}^H \mathbf{B} \mathbf{w}, \\ \mathbf{h}_{\text{rest}}^H \mathbf{h}_{\text{rest}} &= \mathbf{w}^H \mathbf{H}_{\text{rest}}^H \mathbf{H}_{\text{rest}} \mathbf{w} = \mathbf{w}^H \mathbf{C} \mathbf{w}, \end{aligned}$$

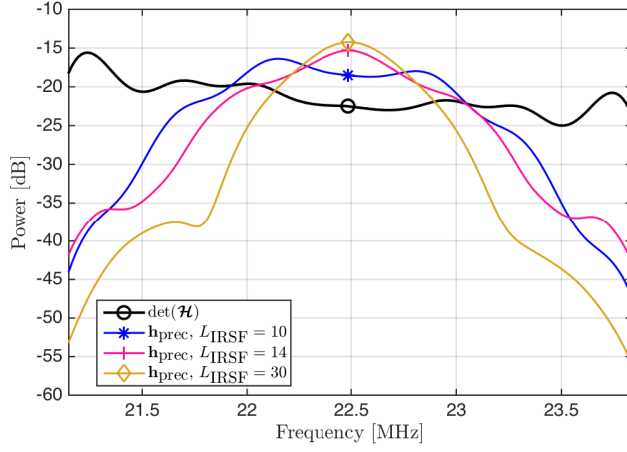
where $\mathbf{B} = \mathbf{H}_{\text{eff}}^H \mathbf{H}_{\text{eff}}$ and $\mathbf{C} = \mathbf{H}_{\text{rest}}^H \mathbf{H}_{\text{rest}}$. Implementing eigen-decomposition as in [14] and summarized in Table 1, the optimal IRSF that maximizes the SSNR is given by

$$\begin{aligned} \mathbf{w}_{\text{opt}} &= \max_{\mathbf{w}} [\text{SSNR}] \\ &= \max_{\mathbf{w}} \left[10 \log_{10} \left(\frac{\mathbf{w}^H \mathbf{B} \mathbf{w}}{\mathbf{w}^H \mathbf{C} \mathbf{w}} \right) \right]. \end{aligned} \quad (8)$$

The length relation between L_{target} and L_{IRSF} differentiated in Table 1 determines the singularity of matrix \mathbf{B} .



(a) Time-domain channel representation.



(b) Frequency-domain channel representation.

Fig. 7: Direct channel impulse response shortening (IRS) for $L_{\text{target}} = 15$, considering channel measurements between 21 MHz and 24 MHz.

Fig. 7 reveals that there is a trade-off between the time-domain shortening effectiveness and the frequency-domain effective channel gain. A longer shortening filter (*e.g.*, $L_{\text{IRSF}} = 30$, yellow diamond-marked line in Fig. 7a) suppresses the channel spread outside L_{target} to a much lower level compared to a shorter

filter (*e.g.*, $L_{\text{IRSF}} = 10$, blue star-marked line). The counterparts in frequency-domain in Fig. 7b show that the effective channel using a shorter filter (*e.g.*, $L_{\text{IRSF}} = 10$) has a higher channel gain over the 3 MHz bandwidth compared to that of a longer filter (*e.g.*, $L_{\text{IRSF}} = 30$). Since the time-domain spread affects the ISI and the frequency-domain effective channel gain affects the receive signal power, using a longer L_{IRSF} does not necessarily result in a higher receive SNR. The effect of this trade-off is illustrated in terms of SNR in the next subsection.

In summary, the time-domain precoder is formulated as

$$\mathbf{P} = \mu \cdot \text{adj}(\mathbf{H}) * \mathbf{w}', \quad (9)$$

where $\text{adj}(\mathbf{H})$ diagonalizes the interference channel as defined in Eq. (6). $\mathbf{w}' = \mathbf{w}_{\text{opt}}$ is the filter given by Eq. (8) if the direct CIR shortening is needed; otherwise $\mathbf{w}' = \boldsymbol{\delta}$. The power normalization factor μ that constrains the transmit power is defined as

$$\mu = \frac{1}{\max_{i \in [1, \dots, K]} \sum_{j=1}^K \left\| [\text{adj}(\mathbf{H}) * \mathbf{w}']_{i,j} \right\|_2}.$$

4.3 Precoding Simulation Results

In Fig. 8, the average receive SNR is calculated over a 3 MHz band. The carrier frequency of each band is shifted from 22.5 MHz (referring to a band 21 MHz–24 MHz) to 58.5 MHz (referring to a band 57 MHz–60 MHz) to study the impact of different channel characteristics. A flat transmit PSD of -60 dBm/Hz is applied and a copper channel background noise of -140 dBm/Hz is assumed. The data symbols are 16-QAM modulated as an example.

The single line performance is calculated as a reference using only the direct-path measurements. No crosstalk and transmit power constraint is considered. It can be viewed as an ideal situation after precoding. For the single line and the crosstalk corrupted performances in Fig. 8, average and worst situations are presented respectively. For the other lines that have the time-domain crosstalk cancellation (as in Section 4.1) implemented, the receive SNR for one RRH is presented since we show in Fig. 6 that the crosstalk has been effectively suppressed and the direct paths are identical.

Whether or not the shortening filter should be added is also implementation dependent. If the SNR result without IRS (*e.g.*, black circle-marked line in Fig. 8) is already acceptable, there is no need to add the shortening filter which changes the shape of frequency-domain equivalent channel as shown in Fig. 7b and may increase the complexity of the frequency-domain equalizer. Especially

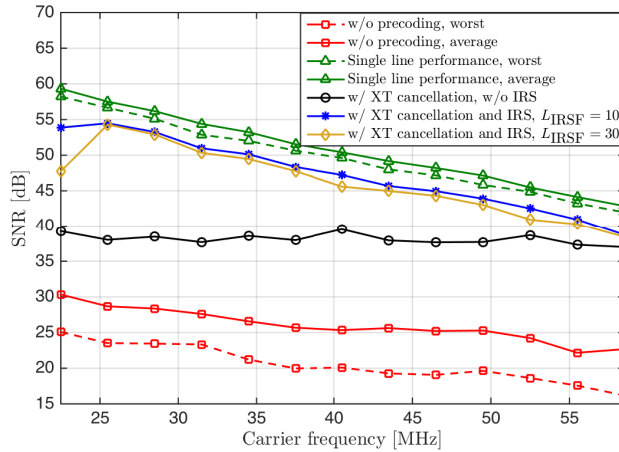


Fig. 8: Receive SNR comparison at the copper and RRH connecting point.

when considering a higher frequency range where the direct coupling magnitude decreases, the SNR difference among the single line performance, the precoded performances with and without IRS becomes much smaller.

5 Conclusion

Time-domain crosstalk cancellation provides more flexibility and is less intrusive than traditional vectoring for LoC systems. The proposed approach exploits LTE reference signals to estimate the copper channel, cancels crosstalk, and yields effective direct paths that are identical for all pairs. The latter enables low-complexity channel shortening in case the desired receive SNR at the RRH-side is not achieved because of the direct channel spread. Simulation results with measured copper channel data confirm that the precoder performance is close to the single-user bound.

Acknowledgement

This work was partly supported by the Celtic-Plus project GOLD, the European Horizon 2020 project Xhaul and the EXAM project of EIT Digital.

References

- [1] J. Gambini and U. Spagnolini, “Wireless over cable for femtocell systems,” in *IEEE Communications Magazine*, pp. 716-720, vol. 51, no. 5, pp. 178-185, May 2013.
- [2] C. Lu, M. Berg, E. Trojer, P.-E. Eriksson, K. Laraqui, O. V. Tidblad, and H. Almeida, “Connecting the dots: small cells shape up for high-performance indoor radio,” *Ericsson Review*, vol. 91, December 2014. [Online]. Available: <http://goo.gl/YvdY5N>
- [3] Y. Huang, E. Medeiros, S. Höst, T. Magesacher, P.-E. Eriksson, C. Lu, P. Ödling, and P. O. Börjesson, “Enabling DSL and Radio on the Same Copper Pair,” in *Proc. 2015 IEEE International Conference on Communications (ICC)*, pp. 1031-1035, June 2015.
- [4] Y. Huang, E. Medeiros, N. Fonseca, S. Höst, T. Magesacher, P.-E. Eriksson, C. Lu, P. Ödling, and P. O. Börjesson, “LTE over Copper – Potential and Limitations,” in *Proc. IEEE 26th Annual International Symposium on Personal, Indoor and Mobile Radio Communications (PIMRC)*, August 2015.
- [5] ITU, “Very high speed digital subscriber line transceivers 2 (VDSL2),” Recommendation ITU-T G.993.2, December 2011. [Online]. Available: <https://www.itu.int/rec/T-REC-G.993.2-201112-I/en>
- [6] G. Ginis and J. Cioffi, “Vectored Transmission for Digital Subscriber Line Systems,” *IEEE Journal on Selected Areas in Communications*, vol. 20, no. 5, pp. 1085-1104, June 2002.
- [7] F. A. Mruck, C. Stierstorfer, J. B. Huber, and R. Tzschoppe, “Time-Domain MIMO Precoding for FEXT Cancellation in DSL Systems,” in *Proc. 2013 17th International ITG Workshop on Smart Antennas (WSA)*, pp. 1-7, March 2013.
- [8] 3GPP, “Evolved Universal Terrestrial Radio Access (E-UTRA); Base Station (BS) radio transmission and reception,” 3rd Generation Partnership Project (3GPP), TS 36.104 V12.6.0, February 2015. [Online]. Available: <http://goo.gl/SCislQ>
- [9] 3GPP, “LTE; Evolved Universal Terrestrial Radio Access (E-UTRA); Physical channels and modulation,” 3rd Generation Partnership Project (3GPP), TS 36.211 V12.6.0, July 2015. [Online]. Available: <http://goo.gl/jepG09>

- [10] E. Medeiros, Y. Huang, T. Magesacher, S. Höst, P.-E. Eriksson, C. Lu, P. Ödling, and P. O. Börjesson, "Frequency-Domain Crosstalk Cancellation for LTE-over-Copper Systems," unpublished.
- [11] Ericsson AB, *Access Network Pair cable, TEL 312*, 2010. [Online]. Available: <http://goo.gl/4RdCXc>
- [12] E. Auger, B. Rankov, M. Kuhn, and A. Wittneben, "Time Domain Precoding for MIMO-OFDM Systems, in *10th International OFDM-Workshop*, August 2005.
- [13] ITU-R, "Propagation data and prediction methods for the planning of indoor radiocommunication systems and radio local area networks in the frequency range 300 MHz to 100 GHz," International Telecommunication Union (ITU), Recommendation P.1238-8, July 2015. [Online]. Available: <https://goo.gl/UG1HmB>
- [14] P. Melsa, R. Younce, and C. Rohrs, "Impulse Response Shortening for Discrete Multitone Transceivers, *IEEE Transactions on Communications*, vol. 44, no. 12, pp. 1662-1672, December 1996.